

NUMERICAL SIMULATION OF THE FINAL STAGES OF
TERRESTRIAL PLANET FORMATION

by

© LARRY PAUL COX

S.B. Physics, Massachusetts Institute of Technology,
(1969)

SUBMITTED IN PARTIAL FULFILLMENT
OF THE REQUIREMENTS FOR THE
DEGREE OF

DOCTOR OF PHILOSOPHY

at the

MASSACHUSETTS INSTITUTE OF TECHNOLOGY
(May, 1978)

Signature of Author
Department of Earth and Planetary Sciences, May, 1978

Certified by Thesis Supervisor

Accepted by
Chairman, Departmental Committee on Graduate Students

WITHDRAWN
FROM
MASSACHUSETTS INSTITUTE
OF TECHNOLOGY
MIT LIBRARIES
AUG 11 1978

LIBRARIES

In Anfwer to the Epicurean Syftem,
 [he argues] How often might a Man, after
 he had jumbled a Set of Letters in a
 Bag, fling them out upon the Ground
 before they would fall into an exact
 Poem, yea or fo much as make a good
 Difcourfe in Profe? And may not a
 little *Book* be as eafily made by
 Chance, as this great *Volume* of the
 World? How long might a Man be fprinkling
 Colours upon a Canvas with a carelefs
 Hand, before they could happen to make
 the exact Picture of a Man? And is a Man
 eafier made by Chance than his Picture?
 How long might twenty thoufand *blind*
Men, which fhould be fent out from the
 feveral remote Parts of *England*, wander
 up and down before they would all meet
 upon *Salisbury-Plains*, and fall into
 Rank and File in the exact Order of an
 Army? And yet this is much more eafy to
 be imagin'd, than how the innumerable
blind Parts of Matter fhould rendezvouze
 themfelves into a World.

John Tillotson
 Archbishop of Canterbury
 in *Maxims and Discourses Moral and Devine*
 (London, 1719)

NUMERICAL SIMULATION OF THE FINAL STAGES OF
TERRESTRIAL PLANET FORMATION

by

LARRY PAUL COX

Submitted to the Department of Earth and Planetary Sciences in May, 1978 in partial fulfillment of the requirements for the degree of Doctor of Philosophy.

Abstract

Four representative numerical simulations of the growth of the terrestrial planets by accretion of large protoplanets are presented. The mass and relative velocity distributions of the bodies in these simulations are free to evolve simultaneously in response to close gravitational encounters and occasional collisions between bodies. The collisions between bodies, therefore, arise in a natural way and the assumption of expressions for the relative velocity distribution and the gravitational collision cross-section is unnecessary.

The relation of the present work to scenarios given by Safronov (1969), Goldreich and Ward (1973), and Greenberg et al. (1977) for the early stages of solar system evolution is discussed. A comparison of predictions of the commonly employed two-body gravitational model with integrations of the equations of motion which include the influence of the Sun indicate that the two-body model is inadequate for the treatment of encounters between large protoplanets, particularly when they move along low eccentricity orbits resulting in encounters with low relative velocities.

A new model is, therefore, proposed for single close encounters between two small masses, m_1 and m_2 , which orbit a much larger mass, M . Comparisons of predictions of the model with integrations of the three-body equations of motion indicate that the model is an adequate approximation

for those encounters with $m_1, m_2 \lesssim 10^{-5} M$ and $\epsilon \geq 4$, where ϵ is the eccentricity of the hyperbolic orbit of m_1 about m_2 . The current simulations represent to my knowledge the only model of planetary accretion taking into account the presence of the Sun in the gravitational interactions between bodies.

The protoplanetary bodies in these simulations are assumed to move along unperturbed co-planar orbits until they pass within a sphere of influence distance $R_s = R_0[m_1(m_1 + m_2)/M^2]^{1/5}$, where R_0 is the heliocentric distance. When a close approach to another body occurs, new orbital elements are computed for each body either by the model or by integration of the regularized equations of motion, depending on the parameters of the encounter. Protoplanets are assumed to accrete and form a body with mass equal to the sum of the masses of the two incoming bodies when a close approach with separation less than the sum of the radii of the bodies (assuming lunar density material) occurs during integration.

All simulations begin with an initial system of one hundred bodies of equal mass having a total mass equal to that of the terrestrial planets. The surface density of the system is assumed to have an $R^{-3/2}$ dependence on heliocentric distance between 0.5 and 1.5 AU and to be zero elsewhere. The orbital eccentricities are randomly chosen from a uniform distribution on the interval from 0 to a given maximum eccentricity, e_{\max} .

These simulations indicate that the growth of bodies with final masses approaching those of Venus and the Earth is possible, at least for the case of a two-dimensional system. Simulations with $e_{\max} < 0.10$ are found to produce final states containing too many bodies with a narrow mass distribution, while simulations with $e_{\max} > 0.20$ result in too many catastrophic collisions between bodies and rapid accretion of planetary-size bodies is prohibited. The $e_{\max} = 0.15$ simulation ends with a state surprisingly similar to that of the present terrestrial planets and, therefore, provides a rough estimate of the range of radial sampling to be expected for the terrestrial planets.

Thesis Supervisor: John S. Lewis

Title: Associate Professor of Geochemistry and
Chemistry

ACKNOWLEDGEMENTS

The preparation of this thesis was an effort involving a number of people besides the author.

The topic emerged as a result of conversations with Myron Lecar, W.R. Ward, and J.S. Lewis. Throughout the research the guidance of my advisor, Professor John Lewis, has been of great help. He has not only made many helpful suggestions and criticisms, but has provided a good balance of enthusiasm and healthy skepticism. During the sabbatical leave of John Lewis in 1976, Professor Charles Counselman ably filled in as my advisor and frequent discussions with him were very helpful in constructing many of the algorithms employed in the simulations. This research has also benefited from the suggestions, criticisms, and interest of Stephen Barshay and Bruce Fegley. I, of course, take full credit for the shortcomings which undoubtedly remain.

During my career in graduate school I was supported by the Earth and Planetary Sciences Department and by the Mathematics Department. The computing time for this research was provided by NASA Grant NGL-22-009-521.

I especially wish to thank my wife, Candace, for her encouragement, support, and love, which were essential to me as well as to this research.

I also wish to thank Roxanne Regan for her efforts
in typing this manuscript.

NUMERICAL SIMULATION OF THE FINAL STAGES OF
TERRESTRIAL PLANET FORMATION

TABLE OF CONTENTS

	<u>page</u>
Frontispiece	2
Abstract	3
Acknowledgements	5
Table of Contents	7
List of Tables	9
I. INTRODUCTION	10
A. The Absence of Known Counterparts of Our Solar System	10
B. Requirements for a Successful Theory of Solar System Formation	13
C. Cosmogonical Hypotheses of the Present Simulations	15
D. Three Scenarios for the Early Stages of Solar System Evolution	17
E. The Late Stages of Solar System Evolution	33
F. The Numerical Simulations	45
II. A NEW MODEL FOR CLOSE GRAVITATIONAL ENCOUNTERS	48
A. Introduction	48
B. A Description of the Model	50
C. Plausibility Arguments for the Model	52
D. The Algorithm for Applying the Model	57
E. Tests of the Model Against Numerical Integration	60
F. Conclusions Drawn from the Numerical Comparisons	68
G. Treatment of Encounters Outside the Range of Validity of the Model	70

	<u>page</u>
III. THE MODEL FOR COLLISIONS BETWEEN BODIES	74
A. A Description of the Collision Model	74
B. An Estimate of Fragment Size After A Collision	76
C. The Requirement of Total Energy Conservation	78
D. Implications of Total Energy Conservation	82
E. Do the Clusters of Fragments Shrink to Solid Density Before Their Next Collision?	84
IV. THE COMPUTER SIMULATION PROCEDURE	90
A. The Basic Assumptions of the Simulations	90
B. The Relative Importance of Close Versus Distant Encounters	92
C. The Algorithm Used for Finding Close Encounters	96
D. A Flowchart of the Simulations	103
V. THE COMPUTER SIMULATIONS	110
A. Results of Four Representative Numerical Simulations	110
B. An Estimate of the Evolution Times Expected for Three-Dimensional Systems	127
C. Heliocentric Distance Sampling of Material for the Final Bodies of the Simulations	130
D. Conclusions Drawn from the Simulations Regarding the Formation of the Terrestrial Planets	134
E. Limitations of the Present Numerical Simulations	136
References	140
Figure Captions	144
Figures	149
Biographical Note	173

LIST OF TABLES

	<u>page</u>
1. Two-Body Gravitational Cross Sections with Keplerian Differential Velocities Gravitational Cross-Sections Obtained by Integration	40
2. Collision Statistics ($e_{\max} = 0.05$)	116
3. Collision Statistics ($e_{\max} = 0.10$)	117
4. Collision Statistics ($e_{\max} = 0.15$)	118
5. Statistics of the Eccentricity Changes Occurring for Encounters and Collisions	120
6. Comparisons of Total System Angular Momentum and Energy	127

CHAPTER I. INTRODUCTION

A. The Absence of Known Counterparts of Our Solar System

The study of the origin of the solar system is hampered considerably by the absence of any known counterparts of our own system. Except for the tentative evidence (van de Kamp, 1969; Gatewood, 1972) in the case of Barnard's star, no extrasolar substellar mass (mass $< 0.01 M_{\odot}$) has been discovered and confirmed. Because of the many uncertainties in the data, it is extremely difficult to determine the characteristics of the Barnard planetary system. Black and Suffolk (1973) and Gatewood (1976) have suggested that if the residuals from rectilinear motion are assumed to be reliable, two bodies with masses similar to that of Jupiter having periods between ten and thirty years, respectively, are indicated. Black and Suffolk further conclude that the two planets cannot be in co-planar orbits. However, it should be noted that the elimination of systematic errors in the observations has been difficult and, therefore, the above conclusions are subject to change.

The tentative detection of planet-like companions of Barnard's star was entirely dependent on the proximity of the star and the small mass of the primary. Since

the existence of such objects can be presently determined only by observing the perturbed motion of the primary and since the motion of the primary relative to the center of mass would be highly complicated by the presence of several massive planets, the observation of even a single counterpart of our own solar system seems unlikely in the near future. Thus, the chance of observing a terrestrial-like system of planets is quite remote. At the very least we are, therefore, deprived of the insights that might result from a classification scheme for planetary systems analogous to those for stars and galaxies.

If it is difficult to observe true counterparts of our planetary system in their completely formed state, it is that much more difficult to observe them in the process of planet formation both because of the small fraction of their age that is thought to be spent in planet formation and because of the probable obscuration of such systems by circumstellar dust grains. Indeed, there is a large body of observational data on nebulae exhibiting strong "excess" infrared emission which surround newly formed stars. These data yield valuable information about the properties of the circumstellar dust grains surrounding these stars and in the case of MWC 349, Thompson et al. (1977) have inferred the existence of a preplanetary

(Amalthea), the seven inner satellites of Saturn (excluding Titan), and the five satellites of Uranus are comparable in mass, but are about two orders of magnitude less than those of the main satellites. These satellites also move in nearly circular, except for Hyperion, prograde orbits in the equatorial planes of their parent bodies. However, there are often substantial mutual perturbations in the orbital motions of these satellite systems. Therefore, a number of possible clues to the problem of satellite formation and perhaps planetary formation have been obscured by the dynamical evolution of these systems subsequent to their formation in much the same way as in the planetary system.

If it is difficult to observe true counterparts of our planetary system in their completely formed state, it is that much more difficult to observe them in the process of planet formation both because of the small fraction of their age that is thought to be spent in planet formation and because of the probable obscuration of such systems by circumstellar dust grains. Indeed, there is a large body of observational data on nebulae exhibiting strong "excess" infrared emission which surround newly formed stars. This data yields valuable information about the properties of the circumstellar dust grains surrounding these stars and in the case of MWC 349, Thompson et al. (1977) have inferred the existence of a preplanetary

disk surrounding the star. The real problem is in obtaining data on the larger bodies and this is observationally very difficult.

Assuming classical models for nucleosynthesis, the extinct radionuclides I^{129} and Pu^{244} have given (for the various meteorites studied so far) time intervals ranging from 90 to 250 million years for the time of isolation of the gas and grains later forming the solar system to the start of xenon retention in meteorites (presumably in small bodies like asteroids). These formation intervals then indicate that no more than about 200 million years of solar-system history, and probably less than that, preceded the cooling of the parent meteorite bodies. Gas-retention ages ($K^{40}-A^{40}$ and $U, Th-He^4$) further indicate that the parent meteorite planets cooled approximately 4.5×10^9 years ago. Finally, the minimum age for the crust of the Earth is the oldest measured for any terrestrial rock. At the moment this age is about 3.7×10^9 years. Therefore, no more than a few times 10^8 years is available for the formation of at least the Earth and Moon.

The processes leading to the formation of the solar system, therefore, occurred approximately 4.5×10^9 years ago and presumably consisted of a relatively rapid succession of non-equilibrium early evolutionary phases.

It is not then surprising that many of the clues to the nature of these processes have been obscured. Consequently, a simple extrapolation backwards in time cannot lead to a plausible picture of the origin and early evolution of the solar system. We then conclude that the chance of observing a counterpart of our system in the process of planet formation is indeed small.

B. Requirements For A Successful Theory Of Solar System Formation

With incomplete knowledge of only one planetary system, the problem of deciding which properties of our solar system are "accidental" or probabilistic and which are expected to be general to other planetary systems is a delicate one indeed. Undaunted by the paucity of our data, we endeavor, like the ancient Greeks, to intuit the essential characteristics of reality. Yet, if we are to propose theories of solar system formation, requirements for a successful theory must be explicitly stated. Many authors, Herczeg (1968), McCrea (1972), Woolfson (1969) among others, have constructed lists of fundamental characteristics of the solar system to be used in verifying any cosmogonical hypothesis. Such a list will now be proposed which is specific to theories of terrestrial planet formation. The criteria proposed here for a

satisfactory theory are listed in a necessarily subjective order of importance.

(1) The existence and approximate number of the terrestrial planets must be accounted for.

(2) To a high degree of approximation planetary orbits are co-planar and circular. With the exceptions of Mercury and Pluto, the eccentricity of planetary orbits is always less than 0.1 and the inclination to the ecliptic less than 3.5° . On the other hand, a theory yielding too nearly circular and co-planar orbits would to my mind be suspect. Also, a corollary of the coherence of orbital inclinations is that all of the planets are observed to have a common sense of orbital motion.

(3) A theory should lead to the formation of terrestrial planets of appropriate masses at appropriate heliocentric distances. This requirement is necessarily an approximate one, since the eventual discovery of even one extrasolar planetary system with a terrestrial planet configuration having planetary masses and orbital spacings identical to our own would to me be extremely remarkable!

(4) A successful theory should also account for the axial rotations of the planets. With the exception of Venus and Uranus, planetary rotation is predominantly direct.

(5) The physical structure and chemical composition of the planets must be taken into account. The terrestrial planets in particular exhibit some characteristic deviations from the cosmic abundance of chemical elements and their isotopes. The most important deviations are:

- (a) an almost complete absence of hydrogen and helium, and a strong depletion of some volatile elements, and
- (b) an overabundance of deuterium, lithium, and other light elements relative to the present solar composition.

(6) As was discussed earlier, no more than a few times 10^8 years are available for the formation of at least the Earth and Moon.

(7) A well-developed theory might include the origin of the Earth-Moon system and we can hope for explanations of the absence of satellites for Mercury and Venus and the presence of Deimos and Phobos.

C. Cosmogonical Hypotheses Of The Present Simulations

Many classifications of theories for the formation of the solar system have been proposed, some of which are thousands of years old. In this century Russell (1935), Herczeg (1968), ter Haar (1948), ter Haar and Cameron (1963), Schatzman (1965), Williams and Cremin (1968), McCrea (1972), and Huang (1972) among others have presented

classifications. In order to categorize the cosmogonical hypotheses of the present numerical simulations, the major divisions common to many of these classifications are presented. Theories of cosmogony can be roughly divided into three classes depending on the intimacy of the connection of the origin of the primitive solar nebula with the formation of the Sun itself.

(A) The Sun is assumed to be a stable main-sequence star with essentially the same structure at the time of formation of the planetary system as today. Here, the raw material of the planets is assumed to be captured from an interstellar cloud either by the intervention of another star or simply by accretion of infalling matter.

(B) The Sun is assumed to be in a late phase of its contraction at the time the planets originated. A pre-dominant central mass is assumed to exist already, enforcing Keplerian motion of the material in the nebula. Since it is inferred that the Sun was formed from diffuse interstellar material, it makes for economy to assume that the solar nebula is simply made up of material left over in forming the Sun.

(C) Here, the proto-Sun is assumed to be in an early phase of its formation, very extended and perhaps much more massive than the final, developed Sun. There may be

no strong central condensation at this stage. Planetary accretion is assumed to have started simultaneously with that of the Sun within the same nebula.

Capture and cataclysmic hypotheses are included in class A. The classical hypotheses of Laplace and Kant are perhaps the earliest representatives of classes B and C, respectively. Many hypotheses rely on a very dense gaseous medium to facilitate planetary accumulation, by reducing relative velocities, thus promoting the coalescence of solid particles. However, in the current simulations only a minimum amount of "circumsolar" matter is assumed, with a density corresponding to the total mass of the terrestrial planets spread over the terrestrial region. The current simulation is based on theories of type B.

D. Three Scenarios For The Early Stages of Solar System Evolution

In this section the scenarios given by Goldreich and Ward (1973), Safronov (1969), and Greenberg et al. (1977) for early stages of the evolution of the solar system are described. These investigations provide a background for the present study of the growth of the largest bodies in the last stage of terrestrial planet formation. They also

permit an assessment of the initial conditions used in the simulations to be described here.

The Goldreich-Ward Scenario:

The Goldreich and Ward (1973) scenario for the accretion of planetesimals is divided into four stages. In the first stage small particles are presumed to condense from the cooling primordial solar nebula as the vapor pressures of various constituents fall below their partial pressures. After nucleation a particle is expected to settle through the gas toward the equatorial plane of the nebula while continuing to grow by collection of material still in the vapor phase at a rate given by Hoyle (1946). The limiting radius a particle can reach in this way is calculated by estimating the rate at which a particle descends to the central plane. Using the velocity of the descending particle relative to the local gas determined by the balance between the vertical component of solar gravity and the gas drag force, Goldreich and Ward obtain a limiting radius of $R \sim 3$ cm and a characteristic descent time of ten years for the condensation of iron in the terrestrial region. The surface density of the nebula was estimated by augmenting the total mass of the terrestrial planets up to solar composition and spreading it over the inner solar system. The half-thickness and resulting gas

density of the nebula are determined by the balance of the vertical pressure gradient and the vertical component of solar gravity. Because of the uncertainty of the number of nucleation sites, the final particle radii may very well be much smaller than the estimated 3 cm especially in light of the fact that no particles approaching this size are found in chondrites, but it is expected that the dust particles will settle into a thin gravitationally unstable disk in any case.

Goldreich and Ward next make use of the dispersion relation for local axisymmetric perturbations of a thin rotating disk to investigate the gravitational stability of the dust disk that forms in the equatorial plane of the solar nebula. This dispersion relation (Toomre, 1964; Goldreich and Lynden-Bell, 1965a, b) is written as

$$\omega^2 = k^2 c^2 + \kappa^2 - 2\pi G \sigma k \quad 1-1$$

where $\kappa^2 = 2\Omega[\Omega + d(r\Omega)/dr]$, σ is the unperturbed surface density, c is the sound speed, Ω is the angular velocity, G is the gravitational constant, ω is the frequency of the disturbance, and $k = 2\pi/\lambda$ is its wavenumber. Using the known masses of the terrestrial planets to estimate the surface density of the protoplanetary dust disk, Goldreich and Ward calculate a critical wavelength below

which all wavelengths become unstable to collapse in the absence of random motions. The largest fragments that form when the unstable disk breaks up are estimated to have masses of order $m \sim 2 \times 10^8 g$, corresponding to a critical wavelength $\lambda_c = 4\pi^2 G \sigma_p / \Omega^2 \sim 5 \times 10^8$ cm. Regions containing total masses as large as this cannot collapse unimpeded, since the required rate of increase of rotational and random kinetic energies of the fragment cannot be met by the release of gravitational potential energy. If the equilibrium contraction size of a region corresponds to spatial densities at least as great as that of the solid material, the fragment may collapse directly to form a solid body.

In the second stage of accretion a first generation of planetesimals having radii up to $R \sim 0.5$ km and masses of the order of $m \lesssim 2 \times 10^{14} g$ is expected to form by direct collapse to solid densities. Since the largest unstable regions have masses $\sim 10^4$ times greater than the regions collapsing directly to solid bodies, it is expected that up to $\sim 10^4$ first-generation objects will be gravitationally bound in larger associations resembling partially contracted clusters.

Collisions between these associations will be induced by the differential rotation of the disk. Some associa-

tions will be disrupted by these collisions while some will probably grow at the expense of others. Gradually, however, gas drag will reduce the internal rotational and random kinetic energy of these associations and they will contract toward solid density. This third stage of accretion ends with the formation of a second generation of planetesimals having masses up to $m \sim 2 \times 10^{18} \text{ g}$ and radii up to $r \sim 5 \text{ km}$.

Goldreich and Ward argue that further growth beyond this third stage is unlikely to occur by means of collective gravitational instabilities. Instead, direct particle-particle collisions resulting from the gravitational relaxation of the disk of planetesimals is expected to be the dominant accretion process following the formation of the second-generation planetesimals.

Since gas drag produces a slow inward drift of the planetesimals toward the sun for as long as the gaseous solar nebula is present, it is essential that the particle growth time be short compared to the orbital lifetime set by this drag at each stage of accretion. Goldreich and Ward demonstrated that at each stage of accretion in their scenario the survival time exceeds the growth time by at least two orders of magnitude.

Before going on to discuss the work of Safronov and co-workers, we will briefly consider the obstacles encountered by attempts to attribute the planetary formation process to gravitational instabilities of the entire gaseous nebula. The dispersion relation used earlier to investigate the stability of the dust disk is not rigorously applicable to the gaseous solar nebula since it is derived for a thin disk; however, it does provide a good estimate of the surface density required for instability. When the value of σ_g obtained by augmenting the terrestrial planets up to solar composition, $\sigma_g \sim 1.5 \times 10^3 \text{ g/cm}^2$, is used, the dispersion relation implies that the gaseous solar nebula is stable against gravitational collapse unless the temperature of the gas is of the order of or less than 0.04°K . This unrealistically low temperature forces one to assume a nebula mass greatly exceeding the value needed to account for the present combined masses of the planets in order to obtain gravitational instabilities of the gaseous nebula. This assumption then leads to difficulties in later accounting for the removal of this excess mass from the solar system. In addition, the fact that the chemical composition of the planets differs from the assumed solar composition of the primordial nebula indicates that the density of the

gaseous component of the nebula was not so high as to lead to gravitational instability and the resulting formation of stable gaseous protoplanets.

The Scenario of Safronov:

Safronov credits Edgeworth (1949) and Gurevich and Lebedinskii (1950) with the independent and almost simultaneous inference of the separation of the dust and gaseous components of the solar nebula with the subsequent gravitational instability of the dust layer resulting in its disintegration into a large number of dust condensations. The effect of turbulence in the primordial nebula on the formation of a thin dust layer was considered by Safronov and it was demonstrated that the gravitational energy released by the cloud as interactions between turbulent eddies caused them to move closer to the Sun was insufficient to maintain turbulence in the cloud. Safronov's description (Safronov, 1969) of the first stage of the planetary formation process is in many ways similar to that of Goldreich and Ward. The initial mass of the dust condensations for the terrestrial zone are calculated to be $m \sim 5 \times 10^{16} \text{g}$, a value which falls between those obtained for first and second generation planetesimals by Goldreich and Ward. In calculating the

above mass for the initial dust condensations, Safronov was apparently unaware of the calculations of the gravitational stability of thin rotating disks carried out by Toomre (1964) and Goldreich and Lynden-Bell (1965a, b). More surprising is the fact that Goldreich and Ward were unaware during their investigation of the work done on instabilities in a thinning dust disk done by Safronov (1969), Edgeworth (1949), and Gurevich and Lebedinskii (1950). Like Goldreich and Ward, Safronov describes a stage of accretion in which "primary condensations" collide sometimes combining and sometimes disrupting. This aggregation process presumably leads to the formation of "secondary condensations" having masses of the order of 10^4 - 10^6 times those of the primary condensations. Next, the entire system of condensations was assumed to be converted into a cluster of bodies within a cosmogonically short time. This is roughly the last stage of evolution considered in any detail by Goldreich and Ward.

Initially, the bodies formed in the flat dust disk are presumed to move in nearly circular orbits and consequently have low relative velocities. Later their mass increases as does their gravitational interaction with other bodies resulting in an increase in relative velocities and orbital eccentricities. Since the relative

velocity of the bodies determines the rate of planetary growth and the extent of fragmentation of colliding bodies, there is a close relation between the relative velocities of the bodies and their size distribution.

Safronov assumes, as is commonly done, that encounters between bodies can be treated as in the two-body problem. For approaching bodies of equal mass m , the relative velocity vector \vec{V} does not change in magnitude, but merely turns through the angle $\psi \approx Gm/DV^2$, where D is the impact parameter and $\psi \ll \pi/2$. In an analysis of the balance between the energy acquired by bodies in encounters and the energy lost in collisions, Safronov concludes that the relative velocities of bodies may be conveniently expressed by $V = \sqrt{Gm/\theta r}$, where m and r are the mass and radius of the largest body in a given accretion zone. For a power law mass distribution of bodies in the terrestrial zone, an estimate of $\theta \approx 3-5$ is obtained.

The two problems of determining the velocity distribution in a system of bodies of varying mass and that of determining the mass distribution of the bodies should be solved simultaneously. However, the complete problem is insoluble in analytic form, especially if one attempts to take into account collisions resulting in fragmentation.

In order to treat the problem analytically it has to be split into two parts, one in which the mass distribution of bodies is assumed known and another in which the relative velocity distribution of the bodies is assumed to be known.

The coagulation theory method used in studying the process of coagulation in colloidal chemistry and the process of rain droplet growth was used to construct equations which describe the evolution of the mass distribution function for protoplanetary bodies. A number of investigations of the coagulation equations, some including fragmentations and some not, have been carried out by Safronov and by other workers. The coagulation coefficient in the most ambitious of these investigations is based on the two-body gravitational collision cross section. The relative velocities of bodies were, therefore, assumed to be given by $V = \sqrt{Gm/\theta r}$ as discussed earlier. When allowance is made for the fragmentation of colliding bodies, quantitative treatment is very difficult, if not impossible. Nevertheless, qualitative considerations (Zvyagina, 1973) and numerical solutions of the coagulation equation (Pechernikova, 1974) indicate that the mass distribution of a system of bodies with fragmentations may be approximated by a power function $n(m) =$

cm^{-q} , where the exponent q of this function lies between 1.5 and 2.0 (more likely closer to 2.0) depending on the exact treatment of the fragmentation process.

There are a number of reasons why the coagulation theory method fails to be of any use in the description of the final stage of accretion during which planet-sized objects form. First, a distribution function description is only useful when the number of bodies within a given mass interval is large enough to permit the use of statistics. In the case of the largest individual bodies statistics cannot be applied. Second, as will be demonstrated later in Chapters II and III, the two-body gravitational collision cross section does not adequately describe the gravitational interactions of bodies in relatively low eccentricity orbits. Finally, a simultaneous treatment of the evolution of the mass and relative velocity distributions of the protoplanetary bodies is much more desirable than a divided approach. Numerical experiments including the coupled evolution of the mass and velocity distributions have recently been carried out by Greenberg et al. (1977).

The Numerical Experiments of Greenberg et al.:

R. Greenberg, J.F. Wacker, W.K. Hartmann, and C.R. Chapman (1977) have developed a numerical model for the

evolution of an initial swarm of kilometer-sized planetesimals into a distribution of bodies which includes several planetoids with diameters up to ~ 1000 km. The low- and moderate-velocity collisions between solid bodies were carefully evaluated using results of low-velocity experiments combined with interpolation based on physical principles. The outcomes of collisions were divided into four categories (depending on the ratio of the masses and the relative velocity at impact for the given collision): (i) elastic rebound, (ii) rebound with cratering of the surfaces of both bodies, (iii) shattering of the smaller body and cratering of the larger one, and (iv) shattering of both bodies. Once the range of mass ratios and relative velocities at impact appropriate to each of these collision outcomes is established, a variety of other parameters specifying collision outcomes remain to be determined. For elastic rebound only the coefficient of restitution, given as the ratio of the rebound velocity to the impact velocity, is required. As the collision outcomes become more complicated, estimates are required for the total ejecta mass as a function of the mass ratio, material, and impact kinetic energy of the colliding bodies; the partitioning of the impact kinetic energy between colliding bodies; the cumulative fraction of ejecta with velocity

greater than V ; the mass distribution of ejecta; the dependence of impact strength on body size; the mass distribution of fragments of shattered bodies; as well as the coefficient of restitution.

Despite the unprecedented detail in this model of collision outcomes, caution must be exercised when extrapolating from results obtained for small laboratory samples to bodies having masses twenty or more orders of magnitude greater. The relationship between material defects in bodies with diameters of several kilometers to defects occurring in small laboratory samples is not at all clear. In addition, gravitational binding energy becomes more important than material binding energy for rocky bodies with radii greater than ~ 40 km (cf. Chapter III). The effect of this dominance of gravitational binding energy for bodies with $R \gtrsim 40$ km on the mass distribution of fragments when such bodies are shattered by collisions is not understood.

Collisions are assumed to result from random relative velocities between bodies as measured by their orbital eccentricities and inclinations rather than from differential Keplerian velocities. The probability of collisions is computed by a "particle-in-a-box" estimate using the two-body gravitational collision cross-section which

neglects the presence of the Sun. Besides collisions, which tend to damp the random velocities, Greenberg et al. have taken into account the rotation of random velocities due to gravitational encounters and the gravitational stirring arising from randomization of Keplerian differential velocities. All of these ways of re-distributing the velocities are based on two-body formulae.

Numerical experiments with a variety of initial mass and velocity distributions and material properties were performed by Greenberg et al.. The main conclusions drawn from their simulations are the following: (a) Collisions between bodies of 1 km diameter rapidly produce a substantial number of 500 to 1000 km diameter bodies, while the bulk of the mass remains in the form of 1 km diameter bodies even after the larger planetoids are formed. (b) Random velocities assume values of the order of the escape velocity of the original bodies, and not of the large bodies, as is maintained by Safronov (1969). These conclusions are held to be true for experiments with a variety of material properties and initial velocity distributions so long as the initial velocity is somewhat less than $20 V_e$, where V_e is the escape velocity of the original bodies.

It will be shown later in this chapter that the two-body

gravitational cross-section assuming relative velocities of the order of the escape velocity of the bodies accounting for the bulk of the mass depends on mass as $\sigma \propto m^{4/3}$, rather than as $\sigma \propto m^{2/3}$ as demonstrated by integrations we have carried out for encounters between bodies initially in circular orbits. Given the very low eccentricity orbits, $e \sim 5.0 \times 10^{-4}$, occurring in the simulations of Greenberg et al., a dependence $\sigma \propto m^{2/3}$ is to be expected rather than the $\sigma \propto m^{4/3}$ dependence assumed. It is not then surprising that the evolution of the mass distribution in these simulations indicates a "runaway" growth of the largest bodies while most of the mass of the system remains in the original 1 km diameter bodies. Presumably, simulations with a more refined treatment of the gravitational encounters between bodies which included the effect of the Sun would produce different evolutions of the mass distribution, but we cannot be sure of this conclusion.

What then can be concluded from these scenarios and simulations about the initial conditions to be used in our simulations? In view of the inadequacy of treating gravitational encounters as isolated two-body interactions, it is difficult to know what confidence to assign to the final mass distributions obtained in the preceeding investigations. Safronov's suggestion that isolated zones of

accretion will begin to merge at some stage of the evolution of the protoplanetary disk and that the masses of the protoplanets at that time will be comparable within an order of magnitude has some physical plausibility, but proof of the occurrence of such a spike in the mass distribution for some value of the mass does not now exist.

For the special case of circular motion, W.R. Ward (1975) has estimated that such a spike is to be expected at a value approximately equal to a lunar mass. This value was obtained by assuming that a body sweeps up material having a mass $m = (2\pi r)(2\Delta r)\sigma_0$, where r is the heliocentric distance, Δr is the half-width of the annulus from which material is accreted, and σ_0 is the surface density computed by "spreading-out" the mass of the present terrestrial planets over their portion of the solar system. Further assuming $\Delta r = R_{L1} = r(m/M_\odot)^{1/3}$, where R_{L1} is the distance to the straight-line Lagrangian point, a spike in the mass distribution is found at

$$m = \frac{[2 \times (M_{\text{V}} + M_{\text{E}} + M_{\text{M}} + M_{\text{J}})]^3}{M_\odot}^{1/2} \approx 1.1 M_{\text{L}} \quad (r = 1 \text{ AU}).$$

1-2

It is not clear how this argument could be modified to take into account non-zero eccentricity orbits of accreting bodies.

E. The Late Stages Of Solar System Evolution

The Safronov Description of the Growth of the Largest Bodies:

Realizing the inadequacy of distribution functions for studying the growth of the largest bodies, Safronov (1969, pp. 105-108) takes a different approach in the investigation of the late stages of planetary accretion. This description serves as an example of the assumptions and physics currently employed in studies of the late stages of the dynamical evolution of the solar system and also raises many questions for which it is hoped that the present numerical simulations will provide some answers.

The gravitational collision cross-section along with the expression for the velocity relative to the circular velocity, $v^2 = Gm/\theta r$, are used to argue that the largest body in a given zone will grow more rapidly than the second-largest both absolutely and relatively. It is further argued that the ratio of the mass of the largest body, m , to that of the second largest, m' , increases only to a certain limit, calculated to be $m/m' \sim 200$ to 1000. Safronov then concludes that a characteristic feature of the accumulation process was the formation of planet "embryos" whose masses were far greater than the masses

of the other bodies in their zone. Confirmation of this conclusion is claimed based on estimates of the masses of the largest bodies falling on the planets as determined by the inclinations of the axes of rotation of the planets relative to the ecliptic plane.

The scenario given by Safronov for the growth of the largest bodies is as follows. As the ratio m/m' increased, the orbit of m became more nearly circular as m grew due to randomly oriented impacts and subsequent accretion of much smaller bodies. The supply zone of m was assumed to be an isolated annular region with a width determined by the mean orbital eccentricity, e , of the main mass of bodies. The zone of gravitational influence of m , as measured by the distance to its libration point, $R_{L1} = (m/3M_{\odot})^{1/3} R$, was calculated to be more than one order of magnitude smaller than the supply zone of m as the final accumulation process began. So long as the bodies in the zone of a planetary "embryo" remained small, the relative velocities and eccentricities remained small and the supply zones were narrow. Outside the given zone were others in which the relative velocities were assumed to be determined by the largest bodies inside them via the assumed relation $v^2 = Gm/\theta r$. These embryos, in turn, grew relatively more rapidly than other bodies in their

zones and their orbits also tended to become circular. As the late stages of solar system evolution began, it was expected that there would be many planet "embryos" present. For as long as they occupied different zones, they were not affected by the law that the largest body of all should grow relatively more rapidly.

As the bodies grew, the relative velocities also grew and the supply zones broadened. When adjacent zones began to overlap, relative velocities equalized and the smaller embryos began to grow more slowly. However, the smaller embryos are expected to continue in nearly circular orbits for some time, since the distance between embryo orbits for which the smaller embryo is susceptible to strong perturbations of the larger is only three to five times greater than the distance to R_{L_1} and several times smaller than the width of the supply zone. Collisions between embryos are expected only after m has increased by 1.5 to 2 orders of magnitude. The gradual reduction in the embryo population due to the mass increase of the larger embryos is expected to continue until all the surrounding material has been used up and the distances between embryos have become so large that mutual perturbations are unable to disrupt the stability of their orbits over large time spans. This is expected to be the primary

process determining the law of planetary distances.

This scenario for the late stages of planetary accretion is, for the most part, a speculative description of what might be expected to occur. It is not clear whether the assumption that the gravitating system of bodies can be treated as a set of isolated zones within each of which the relative velocity distribution of smaller bodies is controlled by the largest body through the expression $v^2 = Gm/\theta r$ can be justified. In any case, the assumed expression for the relative velocities cannot be expected to be of any use in the case of overlapping zones. Also, as was stated earlier, the two-body gravitational model is not an adequate description of the gravitational encounters between the largest bodies ($m \lesssim M_{\oplus}$) when the presence of the sun is taken into account.

Encounter Physics: A Comparison of the Two-Body Model with Integrations Including the Presence of the Sun for Bodies Initially in Circular Orbits:

In order better to understand the gravitational interactions between bodies when their orbital motion about the Sun is taken into account, encounters between bodies initially in co-planar, circular orbits were studied first. These encounters are much more tractable than more general ones, since it is possible to specify these encounters with

only three parameters: the masses of the two bodies and the spacing of their circular orbits. Integrations of the regularized equations of motion, Bettis and Szebehely (1971), were carried out for a range of orbital spacings for the following four sets of values of the two masses: (i) $m_1 = 10^{-5} M_{\oplus}$, $m_2 = 10^{-2} M_{\oplus}$ (Figure 1); (ii) $m_1 = m_2 = 10^{-2} M_{\oplus}$ (Figure 2); (iii) $m_1 = 10^{-3} M_{\oplus}$, $m_2 = M_{\oplus}$ (Figure 3); and (iv) $m_1 = m_2 = M_{\oplus}$ (Figure 4). The separation between bodies at which the encounter integrations were initiated and terminated was taken to be five hundred times the "sphere of influence" radius of the larger body for cases (i) and (ii). This radius is given by $R_s = R_2 [(m_2(m_1 + m_2))/M_{\odot}^2]^{1/5}$ (Battin, 1964), where R_2 denotes the distance from M_{\odot} to m_2 and where m_2 is taken to be the larger mass when m_1 and m_2 are unequal. When the separation value $500 R_s$ resulted in orbital angular separations greater than $\pi/2$, as occurred for $m_2 = M_{\oplus}$, an initial separation corresponding to an orbital angular separation of $\pi/2$ was used. The radius of the orbit of m_2 was in each case taken equal to 1 AU. Only those encounters with m_1 initially outside the orbit of m_2 were integrated, since the encounters with m_1 inside the orbit of m_2 were expected to be approximately symmetric with those outside. These integrations reveal many interesting differences from the behavior predicted

on the basis of the two-body model of gravitational encounters where the presence of the Sun is not taken into account.

Before these differences are described, an expression will be derived for the two-body gravitational cross-section to be employed for the comparison with integrations. The limiting case of grazing impacts defines the edges of the range of the impact parameter, D , for which collisions result. For two bodies having masses of m_1 and m_2 and radii R_1 and R_2 , respectively, the conservation of energy requires

$$\frac{1}{2} \frac{m_1 m_2}{m_1 + m_2} V_o^2 = \frac{1}{2} \frac{m_1 m_2}{m_1 + m_2} V_i^2 - \frac{G m_1 m_2}{R_1 + R_2}, \quad 1-3$$

where V_o is the relative velocity of the bodies at infinite separation and V_i is their relative velocity at the instant of impact. For a grazing impact the conservation of angular momentum requires

$$m_2 V_i (R_1 + R_2) = m_2 V_o D. \quad 1-4$$

Combining the two conservation laws the expression

$$D^2 = (R_1 + R_2)^2 \left[1 + 2G \frac{m_1 + m_2}{R_1 + R_2} \frac{1}{V_o^2} \right] \quad 1-5$$

is obtained for the impact parameter just resulting in grazing collisions. If m_1 and m_2 are assumed to be in

circular orbits about the Sun with radii R_0 and $R_0 + D$, then the relative velocity at infinite separation may be taken to be the Keplerian differential velocity

$$v_0 = \sqrt{GM_\odot} \left[\left(\frac{1}{R_0} \right)^{1/2} - \left(\frac{1}{R_0 + D} \right)^{1/2} \right] \approx \sqrt{\frac{GM_\odot}{R_0}} \left(\frac{D}{2R_0} \right) \quad 1-6$$

($D \ll R_0$).

The collision regions with their widths and impact velocities (given as a fraction of the circular orbital velocity at 1 AU) are obtained by means of the two-body gravitational cross-section with Keplerian differential velocity and tabulated in the upper part of Table 1 for the four sets of values of m_1 and m_2 presented in Figures 1 to 4. The bodies were assumed to be of constant lunar density ($\rho_0 = 3.34 \text{ g/cm}^3$) and R_0 was taken as 1 AU. Also shown in Table 1 are the collision regions, their widths, and impact velocities as obtained by integration of the regularized equations of motion.

After these integrations were performed it was discovered that Dole (1962) and Giuli (1968) in attempting to account for the rotation of the Earth by the gravitational accretion of small bodies had carried out similar integrations, where those encounters with the orbit of m_1 initially inside that of m_2 were also included. In their investigations the body m_1 was assumed to be mass-

Table 1

Two-Body Gravitational Cross-Sections
With Keplerian Differential Velocities

	a(A.U.)		$\Delta a(10^{-5} \text{ A.U.})$	v_i/v_{cir}
	inner boundary	outer boundary		
$m_1=10^{-5}M_{\oplus}, m_2=10^{-2}M_{\oplus}$	0.99809	1.00191	382	0.152
$m_1=m_2=10^{-2}M_{\oplus}$	0.99737	1.00263	526	0.160
$m_1=10^{-3}M_{\oplus}, m_2=M_{\oplus}$	0.99115	1.00885	1770	0.707
$m_1=m_2=M_{\oplus}$	0.98778	1.01222	2444	0.741

Gravitational Cross-Sections Obtained by Integration

	Band	a(A.U.)		$\Delta a(10^{-5} \text{ A.U.})$	v_i/v_{cir}
		inner boundary	outer boundary		
$m_1=10^{-5}M_{\oplus}, m_2=10^{-2}M_{\oplus}$	1_0	1.00446	1.00457	11	0.071
	2_0	1.00512	1.00520	8	0.071
		$\sigma = 2[\Delta a(1_0) + \Delta a(2_0)] = 38$			
$m_1=m_2=10^{-2}M_{\oplus}$	1_0	1.00551	1.00578	27	0.074
	2_0	1.00643	1.00655	12	0.074
		$\sigma = 2[\Delta a(1_0) + \Delta a(2_0)] = 78$			
$m_1=10^{-3}M_{\oplus}, m_2=M_{\oplus}$	1_0	1.02040	1.02110	70	0.329
	2_0	1.02369	1.02407	38	0.329
		$\sigma = 2[\Delta a(1_0) + \Delta a(2_0)] = 216$			
$m_1=m_2=M_{\oplus}$	1_0	1.02560	1.02670	110	0.347
	2_0	1.02985	1.03042	57	0.347
		$\sigma = 2[\Delta a(1_0) + \Delta a(2_0)] = 334$			

less and, therefore, the mathematical structure of the restricted three-body problem was used. For this case Dole found seven distinct inner bands of heliocentric orbits which yielded impacting trajectories in addition to the two outer bands found in the present integrations. Of the seven inner bands found by Dole, two consist of directly approaching trajectories which impact m_2 without looping, and the remaining five consist of trajectories which make one or more loops before impacting m_2 . The two major bands together account for approximately 85% of all the inner impacting trajectories. As we had expected, the two directly approaching inner bands are closely symmetrical with the two outer bands at least for the case when m_1 is assumed to be massless.

The integrations of Giuli can most readily be compared to our own integrations in the case where $m_1 = 10^{-3} M_{\oplus}$ and $m_2 = M_{\oplus}$. Very good agreement is found for the location and width of the two outer bands when the 10% increase in $R_1 + R_2$ due to the radius $R_1 = 10^{-1} M_{\oplus}$ (compared to $R_1 = 0$ for Giuli's integrations) is taken into account along with the sensitivity, exhibited in both our integrations and Giuli's, of the results to the choice of the initial and final separations for the integrations. In computing the total gravitational cross-sections obtained by integration,

$2[\Delta a(1_{\odot}) + \Delta a(2_{\odot})]$, in Table 1, we have made use of the symmetry of inner and outer directly approaching bands found by Dole and Giuli. The major differences between the behavior exhibited for encounters between two small ($m \lesssim M_{\oplus}$) bodies orbiting the Sun when the two-body model, which neglects the presence of the Sun, is used and the behavior observed when these encounters are integrated will be summarized next.

First, the two-body model predicts collisions of m_1 and m_2 for those orbits of m_1 having heliocentric distances in a relatively broad range centered on and symmetric about the orbital radius of m_2 . The extent of that range is given for four sets of values of m_1 and m_2 in the first part of Table 1. Integrations of the regularized equations of motion of m_1 and m_2 about M , on the other hand, demonstrate that collisions of m_1 and m_2 occur instead for orbits of m_1 having orbital radii falling in nine distinct bands of heliocentric distance. As stated earlier, Giuli and Dole have shown that five of these bands consist of trajectories which make one or more loops before collision and that these five bands contribute only 7 to 8% of all impacting trajectories. The remaining four major bands are approximately symmetric about the orbit of m_2 . The two inner bands are observed much closer and

the two outer bands much further from the sun than the range of trajectories predicted on the basis of the two-body model to result in collisions. Consequently, it is expected that m_2 will experience collisions with bodies in orbits further from its own than is predicted by the two-body model. Second, the total collision cross-section, taken as the sum of the four major band widths, obtained from the integrations is approximately one order of magnitude smaller for each of the four sets of values of m_1 and m_2 than is predicted by the two-body model. Third, the relative velocity upon collision determined from the integrations was approximately half of the value expected on the basis of the two-body model. This result clearly has profound significance for accretion models of the formation of planets. Finally, the dependence of the gravitational collision cross-section on the mass m_2 is found from both the integration ratios $\sigma(m_1 = m_2 = M_\oplus) / \sigma(m_1 = m_2 = 10^{-2} M_\oplus)$ and $\sigma(m_1 = 10^{-3} M_\oplus, m_2 = M_\oplus) / \sigma(m_1 = 10^{-5} M_\oplus, m_2 = 10^{-2} M_\oplus)$ to be given approximately by $\sigma \propto m_2^{1/3}$. These same ratios computed for the two-body model with Keplerian differential velocities show the same approximate dependence of σ on m_2 , namely $\sigma \propto m_2^{1/3}$. When encounters between bodies in circular but inclined orbits are considered, the mass dependence of the cross-section is expected to be given by $\sigma \propto m_2^{2/3}$.

This dependence of σ on mass is in sharp contrast to the dependence obtained by Safronov (1969, pp. 105-108) in considering the growth features of the largest bodies in a given isolated zone. The gravitational two-body collision cross-section was used to obtain this dependence assuming the mean velocity of the smaller incident bodies relative to the circular velocity of the larger body to be given by $V = \sqrt{Gm/\theta r}$, where m and r are the mass and radius, respectively, of the largest body in the isolated zone and θ is a parameter computed to be in the range 3 to 5. The dependence of σ on mass obtained by Safronov in this way is given by $\sigma \propto m^{4/3}$. This is to be compared with the dependence $\sigma \propto m^{2/3}$ inferred for the three-dimensional case from the integrations of encounters between bodies initially in circular orbits. The significance of this difference is that for $\sigma \propto m^{4/3}$ the mass of the largest body increases by accretion faster than the masses of the smaller bodies in a given zone, thus running away to large mass. For $\sigma \propto m^{2/3}$ the bodies in a given zone will tend towards similar mass values, since the smaller bodies will increase their mass faster than the largest ones.

The importance of the difference in the present investigation is in the choice of the initial mass

distribution of bodies to be used in the numerical simulations. The choice of equal mass bodies for this initial distribution appears to be defensible in either case, since if $\sigma \propto m^{4/3}$ the largest bodies in each isolated zone are expected to have similar masses once most of the material in each zone has been swept up by the largest body in a zone. For the case $\sigma \propto m^{2/3}$ the bodies are expected to attain similar masses at an earlier stage of evolution. Since only one or two hundred bodies can presently be accommodated by the numerical simulation programs, the choice of equal mass bodies for the initial distribution also seems to be the most convenient.

F. The Numerical Simulations

The numerical simulations carried out here have a number of advantages over treatments such as those described in some detail earlier in this chapter. First, the mass and relative velocity distributions of the proto-planetary bodies are free to evolve simultaneously. Once the initial conditions are chosen and the algorithm for handling encounters is established, the distributions of the orbital elements of the bodies evolve in response to the gravitational close encounters and occasional collisions occurring between bodies. Events involving larger

bodies and moderate mass ratios are included and are treated in the same way as events between pairs of bodies with large mass ratios. Collisions between bodies arise in a natural way in these simulations and assumed expressions for the relative velocity distribution and the gravitational collision cross-section are not needed. This is a fortunate feature, since as we saw earlier, integrations of close encounters between small bodies initially in circular orbits show characteristics that are not at all explicable by two-body gravitational models. Integrations of close encounters between bodies initially in small eccentricity orbits, $e \lesssim 0.02$ say, also indicate more complicated behavior than can be accounted for by two-body models. Finally, no reliance on isolated zones or other such artificial constructions is necessary. Next, a brief outline for the remainder of this thesis will be given.

It is the primary purpose of this dissertation to determine whether terrestrial-like planetary systems can be produced as a result of the gravitationally-induced collisions and accretions occurring in a swarm of approximately lunar-mass protoplanets, at least when the bodies form a co-planar system. A new model for close gravitational encounters is described in Chapter II and

plausibility arguments are given for it. In the same chapter, predictions of the model are compared with the results of integrations of the regularized equations of motion and a brief discussion of the treatment of the slow encounters is also given. In the next chapter (III) a scenario is developed for collisions between proto-planets. Chapter IV describes the numerical simulations and in Chapter V the results of several computer simulations are presented. A discussion of conclusions drawn from the simulations about the terrestrial planet formation process and a short consideration of possible future investigations are also given in this final chapter.

.

CHAPTER II. A NEW MODEL FOR CLOSE GRAVITATIONAL ENCOUNTERS

A. Introduction

A model is described for single close encounters between two small masses, m_1 and m_2 , orbiting a large mass, M ($m_1, m_2 \ll M$). The special case where m_1 and m_2 are comparable will receive particular consideration, but the model will be shown to be equally valid when m_1 and m_2 are not comparable. A close encounter is taken to be an approach of m_1 and m_2 for which their minimum separation, as they move along unperturbed orbits about M , is less than the "sphere of influence" radius of the larger of the small bodies. This radius is given by $R_s \approx R_1 [(m_1(m_1 + m_2)/M^2)]^{1/5}$ (Battin, 1964), where m_1 is now taken to be the larger mass when m_1 and m_2 are unequal. The radius R_1 denotes the distance from M to m_1 .

The radius R_s serves in this model to divide the motion of m_1 and m_2 about M into two parts:

- (i) the unperturbed two-body motion of m_1 and m_2 about M when the separation of m_1 and m_2 is greater than R_s , and
- (ii) the unperturbed two-body motion of m_2 about m_1 when the separation of m_1 and m_2 is less than R_s .

The motion of m_1 and m_2 inside the radius R_s is further analyzed into two parts. It is assumed in this approxima-

tion that the center of mass of m_1 and m_2 describes an orbit in the gravitational field of M and that m_1 and m_2 have residual motions with respect to their center of mass. The reference frame to which these residual motions are referred is clearly an accelerated one in contrast to the usual inertial frame employed by Chandrasekhar (1941) and Williamson and Chandrasekhar (1941) in their classic treatment of stellar encounters. Indeed, the assumption of conic motion of the m_1, m_2 center of mass accounts for much of the improvement of the present model over that of Williamson and Chandrasekhar in which straight-line motion of the m_1, m_2 center of mass is assumed. The variation of the gravitational field of M over the region occupied by m_1 and m_2 will give rise to a tidal field. However, we will require that R_s be sufficiently small, by requiring $m_1, m_2 \ll M$, to assure only negligible influence of the tidal field, at least for all encounters completed within a time sufficiently small relative to the time required for the motion of the m_1, m_2 center of mass about M .

The special case of encounters between two bodies of comparable mass orbiting a much larger mass has been considered recently only by Horedt (1972) and Steins and Zalkalne (1970). Horedt considers only the special

case where m_1 initially moves in a circular orbit around the large mass, M , and m_2 moves in an unperturbed hyperbolic orbit around M . The primary interest in these studies seems to be in encounters of comets with satellites or asteroids and indeed Horedt's model seems applicable only to very rapid encounters of this type, since no allowance is made for changes in the velocities of m_1 and m_2 arising from their motion about M during the encounter. On the other hand, our model will be shown to be an adequate approximation for many purposes in the more general case where the two small bodies move in initially unperturbed elliptic orbits about M , provided the eccentricity of the hyperbolic motion of m_2 about m_1 satisfies the condition $\epsilon \geq 4$.

Kaula (1975) has stated that the evolution of a system of planet embryos accreting much smaller planetesimals may be "significantly affected by the small fraction of events involving larger bodies and moderate mass ratios." The present model is uniquely suitable for the numerical simulation of such a system.

B. A Description of the Model

The essential features of the model are as follows. When m_1 and m_2 reach a separation $\Delta r = R_s$, the position and velocity of the center of mass of m_1, m_2 are used to

determine a conic section orbit about M . This orbit is always an ellipse in this study, but is not required to be by the model. The center of mass is assumed to move along this ellipse for the duration of the encounter. Meanwhile, m_1 and m_2 execute two-body motion, always along hyperbolic orbits here, with respect to their center of mass for as long as their separation is less than R_s . The frame of reference chosen for the motion of m_1 and m_2 about their center of mass has its origin at their center of mass and its axes parallel to the axes of an initially specified inertial frame. This frame is then accelerated in accordance with motion along a conic but does not rotate. The duration of the encounter and the extent of the simultaneous motion of the center of mass are determined by the time required for m_1 and m_2 to execute their hyperbolic motion about their center of mass from a separation $\Delta r = R_s$ to closest approach and back again to $\Delta r = R_s$. The algorithm for treating close encounters using the model will be described in more detail in the last part of this section, but we will next argue for the plausibility of the above features of the model.

C. Plausibility Arguments for the Model

First, we examine the assumption that the motion of the m_1, m_2 center of mass relative to M is along a conic section with focus at M for separations of m_1 and m_2 less than the sphere of influence radius. The equations of motion of m_1 and m_2 with M as origin are given by

$$\ddot{\vec{R}}_1 + G(m_1 + M) \frac{\vec{R}_1}{R_1^3} = Gm_2 \left(\frac{\vec{R}_2 - \vec{R}_1}{R_{12}^3} - \frac{\vec{R}_2}{R_2^3} \right) \quad 2-1$$

$$\ddot{\vec{R}}_2 + G(m_2 + M) \frac{\vec{R}_2}{R_2^3} = Gm_1 \left(\frac{\vec{R}_1 - \vec{R}_2}{R_{12}^3} - \frac{\vec{R}_1}{R_1^3} \right), \quad 2-2$$

where \vec{R}_1 and \vec{R}_2 are the position vectors of m_1 and m_2 with respect to M , $R_{12} = |\vec{R}_2 - \vec{R}_1|$, and G is the gravitational constant. The exact equation of motion of the center of mass of m_1, m_2 relative to M is then

$$m_1 \ddot{\vec{R}}_1 + m_2 \ddot{\vec{R}}_2 = (m_1 + m_2) \ddot{\vec{R}}_0 = -G(M + m_1 + m_2) \left(\frac{m_1 \vec{R}_1}{R_1^3} + \frac{m_2 \vec{R}_2}{R_2^3} \right), \quad 2-3$$

where \vec{R}_0 is the position vector of the m_1, m_2 center of mass.

Denoting the position vectors of m_1 and m_2 with respect to their center of mass by \vec{r}_1 and \vec{r}_2 , we may express R_1^{-3} and R_2^{-3} in Eq. 2-3 as

$$R_i^{-3} = (R_0^2 + 2\vec{R}_0 \cdot \vec{r}_i + r_i^2)^{-3/2} = R_0^{-3} \left(1 + \frac{2\vec{R}_0 \cdot \vec{r}_i}{R_0^2} + \frac{r_i^2}{R_0^2} \right)^{-3/2}$$

$$i = 1, 2$$

2-4

Taking into account the assumption that $m_1, m_2 \ll M$ in $r_1, r_2 \leq R_s \sim R_0 [(m_1(m_1 + m_2))/M^2]^{1/5}$ yields the result $r_1, r_2 \ll R_0$. Expanding R_i^{-3} and keeping terms to second order in r_i/R_0 , we find

$$R_i^{-3} \sim R_0^{-3} \left[1 - \frac{3\vec{R}_0 \cdot \vec{r}_i}{R_0^2} - \frac{3}{2} \frac{r_i^2}{R_0^2} + \frac{15}{2} \frac{(\vec{R}_0 \cdot \vec{r}_i)^2}{R_0^4} \right]. \quad 2-5$$

Substituting this result into Eq. 2-3 and dropping terms of order higher than the second in r_i/R_0 we obtain the following approximate equation of motion of the m_1, m_2 center of mass,

$$\begin{aligned} \ddot{\vec{R}}_0 \sim & - \frac{G(M + m_1 + m_2)}{R_0^2} \{ \hat{\vec{R}}_0 - \left(\frac{r}{R_0} \right)^2 \frac{m_1 m_2}{(m_1 + m_2)^2} \times \\ & [3(\hat{\vec{R}}_0 \cdot \hat{\vec{r}}) \hat{\vec{r}} + \frac{3}{2} (1 - 5(\hat{\vec{R}}_0 \cdot \hat{\vec{r}})^2) \hat{\vec{R}}_0] \}, \end{aligned} \quad 2-6$$

where $\vec{r} = \vec{r}_2 - \vec{r}_1$. The ratio of the non-central force term to the central force term in Eq. 2-6 can be seen to be of order

$$\left(\frac{r}{R_0} \right)^2 \leq \left(\frac{R_s}{R_0} \right)^2 \sim \left(\frac{m_1}{M} \right)^{4/5},$$

so the assumption of conic motion of the m_1, m_2 center of mass is a very good approximation. Next, we consider the justification for assuming conic motion of m_1 and m_2 about their center of mass.

The exact equation of motion of m_2 relative to m_1 is obtained by subtracting Eq. 2-1 from Eq. 2-2,

$$\ddot{\vec{R}}_2 - \ddot{\vec{R}}_1 = \ddot{\vec{r}} = -G(m_1 + m_2) \frac{\vec{r}}{r^3} + GM \left(\frac{\vec{R}_1}{R_1^3} - \frac{\vec{R}_2}{R_2^3} \right). \quad 2-7$$

From this equation of motion we obtain the equations of motion of m_1 and m_2 relative to their center of mass

$$\ddot{\vec{r}}_i + G \frac{m_j}{(m_i + m_j)^2} \frac{\vec{r}_i}{r_i^3} = \frac{GM m_j}{m_i + m_j} \left(\frac{\vec{R}_j}{R_j^3} - \frac{\vec{R}_i}{R_i^3} \right). \quad 2-8$$

$$i = 1, 2 \quad i \neq j$$

Again, making use of the condition $r_1, r_2 \leq R_s \ll R_0$ in expanding R_i^{-3} , but this time keeping terms only to first order in r_i/R_0 we have

$$R_i^{-3} \approx R_0^{-3} \left(1 - \frac{3\vec{R}_0 \cdot \vec{r}_i}{R_0^2} \right). \quad 2-9$$

Substituting this expression for R_i^{-3} into Eq. 2-8 and dropping terms on the right-hand side of higher order than

the first in r_i/R_0 gives the following approximate equations of motion of m_1 and m_2 relative to their center of mass

$$\ddot{\vec{r}}_i \sim - \frac{Gm_j^3}{(m_i + m_j)^2} \frac{1}{r_i^2} \left\{ \hat{r}_i + \frac{M}{m_i + m_j} \left(\frac{r}{R_0} \right)^3 [3(\hat{R}_0 \cdot \hat{r}_i) \hat{R}_0 - \hat{r}_i] \right\}.$$

$$i = 1, 2 \quad i \neq j \quad 2-10$$

The ratio of the non-central force term to the central force term in Eq. 2-10 is of order

$$\frac{M}{m_i} \left(\frac{r}{R_0} \right)^3 \leq \frac{M}{m_i} \left(\frac{R_s}{R_0} \right)^3 \sim \left(\frac{m_1}{M} \right)^{1/5},$$

so the assumption of conic motion of m_1 and m_2 relative to their center of mass is a valid assumption for m_1 , $m_2 \lesssim 10^{-5} M$. It is not as good an assumption, however, as that of conic motion of the m_1, m_2 center of mass.

Finally, a brief explanation of the origin of the expression for the sphere of influence radius, R_s , is given. The equation of motion of m_2 relative to m_1 is from Eq. 2-7

$$\ddot{\vec{r}} + G(m_1 + m_2) \frac{\vec{r}}{r^3} = GM \left(\frac{\vec{R}_1}{R_1^3} - \frac{\vec{R}_2}{R_2^3} \right). \quad 2-11$$

The right-hand side of this equation is, of course, the

disturbing force due to M. Recall from Eq. 2-2 that the motion of m_2 relative to M is given by

$$\ddot{\vec{R}}_2 + G(m_2 + M) \frac{\vec{R}_2}{R_2^3} = -Gm_1 \left(\frac{\vec{r}}{r^3} + \frac{\vec{R}_1}{R_1^3} \right), \quad 2-12$$

where the right-hand side is the disturbing force due to m_1 . According to Laplace, the advantage of either equation of motion depends on the ratio of the disturbing force to the corresponding central attraction. The preferred equation of motion is the one providing the smaller ratio. It can be demonstrated (Battin, 1964) that the surface boundary over which these two ratios are equal is almost spherical with radius

$$R_s \approx R_0 \left[\frac{m_1(m_1 + m_2)}{M^2} \right]^{1/5}$$

if $r \ll R_0$, where m_1 is taken to be the larger mass.

While these arguments lend plausibility to the present model, comparisons for a large variety of close encounters of predictions of the model with results of numerical integration of the equations of motion are desirable. These comparisons will be presented in Section E, but first the algorithm for applying the model must be described in a little more detail. The following description of the algorithm will also serve to define the

parameter space to be used in the comparisons.

D. The Algorithm for Applying the Model

When m_1 and m_2 reach a separation equal to the sphere of influence radius of m_1 , it is assumed that their positions and velocities with respect to a reference frame (X,Y) with origin at M are known. At this instant the positions and velocities of the center of mass of m_1 and m_2 and of m_1 and m_2 relative to their center of mass are computed. Next, the eccentricity vector, \vec{e}_1 , of the orbit of m_1 with respect to the m_1, m_2 center of mass is calculated in the standard way from the initial position and velocity of m_1 with respect to the m_1, m_2 center of mass. The orientation of the hyperbolae along which m_1 and m_2 move with respect to their center of mass is then specified by the direction of \vec{e}_1 which corresponds to an orientation angle, ϕ , in the X,Y coordinate system (Figure 5). Now, define two sets of orthogonal coordinates which have their origins at the m_1, m_2 center of mass. The first, (x,y) , has axes parallel to those of (X,Y) and the second, (\tilde{x},\tilde{y}) , is rotated relative to (x,y) through the angle ϕ , so that its x axis is parallel to \vec{e}_1 . The coordinates and velocities of m_1 and m_2 in the rotated coordinate system (\tilde{x},\tilde{y}) are given by the transformations

$$\begin{pmatrix} \tilde{x}_1 \\ \tilde{y}_1 \end{pmatrix} = \begin{pmatrix} \cos\phi & \sin\phi \\ -\sin\phi & \cos\phi \end{pmatrix} \begin{pmatrix} x_1 \\ y_1 \end{pmatrix} \quad \begin{pmatrix} \dot{\tilde{x}}_1 \\ \dot{\tilde{y}}_1 \end{pmatrix} = \begin{pmatrix} \cos\phi & \sin\phi \\ -\sin\phi & \cos\phi \end{pmatrix} \begin{pmatrix} \dot{x}_1 \\ \dot{y}_1 \end{pmatrix}$$

2-13

$$\begin{pmatrix} \tilde{x}_2 \\ \tilde{y}_2 \end{pmatrix} = -\frac{m_1}{m_2} \begin{pmatrix} \tilde{x}_1 \\ \tilde{y}_1 \end{pmatrix} \quad \begin{pmatrix} \dot{\tilde{x}}_2 \\ \dot{\tilde{y}}_2 \end{pmatrix} = -\frac{m_1}{m_2} \begin{pmatrix} \dot{\tilde{x}}_1 \\ \dot{\tilde{y}}_1 \end{pmatrix}.$$

Making use of the symmetry properties of the hyperbola,

$$\begin{aligned} \tilde{x}_i' &= \tilde{x}_i & \dot{\tilde{x}}_i' &= -\dot{\tilde{x}}_i \\ \tilde{y}_i' &= -\tilde{y}_i & \dot{\tilde{y}}_i' &= \dot{\tilde{y}}_i, \end{aligned} \quad i = 1, 2 \quad 2-14$$

where the primes indicate values at the end of the encounter. Reversing the transformations in (2-13), the final coordinates and velocities in the (x,y) coordinate system become

$$\begin{pmatrix} x_1' \\ y_1' \end{pmatrix} = \begin{pmatrix} \cos\phi & -\sin\phi \\ \sin\phi & \cos\phi \end{pmatrix} \begin{pmatrix} \tilde{x}_1' \\ \tilde{y}_1' \end{pmatrix} \quad \begin{pmatrix} \dot{x}_1' \\ \dot{y}_1' \end{pmatrix} = \begin{pmatrix} \cos\phi & -\sin\phi \\ \sin\phi & \cos\phi \end{pmatrix} \begin{pmatrix} \dot{\tilde{x}}_1' \\ \dot{\tilde{y}}_1' \end{pmatrix}$$

2-15

$$\begin{pmatrix} x_2' \\ y_2' \end{pmatrix} = -\frac{m_1}{m_2} \begin{pmatrix} x_1' \\ y_1' \end{pmatrix} \quad \begin{pmatrix} \dot{x}_2' \\ \dot{y}_2' \end{pmatrix} = -\frac{m_1}{m_2} \begin{pmatrix} \dot{x}_1' \\ \dot{y}_1' \end{pmatrix}.$$

The coordinates and velocities of the m_1, m_2 center of mass after the encounter must be determined next, but

these quantities depend on the duration of the relative encounter. For a partial hyperbolic encounter this duration is given by

$$\Delta t = 2\sqrt{\frac{\bar{a}^3}{G(m_1 + m_2)}} (\epsilon \sinh |H| - |H|) \quad 2-16$$

$$\text{with } H = \cosh^{-1} \left(\frac{\bar{a} + R_s}{\bar{a} \epsilon} \right),$$

where \bar{a} and ϵ are the semi-major axis and eccentricity, respectively, of the orbit of m_2 about m_1 . The final eccentric anomaly, E_0' , of the m_1, m_2 center of mass can now be determined by solving Kepler's equation making use of the duration, Δt , along with the semi-major axis (a_0), eccentricity (e_0), and initial eccentric anomaly (E_0) computed for the m_1, m_2 center of mass. The final coordinates (X_0', Y_0') and velocities (\dot{X}_0', \dot{Y}_0') of the center of mass may then be obtained from a_0, e_0, \dot{E}_0' by standard formulae (e.g., Eqns. 6.4.3 and 6.4.15 of Fitzpatrick, 1970). The final coordinates and velocities of m_1 and m_2 relative to M are then

$$\begin{aligned} x_i' &= x_0' + x_i' & \dot{x}_i' &= \dot{x}_0' + \dot{x}_i' \\ y_i' &= y_0' + y_i' & \dot{y}_i' &= \dot{y}_0' + \dot{y}_i' \end{aligned} \quad i = 1, 2 \quad 2-17$$

If desired, the initial and final coordinates and velocities of m_1 and m_2 relative to M may be expressed instead as orbital elements of two ellipses with foci at M .

E. Tests of the Model Against Numerical Integration

Changes in the eccentricities and semi-major axes of the orbits of m_1 and m_2 about M are calculated for many close encounters using the model. These changes are then compared to the corresponding changes obtained by numerical integration of the three-body equations of motion. Before presenting these comparisons it is necessary to describe the parameter space to be used in specifying the encounters.

First, there are the values of the masses m_1 and m_2 . The remaining parameters adopted for the present comparisons can be divided into two groups: those describing the motion of m_1 and m_2 with respect to their center of mass ($\alpha, \epsilon, \phi, \pm$) and those describing the motion of the m_1, m_2 center of mass (a_0, e_0, θ_0). From Section D the eccentricity of the hyperbolic orbits along which m_1 and m_2 move with respect to their center of mass is given by ϵ . The parameter α specifies the separation of m_1 and m_2 at their point of closest approach as a fraction of

the sphere of influence radius. The orientation of the hyperbolic orbits, specified by ϕ , is defined to be the angle between the eccentricity vector of the m_1 orbit about the m_1, m_2 center of mass and the X-axis of the X,Y reference frame with origin at M. The sphere of influence radius, R_s , along with α and ϵ determine the duration of the encounter. The sign \pm specifies the direction of motion of m_1 and m_2 along their hyperbolic orbits. Motion of m_1 and m_2 about their center of mass in the same sense of rotation as the motion of their center of mass about M is denoted by +, and motion of m_1 and m_2 about their center of mass in the opposite sense is denoted by -. Finally, the motion of the m_1, m_2 center of mass is specified by the semi-major axis (a_0) and eccentricity (e_0) of its orbit about M along with its mean anomaly (θ_0). The orientation of the m_1, m_2 center of mass orbit relative to the reference frame, X,Y may be arbitrarily chosen. It will be assumed in all of the comparisons to follow that the orbits of m_1 and m_2 about M are co-planar, and that m_1 and m_2 orbit M in the same direction, but these conditions are not required by the model.

When all of the above parameters are specified, the elements of the m_1 and m_2 orbits about M prior to

the encounter are determined. The integrations are started with initial positions and velocities for m_1 and m_2 , derived from the above elements, at a time prior to close approach for which the separation between m_1 and m_2 is approximately $R_0/10$. The integrations then proceed to closest approach of m_1 and m_2 and are terminated when their separation again reaches $R_0/10$. For certain encounters the separation of m_1 and m_2 prior to close approach reaches a local maximum which is less than $R_0/10$. When this occurs, the initial positions and velocities of m_1 and m_2 used to start the integration are chosen at this local maximum provided the separation there is of the order of $R_0/20$ or greater. The numerical integration, therefore, includes virtually all of the effect of the interactions of m_1 and m_2 on their orbital elements, since the above choice of initial separation is typically two orders of magnitude greater than the sphere of influence radius. The integrator used is one developed by Myron Lecar, Rudolf Loesser, and Jerome R. Cherniak (1974) using Taylor series expansions of the positions and velocities in time. The use of this integrator seems appropriate, since it has been shown to be particularly efficient for n-body integrations similar to the present one where n is small.

A complete test of the model for a grid spanning all of the nine parameters described earlier for specifying encounters is clearly not possible. In the remainder of this section results of certain parameter searches are described where all but one or two parameters are held fixed while the remaining ones are allowed to vary. An attempt has been made to select these searches carefully in such a way as to gain insight into the effect of various parameters on the outcome of a close encounter.

First, the dependence on α and ϵ of changes in the eccentricities ($\Delta e_1, \Delta e_2$) and semi-major axes ($\Delta a_1, \Delta a_2$) of the orbits of m_1 and m_2 about M was investigated for two different orientations, $\phi = \pi/10$ (Figure 6) and $\phi = 7\pi/10$ (Figure 7). The m_1, m_2 center of mass motion for the encounters in both these figures was assumed to be along a circular orbit with $a_0 = R_0 = 1$ AU. Also, the sense of motion of m_1 and m_2 about their center of mass was taken to be opposite (-) to the sense of rotation of their center of mass about M . The masses were chosen such that $m_1 = m_2 = m_0$ with the ratio $m_0/M = .01M_\oplus/M_\odot = 3.0 \times 10^{-8}$, where M_\oplus and M_\odot denote the mass of the Earth and of the Sun, respectively. Values of $\Delta e_1, \Delta e_2, \Delta a_1, \Delta a_2$ were obtained by application of the model and by numerical integration for all of the encounters represen-

ted by the grid intersection points in Figures 6 and 7. The values of Δe_1 , Δe_2 , Δa_1 , Δa_2 given by the model were used to produce the contour plots by interpolation.

For a particular value of ε the values of Δe and Δa decrease as the close approach distance, given by α as a fraction of R_s , increases as one would expect. Above a critical value of ε ($\varepsilon \sim 2$), the values of Δe and Δa decrease as ε increases for a given value of α . This decrease in Δa and Δe is due to the increasing relative velocity of m_1 and m_2 at their point of closest approach as ε increases.

A measure of the agreement between the model and the numerical integration is afforded by the values of E_e and E_a , where

$$E_e = \frac{|\Delta e_1 - \Delta e_1'| + |\Delta e_2 - \Delta e_2'|}{|\Delta e_1'| + |\Delta e_2'|} \quad 2-18$$

$$E_a = \frac{|\Delta a_1 - \Delta a_1'| + |\Delta a_2 - \Delta a_2'|}{|\Delta a_1'| + |\Delta a_2'|} \quad 2-19$$

The primed quantities refer to values obtained by integration and the unprimed ones to values obtained from the model. Contours of E_e and E_a are plotted in Figures 5 and 6 for the same grid as was used for the contours of

eccentricity and semi-major axis changes.

All of the contour plots show a dependence on ϕ . For instance, the E_e and E_a contours show that the model is in agreement with the integrations for lower values of ϵ with $\phi = \pi/10$ than when $\phi = 7\pi/10$. In order to better understand the effect of ϕ , a new set of encounters was run with ϕ spaced by intervals of $\pi/20$, with $\epsilon = 4$, and with $\alpha = 0.04, 0.08, 0.16, 0.32, 0.64$. Again, it was assumed that $m_1 = m_2 = m_0$, and that the center of mass motion was along a circular orbit with $a_0 = R_0 = 1$ A.U. This sequence of encounters was run for both senses of motion (\pm) of m_1 and m_2 about their center of mass. For $m_1 = m_2$ it is not necessary to study encounters with $\phi > \pi$, since an interchange of m_1 and m_2 gives results for $\pi \leq \phi \leq 2\pi$ which are identical with those for $0 \leq \phi \leq \pi$. The values of $\Delta e_1'$, $\Delta e_2'$, $\Delta a_1'$, $\Delta a_2'$ obtained by numerical integration for the encounters with $\alpha = 0.16$ and $\epsilon = 4$ are plotted in Figure 8 for both senses of motion. The percentage errors are again given by Eqs. 2-18 and 2-19 and the absolute errors are given by

$$E_e = (|\Delta e_1 - \Delta e_1'| + |\Delta e_2 - \Delta e_2'|)/2 \quad 2-20$$

$$E_a = (|\Delta a_1 - \Delta a_1'| + |\Delta a_2 - \Delta a_2'|)/2. \quad 2-21$$

The near identity of Δe_1 and Δe_2 and of $|\Delta a_1|$ and $|\Delta a_2|$ is due to the symmetry of these encounters with $m_1 = m_2$ and with circular motion of the m_1, m_2 center of mass. The percentage of error E_e exceeds 50% only in the vicinity of $\phi = 0$ and $\phi = \pi/2$ ($\phi = \pi$ is equivalent to $\phi = 0$ for $m_1 = m_2$), and E_a exceeds 50% only in the vicinity of $\phi = 0$. Large percentage errors for Δe and Δa are to be expected for these values of ϕ , since Δa passes through zero near $\phi = 0$ and Δe passes through zero near $\phi = 0$ and $\phi = \pi/2$. At such zero crossings, even relatively small absolute errors give rise to very large percentage errors. The sequence of encounters in Figure 8 then serves to establish a boundary at $\epsilon \sim 4$ such that for encounters with $\epsilon \gtrsim 4$ and $\alpha \lesssim .80$ the model produces values of Δe_1 , Δe_2 , Δa_1 , and Δa_2 with percentage errors less than 50%, generally much less, provided ϕ is not too close to 0 or $\pi/2$. For most purposes it is expected that percentage errors larger than 50% at $\phi = 0$ and $\phi = \pi/2$ will be tolerable, since the absolute errors are quite small for these orientations. So far, only encounters with circular orbits of the m_1, m_2 center of mass have been considered. Now, the effects of variations of the center of mass motion, keeping the remaining parameters fixed, will be described.

The dependence of E_e and E_a on the center of mass parameters (a_0, e_0, θ_0) was determined for several different sets of the remaining fixed parameters $(\alpha, \varepsilon, \phi, \pm)$ for $m_1 = m_2 = m_0$. For most of these sets of fixed parameters, E_e and E_a were quite independent of changes in the center of mass parameters. The largest variations of E_e and E_a were observed for encounters with relatively small values of ε . The boundary case, $\varepsilon = 4$, in Figure 9 then represents the largest dependence of E_e and E_a on e_0 and R_0 among the sets of fixed parameters investigated. Even for this case the dependence of E_e on e_0 is not large considering the marked dependence of Δe_1 and Δe_2 on e_0 . E_a is relatively independent of e_0 , but both E_e and E_a decrease slightly as R_0 increases. Finally, we consider encounters with values of m_1 and m_2 other than $m_1 = m_2 = m_0$.

Only negligible fluctuations in the values of E_e and E_a were found when m_1/m_2 was allowed to assume values within the range $1 \leq m_1/m_2 \leq 32$ subject to $(m_1 + m_2)/2 = m_0$. Next, values of E_e and E_a were determined for the grid of ε, α values used in Figures 5 and 6 for several values of m in the range $m_0/16 \leq m \leq 16 m_0$ where $m = m_1 = m_2$. The orientation of the relative hyperbolae was taken to be $\phi = 9\pi/10$ for these encounters, since, aside from

values of ϕ in the vicinity of the Δe and Δa zero crossings, $\phi = 9\pi/10$ may be considered to be a worst case in the sense of giving the largest values of E_e and E_a (cf. Figure 8). As m decreases the $E_e = 50\%$ and $E_a = 50\%$ boundaries occur at larger values of ϵ . However, this movement of the above boundaries is sufficiently small that a value of ϵ slightly in excess of $\epsilon = 4$ still yields $E_e, E_a \lesssim 50\%$ for $m = m_0/16$. On the other hand, a value of $\epsilon \geq 3$ for $m = 16 m_0$ already assures $E_e, E_a \lesssim 50\%$, at least for encounters with ϕ not in the immediate vicinity of the Δe and Δa zero crossings.

F. Conclusions Drawn from the Numerical Comparisons

The elements of the orbits of m_1 and m_2 about M can theoretically be expressed in terms of the parameters used in Sections D and E to specify close encounters. However, no concise, explicit expression for this transformation is possible, since the determination of the final coordinates and velocities of the m_1, m_2 center of mass requires a solution of Kepler's equation. An estimate of the eccentricities of the orbits of m_1 and m_2 (e_1, e_2) for the case $m_1 = m_2$ and $e_0 = 0$ may, however, be obtained from the approximate relation $e^2 \approx (\epsilon/\alpha)(m/M)^{3/5}$, where $m = m_1 + m_2$, but precise values of e_1 and e_2 can

change by a factor of 2 due to dependence on other parameters, such as ϕ . For $m_1 = m_2 = m_0$ and $\varepsilon = 4$ the values of e_1 and e_2 given by the above relation range from 0.015 at $\alpha = 0.80$ to 0.068 at $\alpha = 0.04$. These values are typical of exact values taking all of the parameters into account, and, therefore, provide an estimate of the lowest values of e_1 and e_2 for which the model works.

In summary, the present model yields changes of the orbital elements of m_1 and m_2 resulting from a close encounter, which are in reasonable agreement with the corresponding changes given by numerical integration, provided the parameters specifying the encounter lie within the region of validity of the model. For the region of parameter space specified by $\varepsilon \gtrsim 4$, $\alpha \lesssim .80$, and $m_1 + m_2 \geq m_0/8$, comparisons of the model with numerical integrations give E_e , $E_a \lesssim 50\%$ except in the vicinity of $\phi = n\pi/2$ ($n = 0, 1, 2, \dots$). These larger values of E_e and E_a near zero-crossings of Δa and Δe do not seem to be a serious concern, since the absolute errors, E_e and E_a , do not increase significantly for these values of ϕ . If greater accuracy is desired, the model errors are bounded by E_e , $E_a \lesssim 10\%$ for $\varepsilon \gtrsim 8$, $\alpha \lesssim .64$, and $m_1 + m_2 \gtrsim 2m_0$.

When straight-line motion of the m_1, m_2 center of mass is assumed (Williamson and Chandrasekhar, 1941), comparisons with integrations indicate that E_e and E_a exceed 100% for all but the fastest encounters, $\epsilon > 128$. Unfortunately, our model is not an analytic one, as is that of Williamson and Chandrasekhar, because of our assumption of conic motion of the m_1, m_2 center of mass. In the context of computer simulations of systems of many small bodies orbiting a much larger body, the present model is nevertheless very simple to use and offers a substantial improvement in handling most close encounters. The model ceases to be a useful approximation only for the very slow encounters between bodies in grazing, nearly circular orbits.

G. Treatment of Encounters Outside the Range of Validity of the Model

Those close encounters having parameters outside the range of validity of the model and those for which a collision is predicted by the model are treated by integration of the equations of motion. The equations of motion of m_1 and m_2 about M , Eqs. 2-1 and 2-2, become singular, however, when $R_{12} = |\vec{R}_2 - \vec{R}_1|$ becomes small during a close approach of m_1 and m_2 . This singularity in the

equations of motion causes a loss of accuracy and a considerable increase in the computer time required for integration. Therefore, the singularity is eliminated by transformations in a process known as regularization before the equations of motion are integrated. A clear, readable account of this process has been given by Bettis and Szebehely (1971).

First, a Jacobian transformation of the coordinates is performed where the vectors \vec{Q} and \vec{R} are defined by $\vec{Q} = (m_1 \vec{R}_1 + m_2 \vec{R}_2) / (m_1 + m_2)$ and $\vec{R} = \vec{R}_1 - \vec{R}_2$. The equations of motion in Jacobian coordinates become

$$\ddot{\vec{R}} = -G(m_1 + m_2) \frac{\vec{R}}{R^3} + \vec{F}; \quad \vec{F} = GM \left(\frac{\vec{r}_2}{r_2^3} - \frac{\vec{r}_1}{r_1^3} \right) \quad 2-22$$

and

$$\ddot{\vec{Q}} = -\frac{G(m_1 + m_2 + M)}{m_1 + m_2} \left(m_1 \frac{\vec{r}_1}{r_1^3} + m_2 \frac{\vec{r}_2}{r_2^3} \right). \quad 2-23$$

The singularity resulting from close approaches of m_1 and m_2 now appears only in the equation for \vec{R} . Next, using Sundman's smoothing transformation, $dt = R d\tau$, for the independent variable in the first equation of motion, one obtains

$$\ddot{\vec{R}} = \frac{R'}{R} \dot{\vec{R}} - \frac{G(m_1 + m_2)}{R} \vec{R} + R^2 \vec{F}, \quad 2-24$$

where the prime denotes differentiation with respect to the new independent variable τ . A singularity remains in the above equation of motion, but its severity has been reduced, i.e. the term R^3 appears in the denominator of Eq. 2-22, while in Eq. 2-24 there is only a factor of R as a divisor.

For motion in two dimensions Levi-Civita introduced a coordinate transformation in addition to a transformation of the independent variable. Levi-Civita's transformation may be written as

$$\vec{R} = \mathcal{L}(\vec{u}) \vec{u} = \begin{pmatrix} u_1 & -u_2 \\ u_2 & u_1 \end{pmatrix} \begin{pmatrix} u_1 \\ u_2 \end{pmatrix} = \begin{pmatrix} u_1^2 - u_2^2 \\ 2u_1 u_2 \end{pmatrix} = \begin{pmatrix} R_1 \\ R_2 \end{pmatrix}, \quad 2-25$$

where u_1 and u_2 are the new dependent variables. Levi-Civita's transformation gives the important relation $R = u_1^2 + u_2^2$ so that the calculation of a square root is not required to determine the relative distance R in \vec{u} -space. Introducing the new dependent variables into the "smoothed" equation of motion for R , Eq. 2-24, one obtains

$$\vec{u}'' + \frac{G(m_1 + m_2) - 2(\vec{u}' \cdot \vec{u}')}{2(\vec{u} \cdot \vec{u})} \vec{u} = \frac{\vec{u} \cdot \vec{u}}{2} \mathcal{L}^T(\vec{u}) \vec{F}. \quad 2-26$$

The coefficient of \vec{u} in the last equation can be shown to be equal to one-half of the negative of the two-body bind-

ing energy per unit mass, ϵ . The transformed "smoothed" equation of motion for \vec{R} can now be written as

$$\vec{u}'' - \frac{\epsilon}{2} \vec{u} = \frac{\vec{u} \cdot \vec{u}}{2} \mathcal{L}^T(\vec{u}) \vec{F}, \quad 2-27$$

where

$$\epsilon = \frac{2(\vec{u}' \cdot \vec{u}') - G(m_1 + m_2)}{\vec{u} \cdot \vec{u}} = \frac{\vec{R} \cdot \vec{R}}{2} - \frac{G(m_1 + m_2)}{R}. \quad 2-28$$

The above expression for ϵ contains a singularity and if used in the above equation of motion would result of course in a singularity in the equation of motion. However, a regular differential equation for the binding energy can be found and is given in \vec{u} -space by

$$\epsilon' = 2(\mathcal{L}(\vec{u}) \vec{u} \cdot \vec{F}). \quad 2-29$$

The system of regular differential equations

$$\begin{aligned} t' &= \vec{u} \cdot \vec{u} \\ \vec{u}'' - \frac{\epsilon}{2} \vec{u} &= \frac{\vec{u} \cdot \vec{u}}{2} \mathcal{L}^T(\vec{u}) \vec{F} \\ \epsilon' &= 2\vec{u}' \cdot \mathcal{L}^T(\vec{u}) \vec{F} \end{aligned} \quad 2-30$$

may then be solved for \vec{u} and for the time, t . \vec{R} may then be obtained from $\vec{R} = \mathcal{L}(\vec{u}) \vec{u}$. A seventh-order Runge-Kutta algorithm with automatic step-size control proposed by Fehlberg (1969) was employed for the numerical integration.

CHAPTER III. THE MODEL FOR COLLISIONS BETWEEN BODIES

A. A Description of the Collision Model

A scenario for events following the collision of two bodies is described and various numerical estimates relevant to the subsequent behavior of the system are given. In particular, the total energy of the two colliding bodies at impact and the total energy of the system at later stages of the scenario are computed in order to demonstrate that the model satisfies the minimum requirement of consistency with total energy conservation. First, however, the various stages of the scenario are outlined.

In a model in which the immediate formation of a solid body is assumed, the primary mechanisms for dissipating the impact kinetic energy are heating of the resultant body and escape of the remaining material. For bodies of equal mass with $m \geq M_c$, the impact kinetic energy, if converted entirely into heat, would be sufficient to melt all of the material in both bodies. The heat capacity and melting temperature of the material in the bodies were taken to be those of ordinary chondrites, 0.166-0.182 cal/g and 1180-1350°C (Alexeyeva, 1958), respectively. Further, for bodies of this size the

comminution energy is far less than the gravitational binding energy. Since heat conduction is quite inefficient over times as short as those elapsing in collisions, it seems much more likely that the two impacting bodies are shattered into smaller fragments. From the computer simulations it is observed that the fraction of collisions with sufficiently high impact kinetic energy to completely disperse the material of both bodies to large distances is quite small provided the orbital eccentricities are not too large (Tables 2-4). We then conclude that although a few high velocity fragments may escape, they carry considerable kinetic energy off with them and most of the fragments, having smaller velocities, will in general form a gravitationally bound cluster of fragments.

The outside radius of such a cluster will necessarily not exceed the distance to the straight-line Lagrangian point corresponding to the total mass of the cluster, since more distant fragments escape the cluster. Since no data are available (or, for that matter, likely to soon become available) on the size distribution of fragments for shattered bodies of this size, where gravitational binding forces dominate over material binding forces, we make the plausible assumption that the mass of a typical fragment is equal to that mass for which

comminution energy equals gravitational binding energy. Since the fragment clusters are relatively small ($\sim 10^{-3}$ AU) and the fragments are on the basis of the above assumption small (a few tens of kilometers in radius) and, therefore, numerous, collisions between fragments will be frequent. These collisions will eventually dissipate the kinetic energy of the cluster as heat, additional comminution energy, etc. If the cluster is not disrupted in the meantime by collisions or close encounters with other clusters or large bodies, it will shrink, primarily by flattening, at least at first, as its kinetic energy is dissipated, eventually forming a solid body of mass approaching that of the cluster.

B. An Estimate of Fragment Size After a Collision

Before the total energy of the system upon formation of the cluster can be computed, we must estimate the mass of the fragment for which material binding energy equals gravitational binding energy. Experiments have been performed by Greenberg and Hartmann (1977), with both finite and semi-infinite targets over a range of velocities (3-300 m/sec), to determine the critical energy per unit volume for catastrophic failure of the target. This parameter, referred to as the "impact strength," was

found to be $I_s \sim 3 \times 10^7$ ergs/cm³ for rocky material. This impact strength has been confirmed for basalt at much higher impact velocities (1-3 km/sec) in experiments by Moore and Gault (1965) and by Fujiwara et al. (1977) and these results indicate that impact strength is independent of velocity. This number most likely represents an upper limit for the material binding energy because of probable flaws in bodies larger than a few kilometers in radius. Since an order of magnitude estimate is sufficient for our purposes, the impact strength cited by Greenberg and Hartmann for small bodies is taken as representative of the material binding strength of the fragments being considered here. Equating this impact strength to the gravitational binding energy per unit mass, the radius of a typical fragment is found to be

$$R_f = \left(\frac{5}{4\pi} \frac{I_s}{\rho_{\text{L}} G} \right)^{1/2} \sim 40 \text{ km.} \quad 3-1$$

The corresponding mass of this fragment is $m_f \sim 1.2 \times 10^{-5} m_{\text{L}}$. The total energy upon formation of a self-gravitating fragment cluster can now be determined on the basis of the above assumption of fragment size.

C. The Requirement of Total Energy Conservation

The gravitational potential energy of the system at the instant of impact is

$$U_i = -\frac{3}{5} \frac{Gm_1^2}{R_1} - \frac{3}{5} \frac{Gm_2^2}{R_2} - \frac{Gm_1 m_2}{R_1 + R_2}, \quad 3-2$$

where the first two terms represent the work done to bring the material comprising the bodies, assumed to be of constant density, into the given spherical distributions, and the third term is the mutual potential energy of the bodies. The incoming kinetic energy at impact is

$$T_i = \frac{1}{2} \mu V_i^2; \quad \mu = \frac{m_1 m_2}{m_1 + m_2} \quad 3-3$$

where V_i is the relative velocity at impact. For simplicity the bodies are for now assumed to be of equal mass and density, $m_1 = m_2 = m$, $R_1 = R_2 = R$. For this case the total energy of the system at the instant of impact is then

$$E_i = \frac{m}{4} V_i^2 - \frac{17}{10} \frac{Gm^2}{R}. \quad 3-4$$

As was stated earlier, collisions with $E_i > 0$ very seldom occur in the simulations.

Next, let m_c denote the mass of the bound cluster and m_e the total escaping mass. Total mass conservation then

requires $m_1 + m_2 = 2m = m_c + m_e$. The total energy of the system, once the cluster has been established and any escaping fragments are far away, may be expressed as

$$E' = U_f + U_c + T_c + T_e + Q. \quad 3-5$$

Here, U_f is the sum of the gravitational binding energies of the cluster fragments, U_c is the gravitational potential energy of the fragment cluster, T_c is the total internal kinetic energy of the fragment cluster, T_e is the kinetic energy carried away by escaping material, and Q is a term including energy dissipated in a variety of ways such as in comminuting or compacting material, in phase transitions, etc., but primarily includes energy dissipated as heat. (Note that the energy required to raise the temperature of the rock by a little more than 1°K is sufficient to crush the rock!).

Since the cluster is a self-gravitating system, it satisfies the virial theorem which states that

$$2\langle T_c \rangle = - \langle U_c \rangle, \quad 3-6$$

where the brackets indicate time averages. Dropping the brackets, the total energy of the cluster may be written as

$$E_c = U_c + T_c = U_c/2, \quad 3-7$$

and the cluster may be said to be bound by an energy $U_c/2$. If for simplicity all fragments in the cluster are assumed to have the same mass, m_f , and their mass is taken to be equal to that mass for which gravitational and binding energies are equal, then U_c is given in this case by

$$U_c = - \sum_{\substack{i,j \\ i \neq j}} G \frac{m_i m_j}{r_{ij}} = -Gm_f^2 \sum_{\substack{i,j \\ i \neq j}} \frac{1}{r_{ij}} = -Gm_f^2 \frac{n(n-1)}{2} \frac{1}{R_c}, \quad 3-8$$

where R_c is the harmonic mean value of the separation, r_{ij} , over all pairs of fragments. Since $n \gg 1$, the total potential energy of the cluster may be expressed as

$$U_c = - \frac{Gm_c^2}{2R_c}. \quad 3-9$$

The quantity R_c is a characteristic scale size for the cluster; as a harmonic mean it clearly refers to the central bulk rather than to the outlying extremities of the cluster. Since the distance from the cluster center to the outlying extremities is limited by the distance to the straight-line Lagrangian points, the core radius may be taken to be a fraction, f , of the distance to the extremities. It may then be written as

$$R_c = f R_L = f R_0 \left(\frac{m_c}{3M_\odot} \right)^{1/3}, \quad 3-10$$

where R_0 is the heliocentric distance of the cluster and M_\odot is the solar mass. The total energy of the cluster is then given by

$$E_c = - \frac{G}{4R_0 f} (3M_\odot)^{1/3} m_c^{5/3}. \quad 3-11$$

The total gravitational binding energy of the cluster fragments is

$$U_f = - \frac{3}{5} G \sum_{i=1}^n \frac{m_i^2}{R_i}. \quad 3-12$$

If the fragments are assumed to have the same mass, m_f , and to have uniform densities equal to the density of the colliding bodies, ρ_c , then

$$U_f = - \frac{3}{5} G n \frac{m_f^2}{R_f} = - \frac{3}{5} G \frac{m_c m_f}{R_f} = - \frac{3}{5} G \left(\frac{4\pi\rho_c}{3} \right)^{1/3} m_f^{2/3} m_c. \quad 3-13$$

In the absence of predictions of the total escaping mass, the distributions of mass and velocity of the escaping fragments, and the energy dissipated as heat for collisions between bodies of mass $m \geq M_c$, we will choose the most conservative assumption and set $T_e = Q = 0$. With either

calculated or assumed values for each term in E' , the total energy of the system upon establishment of the cluster may be written as

$$E' = - \frac{G(3M_{\odot})^{1/3}}{4R_0} \frac{m_c^{5/3}}{f} - \frac{3}{5} G \left(\frac{4\pi\rho}{3} \right) m_f^{2/3} m_c . \quad 3-14$$

We may now ask how much of the initial impact kinetic energy could be absorbed in fragmenting the colliding bodies, assuming the formation of a cluster of fragments of equal mass, m_f ?

D. Implications of Total Energy Conservation

Earlier in this chapter the total energy at the instant of impact was determined to be

$$E_i = T_i + U_i = \frac{m}{4} V_i^2 - \frac{17}{10} \frac{Gm^2}{R} \quad 3-4'$$

for the case of colliding bodies of equal mass and density. The kinetic energy at impact is further taken to be a fraction, λ , of the total potential energy at impact. The total energy of the system at impact may then be expressed as

$$E_i = (1 - \lambda)U_i , \quad 3-15$$

where $\lambda < 1$ for $E_i < 0$. No accretion is to be expected of course for $E_i > 0$. Since the kinetic energy of escaping material was set equal to zero, the escaping mass is also zero and $m_c = 2m$. An expression for $f = R_c/R_L$ in terms of $\lambda = T_i/(-U_i)$ and m_f/m_c may be obtained by equating the total energy of the system at impact and upon formation of the fragment cluster,

$$f = \frac{\frac{(3M_\odot)^{1/3}}{4R_0}}{\left(\frac{4\pi\rho_\odot}{3}\right)^{1/3} \left[\frac{17}{10 \cdot 2^{5/3}} (1 - \lambda) - \frac{3}{5} \left(\frac{m_f}{m_c}\right)^{2/3} \right]} \quad 3-16$$

For the small value of the ratio m_f/m_c being considered here, λ is the primary factor determining the value of f . With $\rho_\odot = 3.34 \text{ gm/cm}^3$ (lunar density), $m_f = 1.2 \times 10^{-5} m_\odot$ (the mass for which impact strength equals gravitational binding energy per unit mass), $m_c = 2m_\odot$, $R_0 = 1 \text{ AU}$, and $\lambda = 0.95$, the above expression gives $f \lesssim 1/20$. Thus, energy conservation permits the formation of a quite compact cluster even in the case of a collision with relatively high impact kinetic energy. When, in addition, the impact kinetic energy dissipated in heating, comminution, and compaction of material is taken into account, we conclude that at least for

$\lambda \leq 0.95$ practically all of the material from the impacting bodies is gravitationally bound in the fragment cluster. Having hypothesized the formation of gravitationally bound clusters of fragments of the shattered colliding bodies as a stage in the process of accretion, it remains to show that these clusters will shrink, by dissipating energy in collisions between fragments, to solid densities in a time less than the characteristic collision time for the protoplanetary bodies.

E. Do the Clusters of Fragments Shrink to Solid Density Before Their Next Collision?

The collision probability per unit time for one fragment is given by

$$\frac{1}{\tau} = \bar{V} N \sigma, \quad 3-17$$

where N is the number of fragments per unit volume, \bar{V} is the mean relative speed of the fragments, and σ is the collision cross-section of the fragments. Suppose that in each collision between fragments an amount of kinetic energy

$$\Delta T = \frac{1}{2} \beta \frac{m_1 m_2}{m_1 + m_2} \bar{V}^2 \quad 3-18$$

is dissipated as heat, comminution energy, etc., where β is the fraction of the relative kinetic energy dissipated. For $m_1 = m_2 = m_f$ this dissipated energy is

$$\Delta T = \beta \frac{m_f}{4} \bar{v}^2 \quad 3-19$$

per collision. In the mean collision time, τ , there will be n collisions in the cluster dissipating an amount of kinetic energy

$$T_\tau = n\beta \frac{m_f}{4} \bar{v}^2, \quad 3-20$$

where n is the number of fragments in the cluster.

The total kinetic energy of the cluster is

$$T_c = \frac{1}{2} m_c \bar{v}^2, \quad 3-21$$

where \bar{v}^2 is the mass average speed of the fragments. To facilitate comparison of T_c and T_τ , a relation between \bar{v} and \bar{v}^2 is needed. Identical fragments have been assumed in this computation, and it is easy to show that in this case $\bar{v}^2 = 2\bar{v}^2$. For present purposes the difference between rms and average values may be neglected, and the relation $\bar{v}^2 = 2\bar{v}^2$ results. The total kinetic energy of the cluster may then be written as

$$T_c = \frac{1}{4} m_c \bar{V}^2. \quad 3-22$$

It comes as no great surprise that the number of collisions per body required to dissipate the kinetic energy of the cluster is

$$n = \frac{T_c}{T_\tau} = \frac{1}{\beta}. \quad 3-23$$

Assuming that τ remains constant as the cluster evolves, the time required for the cluster to dissipate enough kinetic energy to shrink to solid density may be approximated by

$$t_s = \frac{\tau}{\beta}. \quad 3-24$$

The behavior of a cluster of fragments as it dissipates kinetic energy and subsequently shrinks is certainly much more complicated than the simple model described here indicates, but an order of magnitude estimate of settling time will suffice. It remains then to evaluate τ .

Invoking the virial theorem once again and recalling the total potential energy of the cluster

$$2\langle T_c \rangle = \frac{1}{2} m_c \bar{V}^2 = -U_c = \frac{Gm_c^2}{2R_c}, \quad 3-25$$

the mean relative speed of a cluster fragment is determined to be

$$\bar{V} = \sqrt{\frac{Gm_c}{R_c}}. \quad 3-26$$

Given the mean relative speed of the fragments and their mass, the effect of gravitational focusing in encounters between fragments can be readily estimated and is found to be negligible. Therefore, the collision cross-section for the fragments is taken to be their effective geometric cross-section, $\sigma = \pi(2R_f)^2$. With the relations $m_f = \frac{4\pi}{3} \rho_c R_f^3$ and $R_c = f R_0 (m_c/3M_\odot)^{1/3}$, the mean collision time may be written as

$$\tau = C f^{7/2} \left(\frac{m_f}{m_c}\right)^{1/3}, \quad 3-27$$

where the proportionality constant C is given by

$$C = \frac{1}{3\sqrt{G}} \left(\frac{R_0}{3M_\odot}\right)^{7/6} \left(\frac{4\pi\rho_c}{3}\right)^{2/3} = 1210 \text{ years at } R_0=1 \text{ AU}. \quad 3-28$$

The largest mean collision times occur for the least massive fragment clusters and for those clusters with the largest values of $f = R_c/R_L$. The mean collision time between fragments for the least massive clusters in our simulations, $m_c \sim 0.04 M_\oplus$, assuming $f \sim 1/20$ is of the

order of 5 hours. Even for the extreme values of $f = 1/4$ and $\beta = 1/10$, the mean collision time between fragments is expected on the basis of these estimates to be of the order of 50 days with a corresponding settling time for the cluster of the order of 1.5 years. On the other hand, the mean collision time between bodies in the early stages ($t < 1000$ years) of the planar simulations carried out here are of the order of 40 years. Considerably greater mean collision times between bodies are expected for a more realistic non-planar system. A more detailed treatment of the collisions between protoplanets and the subsequent evolution of their collision remnants would of course be highly desirable, but is certainly too ambitious for the present computer simulations.

Collisions between bodies are then treated in the simulations as follows. When a close approach with separation less than the sum of the two radii is found by integration, the two colliding protoplanets are assumed to accrete and form a body with mass equal to the sum of the masses of the two incoming bodies. The orbital elements of the newly formed body are determined from the position and velocity of the center of mass of the two colliding bodies at the instant of impact. The

relative velocity of the bodies upon impact is recorded and used to calculate a value for λ (Eq. 3-15) which in turn is used to decide whether the assumption of accretion was a valid one. Relative impact velocities and corresponding values of λ are tabulated for the collisions in three simulations in Chapter V.

CHAPTER IV. THE COMPUTER SIMULATION PROCEDURE

A. The Basic Assumptions of the Simulations

In the present simulations of the growth of the terrestrial planets by accretion of large protoplanets ($m \sim M_{\oplus}/50$), the protoplanetary bodies are assumed to move along unperturbed co-planar orbits until they pass within a sphere of influence distance, R_s , of another body. If a close approach to another body occurs, new orbital elements are computed for each body. When the parameters of the encounter fall within the region of validity of the model described in Chapter II for close encounters, the new orbital elements are computed using the model. Those encounters having parameters outside the range of validity of the model and those predicted by the model to have separations at closest approach less than the sum of the radii of the two protoplanets are treated by integration of the regularized equations of motion (cf. Section G of Chapter II). The motion of the bodies during these latter encounters is integrated starting at an initial separation of $50 R_s$, and continuing through close approach to a final separation of $50 R_s$, where new orbital elements are computed for each body.

As stated in the previous chapter, two protoplanets are assumed to accrete and form a body with mass equal to the sum of the masses of the two incoming bodies when a close approach with separation less than the sum of the radii of the bodies (assuming lunar density material) occurs during integration. The orbital elements of the newly formed body are of course determined by the position and velocity of the center of mass of the colliding bodies at the instant of impact.

Several considerations influence the choice of $50 R_s$ as the separation distance at which integrations are initiated and terminated. Clearly, the separation must be large enough to include in the integration as much as possible of the effect of the encounter on the orbital elements of the two protoplanets. At the same time the separation should be sufficiently smaller than the typical spacing between protoplanets that the effect of the nearest neighboring protoplanets on the encounter between the two under consideration can generally be neglected. For a system of one hundred protoplanets having a total mass equal to the sum of the masses of the terrestrial planets, with uniform spacing of the protoplanets in the ecliptic plane between the heliocentric distances 0.5 and 1.5 AU, the typical spacing is $\sim 170 R_s$.

The separation $50 R_s$ was chosen as a compromise between the above two requirements. It should be noted that only the effects of those encounters expected on the basis of unperturbed orbits to result in separations less than the sphere of influence are included in this simulation.

B. The Relative Importance of Close Versus Distant Encounters

One can ask what fraction of the changes in the orbital elements of the protoplanets might be expected to result from close encounters, $(\Delta r)_{\min} < R_s$, as opposed to more distant encounters, $(\Delta r)_{\min} > R_s$. A rough estimate of the importance of close encounters in the relaxation of the protoplanetary system will now be given. The argument here is very similar to one made for two-dimensional disk systems of stars by Rybicki (1972).

In estimating the relaxation time due to encounters, we assume that encounters between bodies can be treated as two-body interactions neglecting the presence of the Sun. Including the influence of the Sun on the encounters by means of the model described in Chapter II would make the estimation of relaxation time impractically difficult, where an order of magnitude estimate is sufficient and

much simpler. It is not difficult to show that in the center of mass system the orbits of both bodies are hyperbolae, the asymptotes of which make an angle $\pi - \delta$ with the deflection angle δ given by

$$\sin \frac{\delta}{2} = \left[1 + \frac{D^2 V^4}{G^2 (m_1 + m_2)^2} \right]^{-1/2}, \quad 4-1$$

where V is the relative velocity of the bodies and D is the impact parameter. For $D_0 = G(m_1 + m_2)/V^2$ the deflection angle in the center of mass frame is $\delta = \pi/2$. The relaxation time, τ_R , can then be estimated as the time for a typical body to experience an encounter with $D \leq D_0$. This will be an overestimate of the true relaxation time, since the cumulative effect of long-range encounters has been neglected. The number of encounters with $D \leq D_0$ during τ_R is equal to the surface density of bodies, σ , times the area $(V\tau_R) \cdot (2D_0)$ within which another body must pass to satisfy $D \leq D_0$. Setting this number of encounters with $D \leq D_0$ equal to one, we find

$$\tau_R = \frac{V}{2G(m_1 + m_2)\sigma}. \quad 4-2$$

A more refined estimate including the cumulative effects of long-range encounters, $D > D_0$, will now be given. The relaxation time is defined for this case as the time in which the root mean square velocity change due to encounters is the same order of magnitude as the typical relative velocity between bodies. An expression for the deflection angle δ equivalent to the one given earlier is

$$\tan \frac{\delta}{2} = \frac{G(m_1 + m_2)}{DV^2} . \quad 4-3$$

For long-range encounters the deflection angle is small and may be approximated by

$$\delta \sim \frac{2G(m_1 + m_2)}{DV^2} . \quad 4-4$$

The velocity perturbation for distant encounters is then

$$\Delta V \approx \frac{G(m_1 + m_2)}{DV} . \quad 4-5$$

The condition giving τ_R then becomes

$$V^2 \sim \Sigma (\Delta V)^2 \sim \left(\frac{G(m_1 + m_2)}{V} \right)^2 (V\tau_R) \sigma \int_{D_0}^{\infty} \frac{2dD}{D^2} \quad 4-6$$

with the lower limit of the integral taken to be D_0 , where the formula for ΔV breaks down, and the upper limit taken as ∞ since the integral converges rapidly for large D . The relaxation time for long-range encounters is then

$$\tau_R = \frac{V}{2G(m_1 + m_2)\sigma} , \quad 4-7$$

a result identical to that for encounters with $D \leq D_0$. Therefore, the relaxation is substantially due to encounters with $D \leq D_0$, and the cumulative effect of long-range encounters is of no more than the same order of magnitude.

It remains to establish the relationship between D_0 and the sphere of influence radius, R_s , used to define close encounters in the current simulations. For this the typical relative velocity between bodies is expressed as a fraction of the circular orbital velocity at their mutual heliocentric distance, $V = \lambda V_c$, the relative velocities observed for bodies in the current simulations generally fall within the range $.01 < \lambda < .06$ with $\lambda = .025$ being typical. The ratio D_0/R_s , assuming $m_1 = m_2 = m$, may then be written as

$$\frac{D_0}{R_s} = \frac{\frac{2Gm}{\lambda^2 v_c^2}}{\left(\frac{2m}{M_\odot}\right)^{1/5} R} = \frac{2^{4/5}}{\lambda^2} \left(\frac{m}{M_\odot}\right)^{3/5}, \quad 4-8$$

where R is the heliocentric distance. D_0 is then less than R_s for $\lambda > .0078$, which is almost always the case in our simulations. When it is also noted that the relative velocities are greater for long-range encounters than for those with $D < D_0$ due to differential Keplerian motion of the bodies in the system, it can reasonably be argued that encounters with $(\Delta r)_{\min} < R_s$ make the major contribution to the relaxation of the system. The algorithm used for finding those encounters expected on the basis of unperturbed orbits to give close approaches less than the sphere of influence is now described.

C. The Algorithm Used for Finding Close Encounters

i. The Spatial Part

The algorithm is naturally divided into two separate parts, one spatial and one temporal. For a particular pair of bodies, a close encounter is spatially possible only if the minimum distance between the two orbits is less than the sphere of influence radius, R_s ,

of the larger of the two bodies. The orbit of each body is specified by its semi-major axis, eccentricity, and angle of perihelion; $m_i(a_i, e_i, \omega_i)$ and $m_j(a_j, e_j, \omega_j)$. Two simple tests are immediately available to limit the number of pairs of bodies which must be considered. Clearly, no close encounter is possible if

$$a_i(1 - e_i) - R_s > a_j(1 + e_j) + R_s$$

or if

4-9

$$a_j(1 - e_j) - R_s > a_i(1 + e_i) + R_s.$$

Assuming that the given pair of bodies has survived these tests, it remains to be determined whether there is an intersection between the locus of points within R_s of the orbit of m_i and the locus of points within R_s of the orbit of m_j .

The locus of points within R_s of an ellipse with semi-major axis, a , and eccentricity, e , can be shown to be bounded by two ellipses having the same orientation as the original ellipse; an inner ellipse with $a' = a - R_s$ and $e' = (a/(a - R_s))e$ and an outer ellipse with $a'' = a + R_s$ and $e'' = (a/(a + R_s))e$. The inner and outer ellipses exactly bound the locus of points within R_s of the ellipse (a, e) along its semi-major axes; however, along the semi-

minor axes the outer ellipse "bulges" slightly and the inner ellipse is slightly "flat." Therefore, the inner and outer bounding ellipses include an area slightly greater than the locus of points within R_s of (a, e) . For $R_s \ll a$ the error along the semi-minor axes is $\sim R_s e^2/2$. In the current simulations this error is almost always less than 1% of R_s , usually much less, and in any case no close encounters will be missed because of this error since the bounding ellipses enclose slightly more area than necessary.

Denoting the inner and outer bounding ellipses for the orbit of m_i by i' and i'' , respectively, and similarly denoting those for m_j by j' and j'' , the condition of intersection of the locus of points within R_s of the orbit of m_i with the locus of points within R_s of the orbit of m_j is equivalent to the requirements that i intersect j' or j'' and j intersect i' or i'' . In the most common case of overlap of the bands containing points within R_s of each orbit, i intersects both j' and j'' and j intersects both i' and i'' . Two separate regions where a close encounter might occur then exist. Less frequently a "grazing" intersection of the bands occurs and only one region of overlap exists. In this case there are two distinct possibilities: (i) i intersects j' but not j''

and j intersects i'' but not i' , or (ii) i intersects j'' but not j' and j intersects i' but not i'' . Since the problem of finding intersections between two ellipses lying in the same plane has a simple explicit solution, the tabulation of spatially possible close encounters is relatively straightforward.

The values of the angle θ at which two co-planar, confocal ellipses, (a_1, e_1, ω_1) and (a_2, e_2, ω_2) , intersect can be determined by equating the radii from their common focus

$$r_i = \frac{a_i (1 - e_i^2)}{1 + e_i \cos(\theta - \omega_i)} \quad i = 1, 2. \quad 4-10$$

It can be shown without much difficulty that the values of θ for which $r_1 = r_2$ are specified by the relation

$$\cos(\theta - \tan^{-1} \psi) = \frac{\Gamma - 1}{e_2 \sin \omega} \frac{\psi}{\sqrt{1 + \psi^2}}, \quad 4-11$$

where $\omega = \omega_2 - \omega_1$, $\Gamma = (a_2(1 - e_2^2))/(a_1(1 - e_1^2))$, and $\psi = (\sin \omega)/(\cos \omega - e_1 \Gamma / e_2)$. There are in general two values of θ which are determined to modulo 2π , provided of course

$$\left| \frac{\Gamma - 1}{e_2 \sin \omega} \frac{\psi}{\sqrt{1 + \psi^2}} \right| \leq 1. \quad 4-12$$

This last inequality is then the condition for intersection of the two ellipses. Substituting for ψ and simplifying, the condition for intersection may be more succinctly written as

$$\frac{(\Gamma - 1)^2}{e_2^2 + e_1^2 \Gamma^2 - 2e_1 e_2 \Gamma \cos \omega} \leq 1. \quad 4-13$$

With the above condition for the intersection of two ellipses and with the ellipses found earlier to enclose the locus of points within R_s of an elliptic orbit, one can quickly determine whether close encounters are spatially possible for the given pair of bodies. If close encounters are possible for the pair, the explicit solutions for the intersection angles make possible a tabulation of one or two (depending on whether the intersection of bands containing the locus of points within R_s of each orbit is "grazing" or "general") pairs of angular intervals. The points along each of these arc segments then have the property that their distance from the nearest point in the other arc segment is no greater

than R_s . The temporal part of the algorithm for determining potential close encounters consists of determining that time interval for which the bodies next simultaneously occupy corresponding orbital intervals.

ii. The Temporal Part

First, time intervals corresponding to the pairs of angular intervals are computed using Kepler's equation. The time intervals are referenced to the time since pericenter passage either at the time the last encounter involving the given body ended or at the starting time of the simulation, if no encounters involving this body have yet taken place. For a pair of time intervals let t_i and t_j denote the mid-point times of the intervals, let δ_i and δ_j denote the widths of the intervals, and finally let P_i and P_j be the orbital periods associated with m_i and m_j , respectively. The condition that the bodies next simultaneously occupy these corresponding orbital intervals after n orbits of m_j can be shown to be

$$\Delta < (\delta_1 + \delta_2)/2, \quad 4-14$$

where Δ is the lesser of

$$\Delta_1 = |\text{mod}(nP_j + t_j, P_i) - t_i| \quad 4-15$$

and

$$\Delta_2 = P_1 - \Delta_1. \quad 4-16$$

In the expression for Δ_1 , $\text{mod}(x,y)$ is defined as $x - [x/y]y$, where the brackets indicate that the largest integer whose magnitude does not exceed the magnitude of x/y is used.

The above condition that m_i and m_j simultaneously occupy corresponding orbital intervals for which interaction is spatially possible is a necessary condition for a close encounter of m_i and m_j , but not a sufficient one. The bodies may still pass through their intervals in such a way that their minimum separation is never less than R_s . To establish whether the minimum separation between the bodies is in fact less than R_s during the time they are simultaneously occupying their corresponding intervals, a minimum search routine is employed. The routine used, Brent (1973), combines golden section search and successive parabolic interpolation. In actual simulations it is possible in most cases to determine whether the minimum separation is less than R_s with evaluations of the positions of the bodies and their

corresponding separation at only two distinct times. This is so because it has been observed that for relatively small eccentricities the separation does not change very rapidly during the time interval in which the bodies simultaneously occupy their corresponding orbital intervals. Therefore, if the estimate of minimum separation after two evaluations is greater than $4R_s$, it has been found in practice that no close encounter will occur. This completes the discussion of the algorithm for finding close encounters. A verbal flowchart for the simulations follows.

D. A Flowchart of the Simulations

Step 1. (Initial Conditions) First, starting values are chosen for the masses and orbital elements of the bodies in the system whose evolution is to be simulated. All simulations to be presented here begin with one hundred identical bodies with mass equal to 0.02 Earth masses. The total mass of the system is then very nearly equal to the total mass of the present terrestrial planets. The semi-major axes of the orbits of these bodies are required to fall within the range 0.5 to 1.5 AU, corresponding approximately to the range of semi-major axes of the terrestrial planets. The surface density in all of

these simulations was assumed to have an $R^{-3/2}$ dependence on heliocentric distance between 0.5 and 1.5 AU and to be zero elsewhere. The initial eccentricities of the orbits were randomly chosen from a uniform distribution on the interval from 0 to some maximum eccentricity, e_{\max} . The angles of perihelion for the orbits are given by a sequence of random deviates from a uniform distribution on the interval $(0, 2\pi)$. Finally, the time since perihelion passage for each body is taken from a uniform distribution on the interval $(0, P)$ where P is the orbital period of the given body.

Step 2. An initial simulation time step, Δt , is chosen; usually this is taken to be five years.

Step 3. Once the masses and orbital elements for all of the bodies in the system are specified, it can be determined as described earlier whether a close encounter is spatially possible for each pair of bodies. For those pairs of bodies for which a close encounter is possible, angular intervals lying within R_s of the other orbit are determined for each orbit.

Step 4. For each pair of bodies for which a close encounter is spatially possible, determine the starting and ending times using Kepler's equation of those time intervals during which the bodies simultaneously occupy

the sections of their orbits for which spatial interaction is possible. Naturally, only those time intervals with starting times within the current simulation time step are considered.

Step 5. For each time interval obtained in Step 4, a minimum search routine combining golden section search and successive parabolic interpolation is used to determine whether the minimum separation of the bodies, $(\Delta r)_{\min}$, is in fact less than R_s for any time within the given interval. Those times corresponding to minimum separations less than R_s comprise a set of potential close encounter times.

Step 6. The times associated with $(\Delta r)_{\min} < R_s$ are next sorted into ascending numerical order. The least of these times determines the interval within which the next close encounter will take place along with the pair of bodies, m_i and m_j , which will experience that encounter.

Step 7. Again, using the minimum search routine, the time during the approach of m_i and m_j for which their separation is equal to R_s is obtained. For this time the positions and velocities for each of the bodies are calculated and orbital elements for the relative motion of the bodies are then computed from these positions and

velocities. The eccentricity, ϵ , and semi-major axis, \tilde{a} , of the relative motion determine the method to be used in the next step to compute the new elements of the orbital motion of m_i and m_j about the Sun following the encounter.

Step 8. If $\epsilon > 4$ and $(\Delta r)_{\min} = \tilde{a}(\epsilon - 1) < 0.8 R_s$, the new orbital elements for the motion of m_i and m_j about the Sun are computed using the close encounter model described in Chapter II. If $\epsilon < 4$ or $(\Delta r)_{\min} = \tilde{a}(\epsilon - 1) > 0.8 R_s$, the new orbital elements are found by integrating the regularized equations of motion of m_i and m_j in the presence of the Sun. For $\epsilon \lesssim 4$ encounters between m_i and m_j take place relatively slowly and these encounters are, therefore, integrated starting with an initial separation prior to close approach of $50 R_s$ (cf. Section A for justification of this choice). The integrations proceed to close approach of m_i and m_j and terminate when the separation between m_i and m_j again exceeds $50 R_s$. The positions and velocities of the bodies upon termination of the integration are used to compute new orbital elements for the motion of m_i and m_j about the Sun.

Those encounters predicted by the model to have separations at closest approach less than the sum of the radii calculated for the two protoplanets, assuming

homogeneous composition and lunar density material, are also treated by integration. The initial and final separations between bodies used to initiate and terminate the integrations of these encounters were again chosen to be $50 R_s$. When a close approach with separation less than the sum of the two radii is found by integration, the two protoplanets are assumed to accrete and form a body with mass equal to the sum of the masses of the two incoming bodies. The orbital elements of the newly formed body are determined from the position and velocity of the center of mass of the two colliding bodies at the instant of impact. The relative velocity of the bodies upon impact is recorded and used later to determine whether the assumption of accretion was a valid one (cf. Tables 2 to 4).

Step 9. With the new orbital elements for m_i and m_j (only the elements for m_i are required following a collision), determine whether a close encounter is spatially possible for each pair of bodies with i or j as members. For those pairs for which a close encounter is spatially possible, determine as in Step 3 the angular intervals for each orbit which lie within R_s of the other orbit along with their corresponding time intervals.

Step 10. For each pair of bodies including i or j as members and having at least the spatial possibility of a close encounter, determine the starting and ending times of those intervals during which the bodies simultaneously occupy the sections of their orbits for which spatial interaction is possible. Again, only those time intervals with starting times within the current simulation time step are to be considered.

Step 11. For each time interval computed in the previous step, the minimum search routine is used to determine whether the minimum separation of the bodies is in fact less than R_s for any time within the given interval. Those times corresponding to minimum separations less than R_s form a new set of potential close encounter times.

Step 12. If any of the old set of potential encounter pairs includes i or j , delete them and combine the new and old sets of potential encounter pairs along with the times associated with their minimum separation. If the combined set of potential encounter pairs is empty, all close encounters in the current simulation time step have been treated. In this case a new simulation time step is chosen. If the number of close

encounters occurring in the time step just completed is greater than one, the new simulation time step is taken to be one half of the length of the preceeding one. If no close encounters have occurred in the previous two simulation time steps, the new time step is taken to be twice the length of the preceeding one. Otherwise, the simulation time step remains the same. If the starting time of the new simulation interval exceeds a termination time estimated to be greater than that for which the system ceases to experience further close encounters, the simulation is then ended; otherwise, branch to Step 4 and continue, once the new time step has been chosen.

When the combined set of potential encounter pairs is not empty, sort the times corresponding to minimum separation into ascending numerical order. The least of these times is then the time of the next close encounter and determines the pair of bodies, i' and j' , involved in the next close encounter. Branch to Step 7 and determine the new orbital elements for i' and j' .

This completes the description of the algorithm for the computer simulations. In the next chapter the results of four numerical simulations are discussed.

CHAPTER V. THE COMPUTER SIMULATIONS

A. Results of Four Representative Numerical Simulations1. The Plots

Results are presented in Figures 10 through 24 of four representative numerical simulations of the growth of the terrestrial planets by accretion of large proto-planets. These simulations primarily differ in the values chosen for e_{\max} , cf. Section D of Chapter IV. The time evolutions of the orbital eccentricities for the bodies in each simulation are given in Figures 10, 13, 16, and 19; the corresponding semi-major axis evolutions are presented in Figures 11, 14, 17, and 20. An equal abscissa increment has been assigned to each gravitational interaction in the above figures independent of whether the interaction results in a collision or not. The associated times are given as \log_{10} of the time in years. Collisions and subsequent accretions of bodies are denoted in these figures by small boxes. In Figures 12, 15, 18, and 21 the semi-major axes, eccentricities, and masses of the system bodies are shown for nine different stages of each simulation including the initial and final ones. The boundaries of the initial semi-major axis and eccentricity

distributions are indicated by the rectangles in each frame. The areas of the small boxes marking the location of each body are proportional to the masses of the bodies. Finally, the number of system bodies for each of the nine stages is indicated at the top of the frame. Next, several features apparent in these plots of the simulations will be described.

First, in the eccentricity evolution plots we note a redistribution of eccentricities for all of the simulations: the number of bodies with very small values of eccentricity decreases and a "tail" extending toward higher values of eccentricity develops. Also, a rapid initial increase in eccentricity is apparent for the $e_{\max} = 0.025$ and 0.05 simulations. Where the lines in these figures are not too dense, one can observe the range of typical eccentricity changes occurring during close encounters. Later in the chapter quantitative measures of these eccentricity changes are tabulated and discussed for the early ($N \geq 90$) evolution of each simulation. Also note that in the late stages of evolution of each simulation the smallest bodies are commonly perturbed into orbits having relatively high eccentricity values.

In the plots of semi-major axis evolution one observes that "edge effects" are fairly modest in that bodies are only infrequently scattered out of their initial range of heliocentric distance, 0.5 to 1.5 AU. Further, bodies are more frequently scattered outward beyond 1.5 AU than inward of 0.5 AU. One can also make qualitative estimates from these plots of the range of semi-major axis changes typically occurring during close encounters. A detailed examination of the semi-major axis plots reveals that pairs of bodies in orbits having either nearly identical or very dissimilar values of their semi-major axes rarely collide and accrete, even when the orbits approach each other closely enough for collisions to take place. Most collisions then occur for pairs of bodies with only moderately dissimilar values of their semi-major axes. Many instances exist in the simulations where bodies in orbits having nearly identical values for their semi-major axes repeatedly interact without collision until an event happens to scatter one or the other of the bodies into an orbit with a moderately dissimilar semi-major axis value. Usually, a collision soon follows. I would also like to draw attention to the many instances of repeated close encounters between the

same pairs of bodies; for example, the pair of bodies in the $e_{\max} = 0.025$ simulation with a ~ 0.52 AU during the period $3.77 \lesssim \log_{10} t \lesssim 4.12$ and the pair of bodies in the $e_{\max} = 0.05$ simulation with a ~ 1.2 AU during the period $4.38 \leq \log_{10} t \leq 4.60$. One cannot help but wonder what outcomes of these sequences of close encounters might result if tidal dissipation in the bodies were included in the simulation program.

In the plots of system states at selected times (Figures 12, 15, 18, and 21) one can more easily follow the progress of accretion in each simulation, since the masses of the bodies, represented by the box areas, are shown along with the orbital eccentricities and semi-major axes of the bodies. As expected, accretion is more rapid for smaller heliocentric distances since the surface density of bodies is greater in that region. The evolution of the eccentricity and semi-major axis distributions is again apparent in these plots. Also as expected, the more massive bodies tend to have smaller orbital eccentricities since the accretion process averages the eccentricity vectors of the orbits of the accreting bodies. The final states of the $e_{\max} = 0.025, 0.05, \text{ and } 0.10$ simulations contain too many bodies with masses which are too

small relative to those of Venus and Earth. On the other hand, the $e_{\max} = 0.15$ simulation ends with a final state which is very suggestive of the terrestrial system of planets, and two of these bodies approach the Earth and Venus in mass.

The final states of the four simulations are compared with the terrestrial system of planets in Figure 24. The bars indicate the heliocentric range of each body. The numbers above the bars give the mass of the bodies in hundredths of an Earth mass and the numbers between the bars provide a measure of the stability of the heliocentric gaps between orbits. The heliocentric gaps are expressed as fractions of $\Delta = 2.4 R[(m_1 + m_2)/M_\odot]^{1/3}$, where R is the heliocentric distance to the center of the gap between m_1 and m_2 . Birn (1973) has carried out numerical integrations and presented theoretical arguments based on the Jacobian integral which purport to show that bodies in orbits separated by gaps greater than Δ are stable in the sense that, except for oscillations, the semi-major axes of all orbits remain constant over long time scales.

2. The Collision Statistics

The ratio of the total energy at impact for a pair of

colliding bodies to their total gravitational binding energy, $(T + U)/-\Omega$, provides a convenient measure which may be used in deciding whether a given collision is accretive or destructive. When $(T + U)/-\Omega$ is greater than one, a collision is expected to result in the complete disruption and dispersal of the material of both bodies; however, when $(T + U)/-\Omega$ is less than one a collision is expected to result in accretion. Average values of the ratio, $(T + U)/-\Omega$, for collisions occurring in three of the four simulations discussed in this chapter are tabulated in Tables 2 to 4. The numbers of accretive and destructive collisions are also tabulated for each of the m_i - m_j values for which collisions occurred.

There are a number of interesting observations which can be made from these statistics. First, the average $(T + U)/-\Omega$ ratio for all of the collisions occurring in a given simulation increases as e_{\max} increases. Further, the average value of $(T + U)/-\Omega$ for the $m_1 = m_2 = 0.02 M_{\oplus}$ collisions exceeds the average value of $(T + U)/-\Omega$ when all of the collisions for a given simulation are included. It is no surprise then that the $m_1 = m_2 = 0.02 M_{\oplus}$ and $m_1 = 0.04 M_{\oplus}$, $m_2 = 0.02 M_{\oplus}$ collisions account for all of the destructive collisions. Perhaps, the

Table 2Collision Statistics ($e_{\max} = 0.05$)

m_j ($M_{\oplus}/100$)	m_i ($M_{\oplus}/100$)	#(accretive)	#(destructive)	($T + U$)/($-\Omega$) (accretive only)
2	2	34		0.158
2	4	14	1	0.073
2	6	4		0.065
2	8	3		0.065
2	10	2		0.012
2	12	3		0.030
2	14	2		0.030
2	22	1		0.021
2	26	1		0.039
4	4	5		0.084
4	6	3		0.063
4	8	2		0.046
4	10	1		0.004
4	12	1		0.012
4	14	1		0.031
4	16	1		0.022
4	22	1		0.693
6	6	1		0.169
6	8	1		0.033
6	10	1		0.020
6	16	2		0.031
8	8	1		0.037
14	16	1		0.027

Simulation average value of ($T + U$)/($-\Omega$) for the accretive collisions = 0.103

Table 3Collision Statistics ($e_{\max} = 0.10$)

m_j ($M_{\oplus}/100$)	m_i ($M_{\oplus}/100$)	#(accretive)	#(destructive)	(T + U)/(- Ω) (accretive only)
2	2	27	5	0.325
2	4	18		0.153
2	6	6		0.102
2	8	2		0.256
2	10	3		0.096
2	12	1		0.005
2	18	1		0.024
2	20	1		0.009
2	22	1		0.002
2	24	1		0.009
2	30	1		0.101
4	4	2		0.168
4	6	4		0.073
4	8	1		0.061
4	12	1		0.012
4	14	1		0.001
4	16	1		0.002
4	22	1		0.040
4	26	1		0.021
6	6	2		0.094
6	8	1		0.021
6	10	1		0.009
6	12	1		0.043
8	12	1		0.072
8	14	1		0.027
8	22	1		0.033
10	12	1		0.044
10	20	1		0.005
12	20	1		0.281

Simulation average value of (T + U)/(- Ω) for the accretive collisions = 0.171

Table 4Collision Statistics ($e_{\max} = 0.15$)

m_j ($M_\oplus/100$)	m_i ($M_\oplus/100$)	#(accretive)	#(destructive)	(T + U)/(- Ω) (accretive only)
2	2	20	9	0.438
2	4	15	2	0.253
2	6	9		0.266
2	8	6		0.292
2	10	3		0.052
2	12	1		0.208
2	18	1		0.065
2	20	1		0.006
2	24	1		0.022
2	32	1		0.039
2	58	1		0.030
4	4	2		0.163
4	6	3		0.165
4	10	2		0.094
4	14	2		0.051
4	20	1		0.050
6	8	1		0.025
6	18	1		0.0001
6	20	1		0.115
6	24	1		0.068
8	10	1		0.015
8	12	2		0.255
8	24	1		0.192
10	12	1		0.025
10	14	1		0.013
10	30	1		0.089
18	40	1		0.235
26	34	1		0.104
24	60	1		0.012

Simulation average value of (T + U)/(- Ω) for the accretive collisions = 0.238

most significant observation to be made from these statistics is that the number of destructive collisions rapidly increases as e_{\max} increases beyond 0.10, so that for simulations with initial values of $e_{\max} > 0.15$, one is no longer justified in assuming that all collisions result in accretions.

3. Eccentricity Evolution in the Simulations

In Table 5 statistics are tabulated pertaining to the eccentricity changes occurring during the early stages of each of the four representative simulations described in this chapter. The quantity denoted in the table by Δe is the average value of $m_i \Delta e_i + m_j \Delta e_j$ over those events occurring between the simulation starting time and the tenth accretion event, where Δe_i and Δe_j are the eccentricity changes of the two bodies in the given event and the masses m_i and m_j are in units of the initial mass, $0.02 M_{\oplus}$. In these statistics we refer to those gravitational interactions not resulting in collisions as encounters. Note that in all of the simulations, at least for the early stage considered here, the gravitational encounters on the average result in eccentricity increases, but as e_{\max} is increased the mass average eccentricity increase per encounter decreases.

Table 5

Statistics of the Eccentricity Changes Occurring For
Encounters and Collisions

	e_{\max}			
	0.025	0.05	0.10	0.15
$\Delta e/\text{encounter}$	+0.00269	+0.00178	+0.00074	+0.00066
$\Delta e/\text{collision}$	-0.01333	-0.01434	-0.05069	-0.08463
$ \Delta e /\text{encounter}$	0.01007	0.01040	0.00712	0.00569
$\frac{\Delta e/\text{encounter}}{ \Delta e /\text{encounter}}$	0.27	0.17	0.10	0.12
$\frac{\Sigma \Delta e(\text{encounters})}{ \Sigma \Delta e(\text{collisions}) }$	+2.96	+1.59	+0.20	+0.41
collision-encounter balance ratio	5.0	8.0	68.7	128.2
# encounters during the first ten collision events	147	140	137	527

Collisions, on the other hand, always result in eccentricity decreases, and the eccentricity decreases due to collisions increase as e_{\max} is increased. The mass average eccentricity of the system of protoplanetary bodies is then determined by the balance between the eccentricity increases resulting from gravitational encounters and the eccentricity decreases resulting from collisions. The ratio $\Sigma\Delta e(\text{encounters})/|\Sigma\Delta e(\text{collisions})|$ provides a quantitative measure of this balance:

when this ratio is greater than one, the mass average eccentricity is increasing and, conversely, when it is less than one, the mass average eccentricity is decreasing. The collision-encounter balance ratio gives the number of encounters required on the average to offset the eccentricity decreases due to collisions. A measure of the average absolute eccentricity change per encounter is provided by $|\Delta e|/\text{encounter} = (|m_i\Delta e_i| + |m_j\Delta e_j|)/\text{encounter}$ and finally, the ratio $(\Delta e/\text{encounter})/(|\Delta e|/\text{encounter})$ quantifies the rate of the eccentricity increase due to gravitational encounters.

From the simulation starting time to the tenth accretion event, the mass average eccentricity increases quite rapidly for the $e_{\max} = 0.025$ and $e_{\max} = 0.05$ simulations and decreases for the $e_{\max} = 0.10$ and 0.15 simula-

tions. It is expected that an e_{\max} value somewhere between 0.05 and 0.10 would on the average result in a balance between the eccentricity developed in gravitational encounters and that lost in collisions for the coplanar system of bodies chosen here to initiate all the simulations.

In a system where non-zero orbital inclinations are allowed, fewer close gravitational interactions are expected to result in collisions. The number of encounters per collision for a three-dimensional system of bodies with the same members as the system used to initiate the two-dimensional simulations is expected to be at least one order of magnitude greater than the number in the two-dimensional case. The eccentricity balance referred to above is then expected to occur for higher values of e_{\max} in the three-dimensional case than in the two-dimensional one. The necessary eccentricity to produce terrestrial-like final configurations of bodies such as those in the $e_{\max} = 0.15$ simulation might then be built up by the additional gravitational encounters occurring in the three-dimensional case.

A quantitative estimate of the effect of orbital eccentricity averaging of the many bodies accumulating

into a planet has been made by Ziglina and Safronov (1976). A number of assumptions were made in this estimate including a mass distribution for the bodies, the total number of bodies per unit area as a function of the distance to the Sun, and the distribution of orbital eccentricities of the bodies, among others. The estimate they obtained for the orbital eccentricities of the just-formed terrestrial planets may be written as

$$e_{acc} \approx C \left(\frac{m_1}{m} \right)^{1/2} \frac{v_e}{v_c}, \quad 5-1$$

where m_1 is the upper limit of the mass distribution of impacting bodies and m is the present mass of the planet. The parabolic velocity at the surface of the planet is denoted by v_e and the circular Keplerian velocity at the heliocentric distance of the planet by v_c . The constant, C , includes parameters used to specify the mass distribution of bodies and their velocity relative to the circular Keplerian velocity; for the parameter values assumed by Safronov, $C = 0.11$. Values of m_1/m were estimated by Safronov (1969) from the inclinations of the rotation axes of the terrestrial planets. The values of e_{acc} taking $m_1/m = 1.8 \times 10^{-3}$ for Mercury, Venus, and Earth and $m_1/m = 3.5 \times 10^{-3}$ for Mars, are a little more

than one order of magnitude smaller than the current values observed in the terrestrial system. Ziglina and Safronov, without any further arguments or estimates, conclude that the modern orbital eccentricities of the planets must be determined to a greater extent by their prolonged gravitational interaction since the time their accumulation was complete, rather than directly by the process of formation.

On the basis of their estimates of m_1/m from the rotation axis inclinations of the terrestrial planets, Ziglina and Safronov rule out the possibility of collisions and accretions of bodies with moderate mass ratios in the final stage of accumulation of the terrestrial planets. On the other hand, the values of m_1/m occurring in our simulations are a little more than two orders of magnitude greater than those estimated by Safronov and yield values of e_{acc} which are consistent with the present orbital eccentricities for the terrestrial planets. This brings up the intriguing possibility that the present orbital eccentricities of the terrestrial planets might perhaps serve to distinguish between those scenarios for the final stage of accumulation of the terrestrial planets characterized by very small values of

m_1/m , e.g. Safronov (1969) and Weidenshilling (1975), and scenarios characterized by values of m_1/m often greater than 1/10. A careful review of Safronov's estimates of m_1/m along with quantitative estimates of upper limits on the orbital eccentricity changes of the terrestrial planets due to their mutual gravitational interactions and interaction with Jupiter are required in order to determine whether this discrimination between scenarios is possible.

4. Numerical Checks on the Simulations

One numerical simulation was run to check the validity of the encounters model for those close encounters typically occurring in the present simulations. Values for the orbital element changes for each of the close encounters occurring in the simulation were calculated both by use of the model and by integration of the regularized equations of motion. Comparison of these two sets of values revealed that the model, in agreement with the conclusions stated in Chapter II, does indeed provide a useful approximation, $E_e, E_a \lesssim 50\%$, for the orbital element changes occurring in those close encounters for which $\epsilon \gtrsim 4$ and $\alpha \lesssim 0.80$. Even for encounters with $\epsilon < 4$ the model was often a useful approximation,

especially for those encounters with $2 < \epsilon < 4$. However, since there were some encounters for which the predictions of the model were in radical disagreement with the results obtained by numerical integration, it was thought to be more prudent to compute orbital element changes for the encounters having $\epsilon < 4$ by numerical integration of the regularized equations of motion for the duration of the encounter. It was further noted that the model, almost without exception, predicted larger values for the minimum separation between bodies during the encounters with $\epsilon \geq 4$ than was obtained by numerical integration. Therefore, the model consistently somewhat underestimates the orbital element changes relative to the changes obtained by integration for encounters with $\epsilon \geq 4$. Furthermore, since almost all collisions result from encounters with $\epsilon < 4$, the model frequently predicts collisions between bodies for encounters in which integration of the equations of motion produces no collision.

A further check on the accuracy of the simulations was made by calculating the total angular momentum of the system of protoplanetary bodies for the initial and final states of the $e_{\max} = 0.15$ simulation. These values of the total system angular momentum and total system energy are compared to the corresponding values for the current

terrestrial system in Table 6. The total angular momentum is closely conserved, as it should be, while the total system energy decreases by 1.23% between the initial and final states of the $e_{\max} = 0.15$ simulation.

Table 6

Comparisons of Total System Angular Momentum and Energy

	$L_{\text{system}} \text{ (g-cm}^2\text{/sec)}$	$E_{\text{system}} \text{ (g-cm}^2\text{/sec}^2\text{)}$
initial (100 bodies)	5.152×10^{47}	-6.020×10^{40}
final (6 bodies)	5.152×10^{47}	-6.094×10^{40}
terrestrial system	4.95×10^{47}	-6.20×10^{40}

Finally, the numerical integration of the individual encounters was checked by integrating backwards in time to make sure that the initial conditions could be reproduced.

B. An Estimate of the Evolution Times Expected for Three-Dimensional Systems

The evolution time expected for a three-dimensional system is estimated using the ratio of the two-body

collision probability for a three-dimensional system to that for a two-dimensional system along with the evolution times obtained in the two-dimensional computer simulations. The collision probability per unit time for one body may be written as

$$\frac{1}{\tau} = U n \sigma \quad 5-2$$

where U is the mean relative speed of the bodies, n is the number of bodies per unit surface area or volume, and σ is the collision cross-section. The collision cross-section in two dimensions is taken to be $2R$ and in three dimensions to be πR^2 where R is a multiple β_f times the physical radius of the bodies, r . The factor β_f , which provides a measure of the increase of the collision cross-section over the geometric cross-section due to "gravitational focusing," is estimated from the integrations of circular encounters in Chapter I to be approximately 28 for the two-dimensional case with $m_1 = m_2 = 0.02 M_\oplus$. The surface area available to the 100 bodies in the simulations is given by

$$S = \pi (1.5^2 - 0.5^2) = 2\pi (\text{AU})^2. \quad 5-3$$

The corresponding volume assumed to be available to the

100 bodies in a three-dimensional system is taken to be equal to that of the solid of revolution formed by rotating a regular trapezoid, bounded above by $\phi = i_{\max}$, below by $\phi = -i_{\max}$, and by $r_1 = 0.5$ AU and $r_2 = 1.5$ AU in heliocentric distance, one full revolution. Making use of the Pappus-Guldinus theorem we obtain for this volume,

$$V = 2\pi\sqrt{5} \tan i_{\max} (\text{AU})^3. \quad 5-4$$

The ratio of the three-dimensional to the two-dimensional relaxation times is then given by

$$\frac{\tau_{3-D}}{\tau_{2-D}} = \frac{2\sqrt{5}}{\pi} \tan i_{\max} \frac{1 \text{ AU}}{\beta_f R}. \quad 5-5$$

For a set of test bodies having a dimensionless relative velocity,

$$U = u/V_k \quad V_K^2 = \frac{GM_\odot}{a}, \quad 5-6$$

with respect to a field body in a circular orbit of radius, a , there exist expressions for e_{\max} and i_{\max} in terms of U (Öpik, 1951). The maximum possible eccentricity occurs when the orbits are co-planar and when the perihelion of the test body's orbit is at the field body's orbit and

may be written in terms of U as

$$e_{\max} = U^2 + 2U. \quad 5-7$$

For any U , the maximum inclination (relative to the orbital plane of the field body) is according to Öpik

$$i_{\max} = 2 \sin^{-1}(U/2). \quad 5-8$$

For small values of U , $e_{\max} = 2U$ and $i_{\max} = U$ are good approximations.

With the values $e_{\max} = 0.15$ ($i_{\max} = 0.075$ radians), $m_1 = m_2 = 0.02 M_{\oplus}$, and $\beta_f = 28$, the ratio τ_{3-D}/τ_{2-D} is determined to be approximately 280. This ratio with the $e_{\max} = 0.15$ simulation time of 61,400 years yields an estimate of 2×10^7 years for the time required for the stage of accretion considered in our simulations in the case of a three-dimensional system with $e_{\max} = 0.15$ and $i_{\max} = 0.075$ radians. This estimate is well within the limits for the formation time interval discussed in Chapter I.

C. Heliocentric Distance Sampling Of Material for the Final Bodies of the Simulations

It is informative to examine the range of heliocentric distance sampling of material for the bodies in

the simulations at several stages of their evolution. In Figures 22 and 23 the original semi-major axis distributions of component bodies are shown for those bodies with mass greater than $0.1 M_{\oplus}$ at six stages, including the final one, of the $e_{\max} = 0.05$ and $e_{\max} = 0.15$ simulations, respectively. The original semi-major axes of the component bodies are indicated by a (+) and the current semi-major axis and mass of each body are located in the figures by an (x).

As expected the range of heliocentric distance sampling in bodies with smaller mass tends to be narrower than the range of sampling in bodies with larger mass. As also seems reasonable, the range of radial sampling is greater in the $e_{\max} = 0.15$ simulation than in the $e_{\max} = 0.05$ simulation for bodies of a given mass.

The semi-major axis distributions of component bodies are sometimes not at all symmetric about the current semi-major axis of the body being considered. This is often the case when two bodies are accreting material from overlapping heliocentric ranges: the two bodies tend to "repel" each other so that the body closer to the Sun samples more material outside its orbit than inside, and the reverse is of course true for the body farther from the Sun. It must be emphasized, however, that this behavior

is only a tendency and is by no means always observed.

The radial sampling function observed for the bodies in these simulations may generally be described as follows. For a given body, approximately 75% of the material comes from the zone bounded by the orbits of the next inner, i.e. toward the Sun, and next outer bodies, 8% comes from the zone bounded by the orbits of the next inner and second inner bodies, and the remaining 17% comes from the zone bounded by the orbits of the next outer and second outer bodies. However, we must caution that this radial sampling function is based on statistics from a small number of simulations. Furthermore, it undoubtedly reflects the edge effects resulting from our choice of the initial radial distribution of material. The similarity of the final state of the $e_{\max} = 0.15$ simulation to the system of terrestrial planets does permit us to form the above working hypothesis for the radial sampling to be expected for at least the Earth and Venus. Much more complex "edge effects" have no doubt influenced the radial sampling of the material comprising Mercury and Mars. It must be pointed out that although the radial sampling observed for bodies in the simulations represents only the sampling occurring during the last stage of accretion, the range of radial sampling is expected to be

much narrower for bodies with small values of their mass. Therefore, it is apparent that the range of radial sampling exhibited in the final bodies is primarily determined by the last few accretion events involving the given body.

Hartmann (1976) has used Wetherill's (1975) calculations of the gravitational dispersal of planetesimals from different orbits about the Sun to obtain data on the sources of different late-accreted materials added to the terrestrial planet surface layers. Wetherill tabulated the final impact destinations of statistical samples of particles starting in nine different orbits in the terrestrial region of the solar system. In his Table III (p. 555) Hartmann has converted the relative numbers of impacts obtained by Wetherill to obtain the percentage of mass striking target planets from each source orbit. These results indicate that large fractions of the mass added to the terrestrial planets in their later stages of growth probably formed nearer other planet's orbits, in agreement with conclusions drawn from the present simulations. However, our radial sampling function is not directly comparable to that given by Hartmann, but seems to be qualitatively similar.

D. Conclusions Drawn From the Simulations Regarding the Formation of the Terrestrial Planets

Perhaps the primary conclusion is that terrestrial-like planetary systems can be formed as a result of the gravitationally-induced collisions and accretions occurring between bodies in co-planar systems of protoplanets such as those chosen here to initiate the simulations, provided the initial average orbital eccentricity of the system of bodies is in the range $0.05 \leq \langle e \rangle \leq 0.10$. Simulations with initial values of $\langle e \rangle$ smaller than 0.05 are found to result in final-state configurations having many bodies of nearly equal mass, none of which approach the Earth or Venus in mass, Figure 24. On the other hand, initial values of $\langle e \rangle$ greater than 0.10 result in substantial numbers of catastrophically disruptive collisions between bodies and it is expected that the accretion process for this case will at least be dramatically slowed, if not reversed.

The numerical simulations indicate that mass average eccentricity values in the range $0.025 < \langle e \rangle < 0.05$ can be sustained by the gravitational encounters offsetting the eccentricity lost in collisions, at least for the early stages of evolution of the co-planar systems used to begin these simulations. These values of $\langle e \rangle$ are

somewhat too low to produce terrestrial-like systems, but higher values of $\langle e \rangle$ may result from the higher ratio of close gravitational encounters to collisions holding for three-dimensional systems.

Estimates of the time interval required for this stage of accretion in a reasonably thin hypothetical three-dimensional protoplanetary system were made earlier in this chapter. The times required for completion of the two-dimensional numerical simulations from initial systems of 100 equal mass bodies with $m = 0.02 M_{\oplus}$ to the final state configurations are used with theoretical estimates of the ratio of the three- to the two-dimensional relaxation time, based on the two-body gravitational model, to predict a time interval of the order 2×10^7 years for the stage of accretion considered here. This time falls well within the limits of a few times 10^8 years for the formation of the terrestrial planets, based on the oldest ages measured for rocks from the Earth's crust along with the K^{40} - Ar^{40} and U, Th- He^4 gas-retention ages for various meteorites as discussed in Chapter I.

Finally, the original heliocentric distance distribution of component bodies making up the bodies in the final states of the simulations indicate that approximately 75% of the material of a given body comes from

the zone bounded by the orbits of the next inner and next outer bodies. The remaining 25% comes from two zones bounded by the orbits of the next inner and second inner bodies and by the orbits of the next outer and second outer bodies, respectively. This description of the heliocentric distance dependence of the sampling function for a given body is, however, only intended as a general rule of thumb. For certain bodies a number of factors such as edge effects or possible bombarding material perturbed into the terrestrial region by an early-formed Jupiter may significantly modify this sampling function.

E. Limitations of the Present Numerical Simulations

Many of the desirable features of these simulations were described in the final section of Chapter I. In this section we will turn our attention to some of their limitations. First, actual systems of protoplanets, even if they are quite thin, are nevertheless three-dimensional, and this fact presents a whole new set of difficulties in attempting to simulate such systems. It was argued earlier that the number of encounters per collision for a three-dimensional system of bodies having the same

bodies as those in the system used to initiate the two-dimensional simulations is expected to be at least one order of magnitude greater than the number for the two-dimensional case. Therefore, significantly more computer time would be required to simulate the three-dimensional systems. The eccentricity balance might as a result occur for higher values of $\langle e \rangle$ in the three-dimensional case than in the two-dimensional one, but since the character of the encounters presumably also changes in three-dimensions, one cannot be sure that this expectation is justified in fact.

Several simulations which were carried out have not been discussed here, because the orbital spacings between bodies were not stable (Birn, 1973), when no further close approaches, $(\Delta r)_{\min} < R_s$, were predicted and the simulations terminated. In the two-dimensional case this situation is most often the result of an alignment of some number of the orbital eccentricity vectors of the system bodies. Inclusion of the effects of distant encounters in some of these "final" states would give rise to some additional collisions and subsequent evolution of these systems. "Avoidance" mechanisms such as this are expected to be an even greater problem in three-dimensional

simulations which include only the effects of close encounters.

Another limitation of the simulations in their present form is the small number ($N = 100$) of bodies which can currently be handled by the programs. This makes an assessment of the influence of our choice of an initial system of one hundred bodies of equal mass, $m = 0.02 M_{\oplus}$, on the final configurations produced in the simulations difficult. Two-dimensional simulations beginning with protoplanetary systems having more bodies and a variety of mass distributions should elucidate the influence of the initial conditions on the final configurations produced. Such simulations seem feasible upon some improvement and/or modification of the way in which encounters are handled in the simulation programs.

We have attempted here to simulate the last stage of terrestrial planet formation neglecting any outside influences. If, for example, Jupiter has already attained a substantial part of its mass before the stage of accretion considered here, the influence of bombarding material perturbed by Jupiter into orbits crossing the terrestrial region must be included in a realistic scenario.

Finally, some collisions do occur in these simulations which, based on their expected relative velocities at impact, should be completely disruptive, and yet the simulations assume that all collisions result in accretion. This assumption appears to be well justified for collisions occurring in systems with mass average eccentricities $\langle e \rangle \lesssim 0.05$. It cannot be ruled out, however, that bodies were accreted and subsequently dispersed by collisions several times in the process of forming the terrestrial planets. In order to simulate properly this formation process, it would be necessary to construct models of the disruptive collisions commonly occurring in those systems with $\langle e \rangle > 0.05$.

REFERENCES

- Alexeyeva, K.N. (1958), Meteoritika 16, 67, (in Russian).
- Battin, R.H. (1964), Astronautical Guidance, McGraw-Hill, New York.
- Bettis, D.G., and Szebehely, V. (1971), Astrophysics and Space Science 14, 133.
- Birn, J. (1973), Astron. & Astrophys. 24, 283.
- Black, D.C., and Suffolk, G.C.J. (1973), Icarus 19, 353.
- Brent, R.P. (1973), Algorithms for Minimization Without Derivatives, Prentice-Hall, Englewood Cliffs, New Jersey.
- Chandrasekhar, S. (1941), Astrophys. J. 93, 285.
- Dole, S.H. (1962), Planetary Space Science 9, 541.
- Edgeworth, K.E. (1949), M.N.R.A.S. 109, 600.
- Fehlberg, E. (1969), Computing 4, 93.
- Fitzpatrick, P.M. (1970), Principles of Celestial Mechanics, Academic Press, New York/London.
- Fujiwara, A., Kamimoto, G., and Tsukamoto, A. (1977), Icarus 31, 277.
- Gatewood, G. (1972), Ph.D. Dissertation, University of Pittsburgh, Pennsylvania.
- Gatewood, G. (1976), Icarus 27, 1.
- Giuli, R.T. (1968), Icarus 8, 301.

Goldreich, P., and Lynden-Bell, D. (1965), M.N.R.A.S. 130,
97.

_____ (1965), ibid., 130, 125.

Goldreich, P., and Ward, W.R. (1973), Astrophys. J. 183,
1051.

Greenberg, R., and Hartmann, W.K. (1977), abstract in the
8th Annual Meeting Notes of the D.P.S., American
Astronomical Society.

Greenberg, R., Wacker, J.F., Hartmann, W.K., and Chapman,
C.R. (1977), submitted to Icarus.

Gurevich, L.E., and Lebedinskii, A.I. (1950) Izv. AN
SSSR, seriya fizich., 14(6), 765.

Hartmann, W.K. (1976), Icarus 27, 553.

Herczeg, T. (1968), Vistas in Astr. 10, 175.

Horedt, Gp. (1972), Celes. Mech. 1, 232.

Hoyle, F. (1946), M.N.R.A.S. 106, 406.

Huang, S.-S. (1973), Icarus 18, 339.

Kaula, W.M. (1975), Icarus 26, 1.

Lecar, M., Loesser, R., and Cherniak, J.R. (1974), in
Numerical Solution of Ordinary Differential Equations,
Springer-Verlag, New York.

McCrea, W.H. (1972), in Symposium on the Origin of the
Solar System (ed. by Hubert Reeves), Edition du
Centre National de la Recherche Scientifique, Paris.

- Moore, H.J., and Gault, D.E. (1965), Astrogeologic Studies, U.S.G.S. Annual Progress Report, 127.
- Öpik, E.J. (1951), Proc. Roy. Irish Acad. 54A, 165.
- Pechernikova, G.V. (1974), English translation in Soviet Astron. AJ 18, 1305.
- Russell, H.N. (1935), The Solar System and Its Origin, Macmillan, New York.
- Rybicki, G.B. (1972), in Gravitational N-Body Problem (ed. by M. Lecar), D. Reidel, Dordrecht-Holland.
- Safronov, V.S. (1969), in Evolution of the Protoplanetary Cloud and Formation of the Earth and Planets, Israel Program for Scientific Translations, Jerusalem, 1972.
- Schatzman, E. (1965), The Origin and Evolution of the Universe, Basic Books, New York.
- Steins, K., and Zalkalne, I. (1970), in Irregular Forces in the Motion of Comets (Russ.), Riga.
- Ter Haar, D. (1948), Kgl. Dan. Vidensk. Selsk. Mat. Fys. Medd. 25, No. 3, 1.
- Ter Haar, D., and Cameron, A.G.W. (1963), in Origin of the Solar System (R. Jastrow and A.G.W. Cameron, ed.), Academic Press, New York.

- Thompson, R.I., Strittmatter, P.A., Erickson, E.F.,
Witteborn, F.C., and Strecker, D.W. (1977), Astrophys.
J. 218, 170.
- Toomre, A. (1964), Astrophys. J. 139, 1217.
- van de Kamp, P. (1969), Astron. J. 74, 238.
- Ward, W.R. (1975), private communication.
- Weidenschilling, S.J. (1975), Ph.D. Dissertation,
Massachusetts Institute of Technology.
- Wetherill, G.W. (1975), Proc. Sixth Lunar Sci. Conf.
- Williams, I.P., and Cremin, A.W. (1968), Quart. J. Roy.
Astr. Soc. 9, 40.
- Williamson, R.E., and Chandrasekhar, S. (1941), Astrophys.
J. 93, 305.
- Woolfson, M.M. (1969), Rep. Prog. Phys. 32, 135.
- Ziglina, I.N., and Safronov, V.S. (1976), English trans-
lation in Soviet Astronomy AJ 20, 244.
- Zvyagina, E.V., Pechernikova, G.V., and Safronov, V.S.
(1973), English translation in Soviet Astronomy AJ
17, 261.

FIGURE CAPTIONS

Figure 1. Orbital eccentricity and semi-major axis changes are shown along with minimum separation distances for a sequence of encounters between bodies which are initially in co-planar, circular orbits about the Sun with various orbital spacings, given here as multiples of the "sphere of influence" radius of the larger body, $R_s = R[(M_2(M_1 + M_2))/(M_\odot^2)]^{1/5}$. The radius of the initial orbit of M_2 was taken to be 1.0 AU. In addition, M_1 and M_2 were assumed to orbit the Sun in the same sense and only those encounters for which the orbit of M_1 lay outside that of M_2 were considered. The integrations of the regularized equations of motion for all encounters began and ended with separations of $500 R_s$. It proved more convenient to plot $\log_{10}(R_{\text{MIN}}/(R_1 + R_2))$ rather than the minimum separation, R_{MIN} , where R_1 and R_2 are the radii of M_1 and M_2 assuming that they are homogeneous, spherical bodies of lunar density. Therefore, the two regions where $\log_{10}(R_{\text{MIN}}/(R_1 + R_2)) = 0.0$ represent collisions between the bodies. In this sequence of encounters the masses of the two bodies were taken to be $M_1 = 10^{-5} M_\oplus$ and $M_2 = 10^{-2} M_\oplus$.

Figure 2. Same as Figure 1, but with $M_1 = M_2 = 10^{-2} M_{\oplus}$.

Figure 3. Same as Figure 1 and Figure 2, but with $M_1 = 10^{-3} M_{\oplus}$ and $M_2 = M_{\oplus}$.

Figure 4. Same as Figure 1, but with $M_1 = M_2 = M_{\oplus}$.

Figure 5. The parameters specifying encounters in the model.

Figure 6. Contours of Δe and Δa (AU) in α, ε obtained by the model for m_1 and m_2 along with contours of E_e and E_a in α, ε . The motion of the m_1, m_2 center of mass for all these encounters was taken to be along a circular orbit with $R_0 = 1$ AU. The sense of motion of m_1 about m_2 was taken to be $(-)$ and the orientation of the relative hyperbolas was given by $\phi = \pi/10$. The masses were $m_1 = m_2 = m_0$ with $m_0/M = 0.01 M_{\oplus}/M_{\odot}$.

Figure 7. The parameters specifying these encounters are identical to those in Figure 6 except for the orientation angle $\phi = 7\pi/10$.

Figure 8. Dependences of Δe and Δa (AU) on the orientation angle ϕ given by numerical integration. Dependences of $E_e, E_a, E_e,$ and E_a on ϕ are also shown for both senses of motion (\pm) . The motion of the m_1, m_2 center of mass was assumed to be along a circular orbit of radius $R_0 = 1$ AU. The remaining fixed parameters were $\varepsilon = 4, \alpha = 0.16$, and $m_1 = m_2 = m_0$.

Figure 9. Dependences of Δe and Δa (AU) on e_0 and R_0 given by numerical integration. Dependences of E_e and E_a on e_0 and R_0 are also shown. The remaining fixed parameters were $\varepsilon = 4$, $\alpha = 0.16$, $\theta_0 = \pi/2$, $\phi = 0.0$, and $m_1 = m_2 = m_0$. The sense of motion of m_1 and m_2 was taken to be (-).

Figure 10. The time evolutions of the orbital eccentricities are plotted for the bodies in the $e_{\max} = 0.025$ simulation. For clarity in plotting an equal abscissa increment was assigned to each gravitational encounter, whether resulting in a collision or not. The associated event times are given as \log_{10} of the time in years. Collisions and subsequent accretions of bodies are denoted by a vertical line connecting the eccentricity values of the two colliding bodies just prior to the current encounter and by a small box locating the orbital eccentricity of the newly accreted body.

Figure 11. The semi-major axis evolutions corresponding to the eccentricity evolutions in Figure 10 are plotted. Equal abscissa increments were again assigned to each gravitational encounter and accretions are denoted in the same way as in Figure 10.

Figure 12. The semi-major axes, eccentricities, and masses of the system bodies are shown for nine different stages in the $e_{\max} = 0.025$ simulation, including the initial and final ones. The number of system bodies for the nine stages is indicated at the top of each frame. The boundaries of the initial semi-major axis and eccentricity distributions are indicated by the rectangles in each frame. The areas of the small boxes marking the location of each body are proportional to the masses of the bodies.

Figure 13. Same as Figure 10, but for the $e_{\max} = 0.05$ simulation.

Figure 14. Same as Figure 11, but for the $e_{\max} = 0.05$ simulation.

Figure 15. Same as Figure 12, but for the $e_{\max} = 0.05$ simulation.

Figure 16. Same as Figure 10, but for the $e_{\max} = 0.10$ simulation.

Figure 17. Same as Figure 11, but for the $e_{\max} = 0.10$ simulation.

Figure 18. Same as Figure 12, but for the $e_{\max} = 0.10$ simulation.

Figure 19. Same as Figure 10, but for the $e_{\max} = 0.15$ simulation.

Figure 20. Same as Figure 11, but for the $e_{\max} = 0.15$ simulation.

Figure 21. Same as Figure 12, but for the $e_{\max} = 0.15$ simulation.

Figure 22. The original semi-major axis distributions of component bodies are shown for those bodies with mass greater than $0.1 M_{\oplus}$ at six stages, including the final one, of the $e_{\max} = 0.05$ simulation. The original semi-major axes of the component bodies are indicated by a "+" and the current semi-major axis and mass of each body are located by an "x".

Figure 23. Same as Figure 22, but for the $e_{\max} = 0.15$ simulation.

Figure 24. A comparison of the final states of the four representative simulations with the present terrestrial system of planets. The bars indicate the heliocentric range of each body. The numbers above the bars give the mass of the bodies in hundredths of an Earth mass, and the heliocentric distance gaps between orbits are expressed as multiples of $\Delta_s = 2.4 R[(m_1 + m_2)/M_{\oplus}]^{1/3}$, where Δ_s is a gap argued to be stable by Birn (1973).

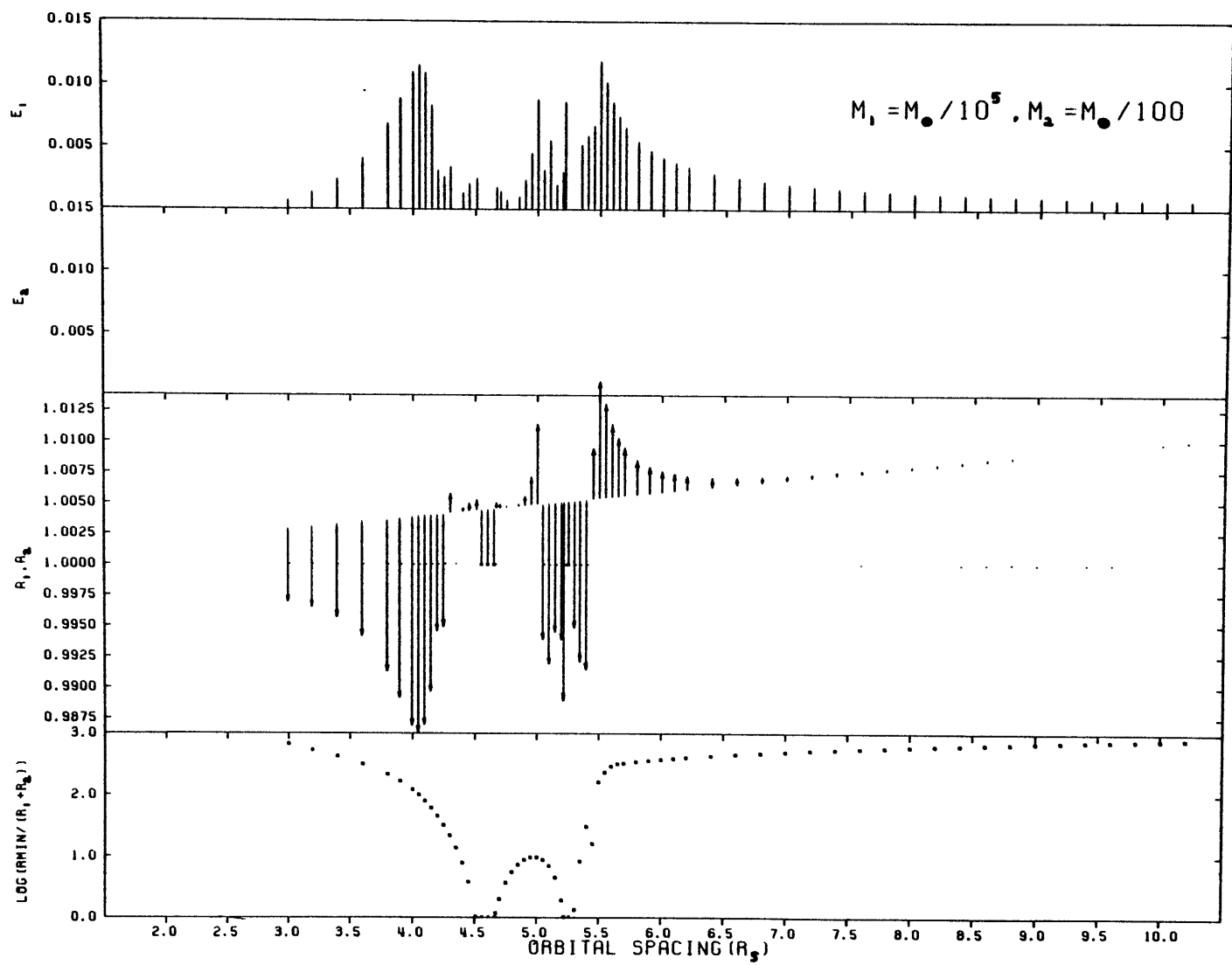
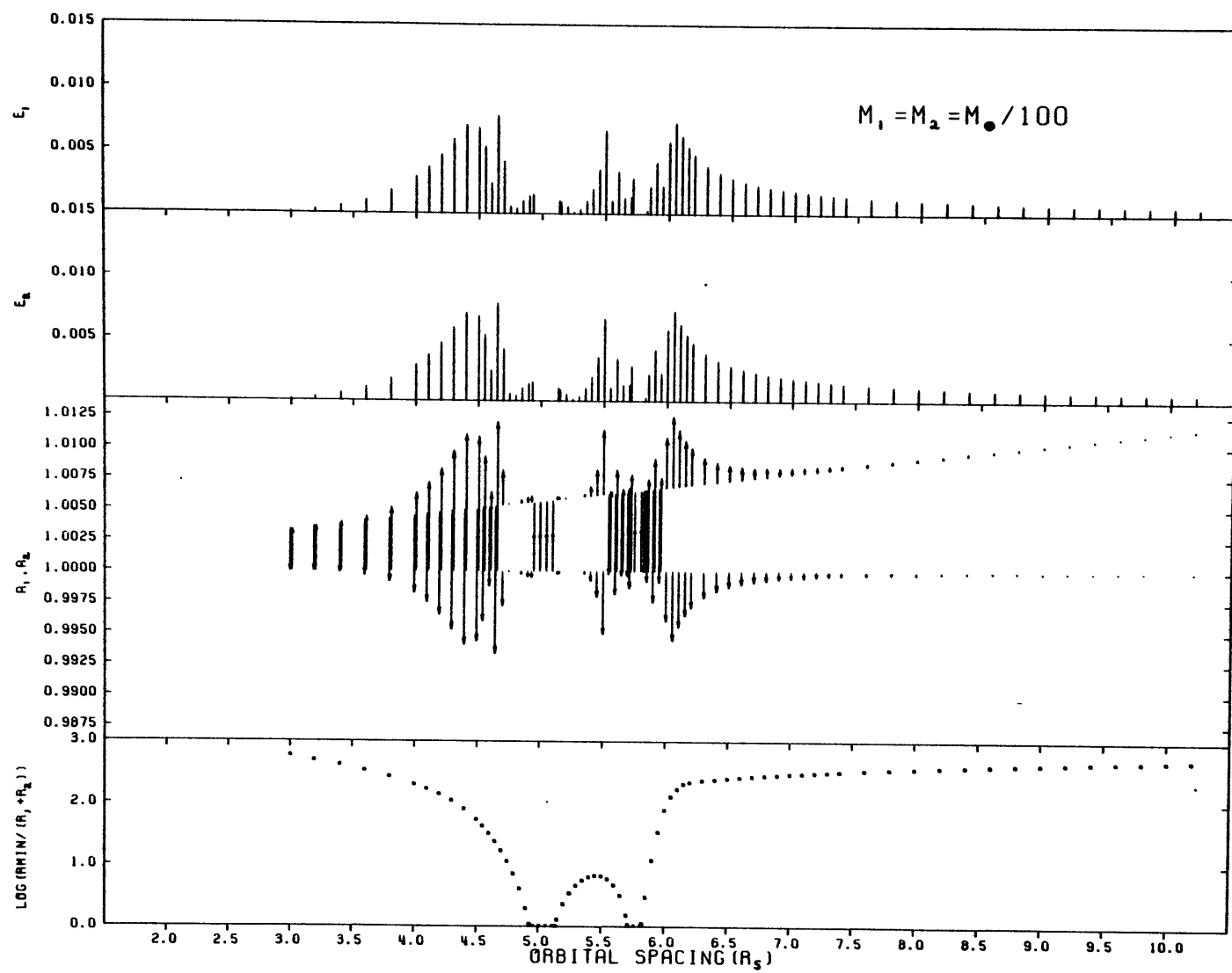


Figure 1

Figure 2



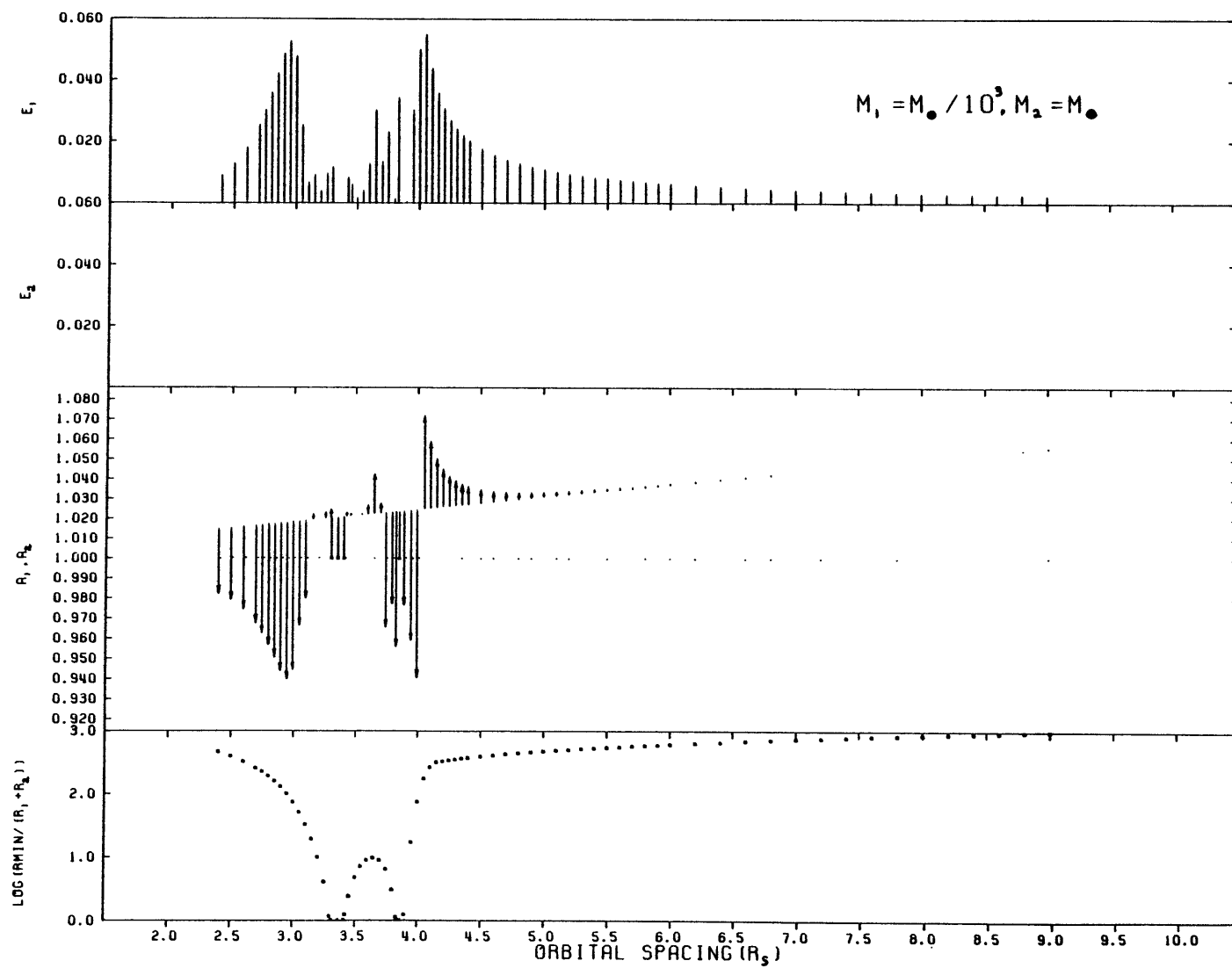


Figure 3

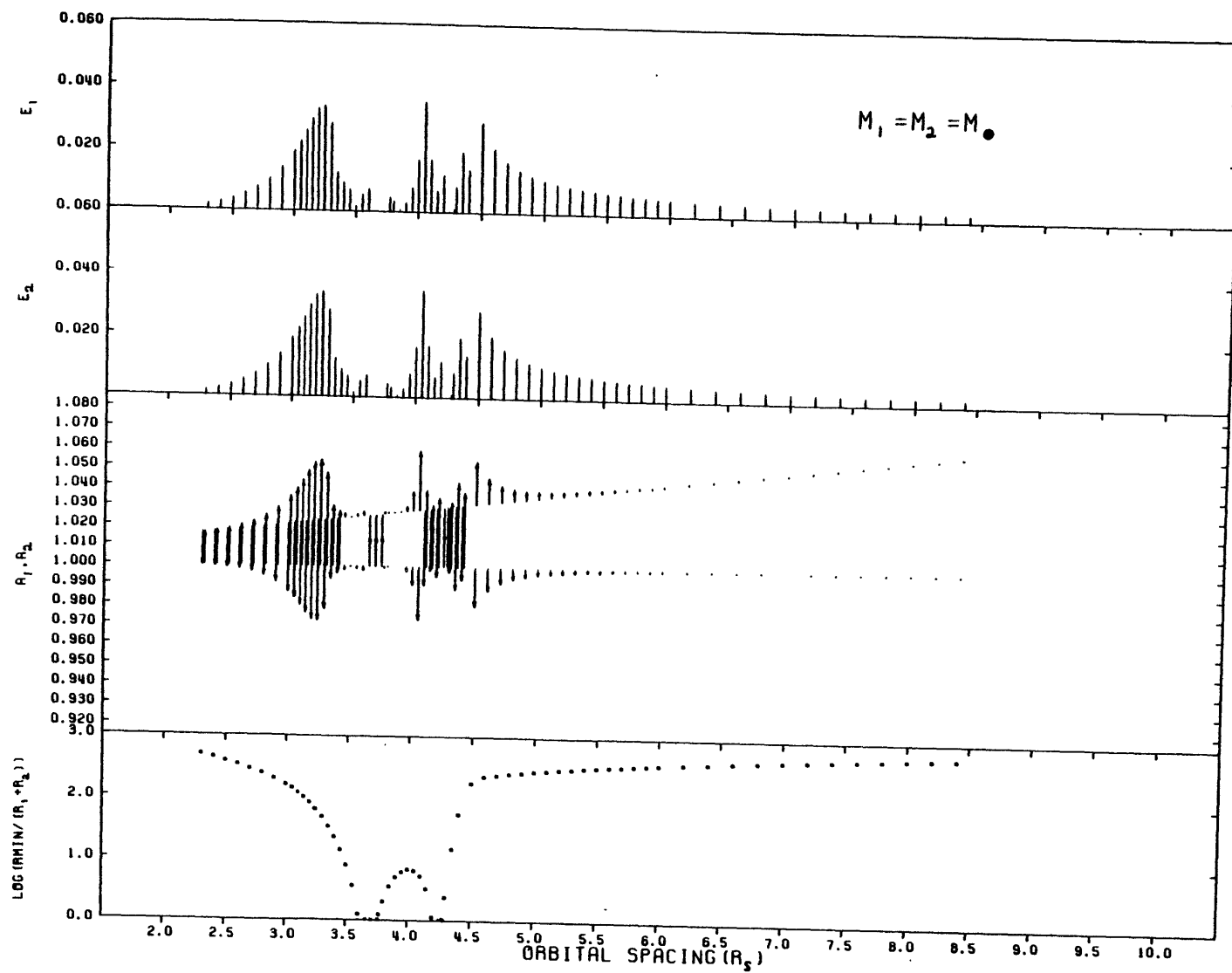
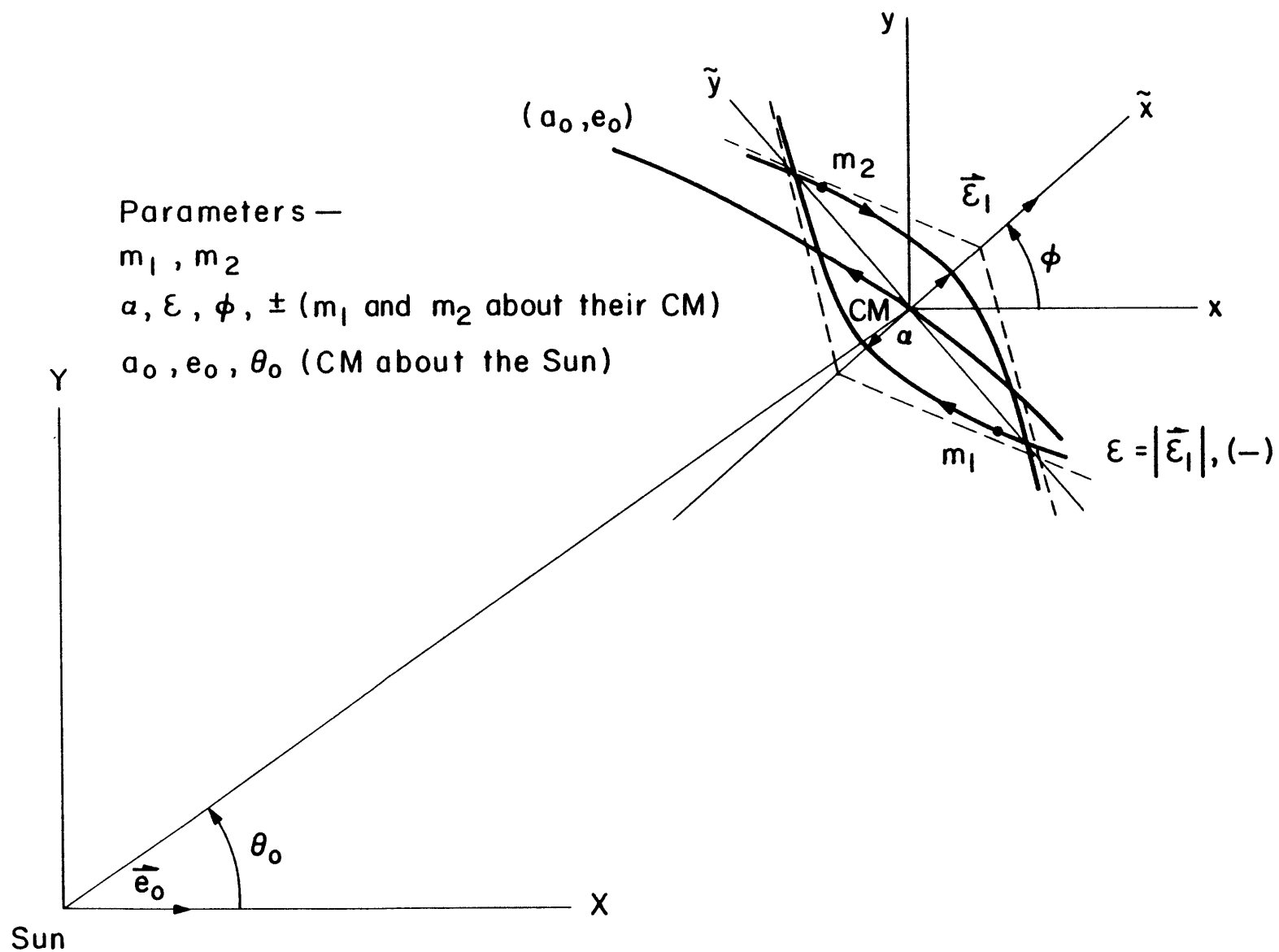


Figure 4

Figure 5



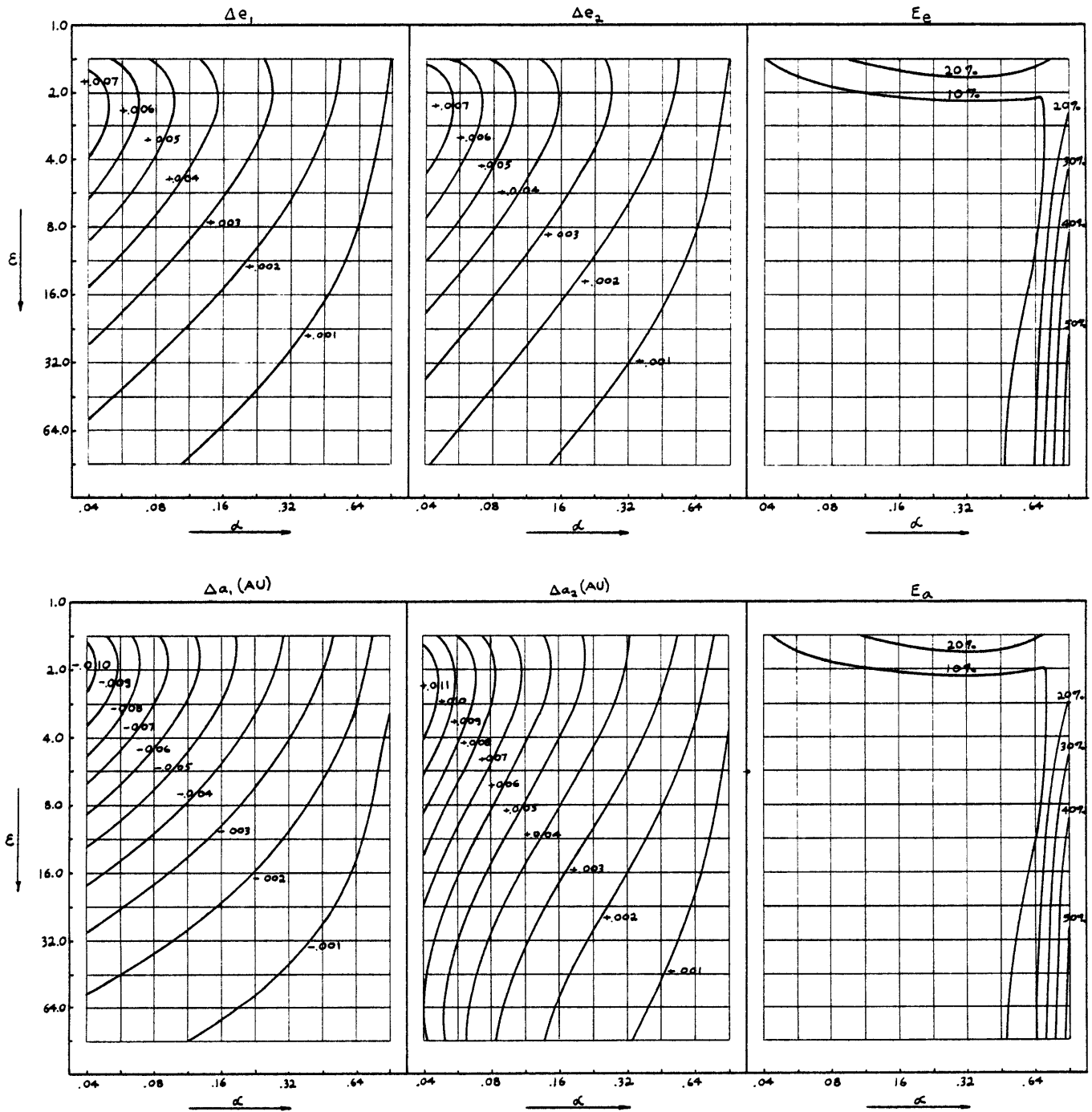


Figure 6

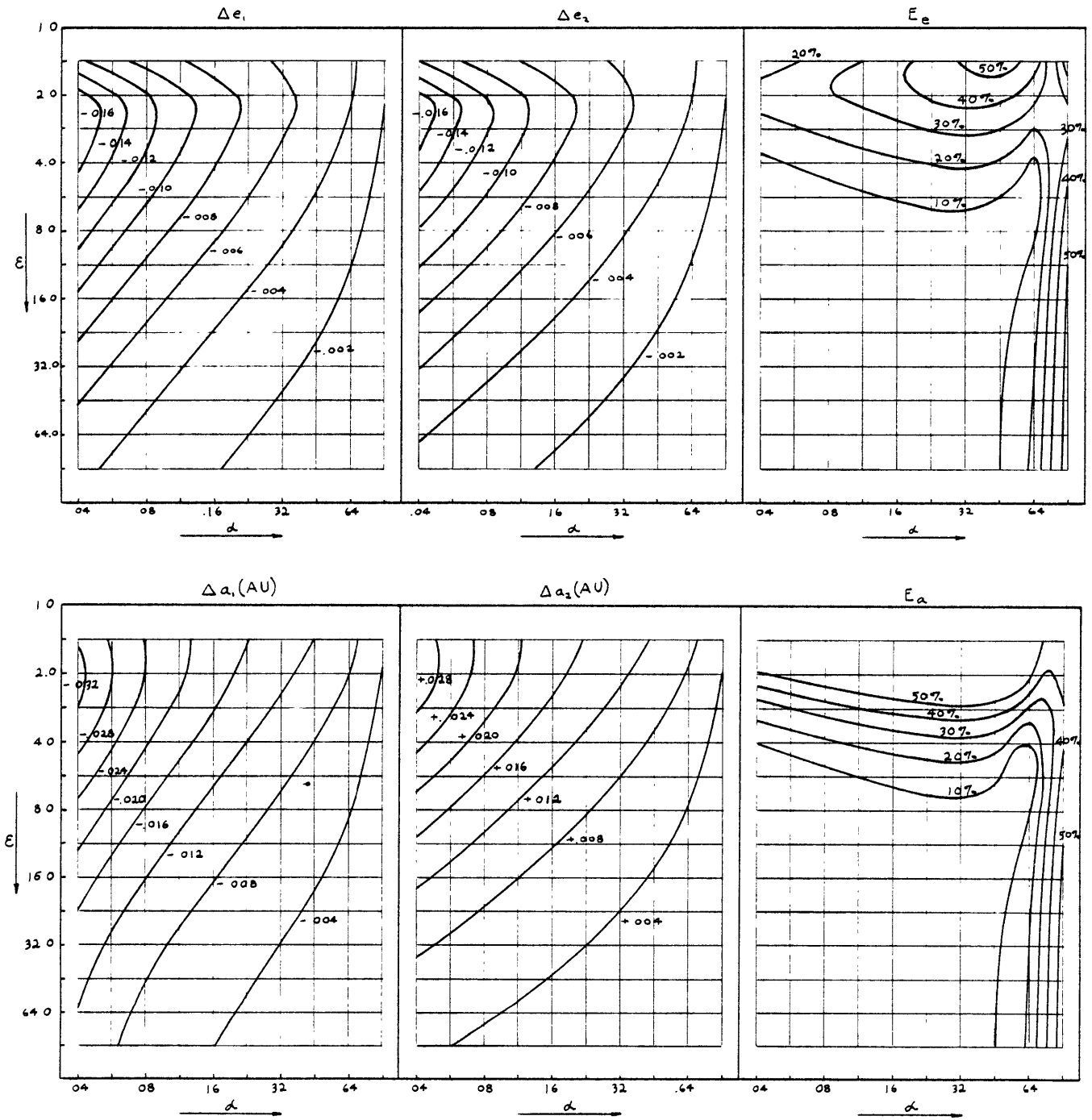


Figure 7

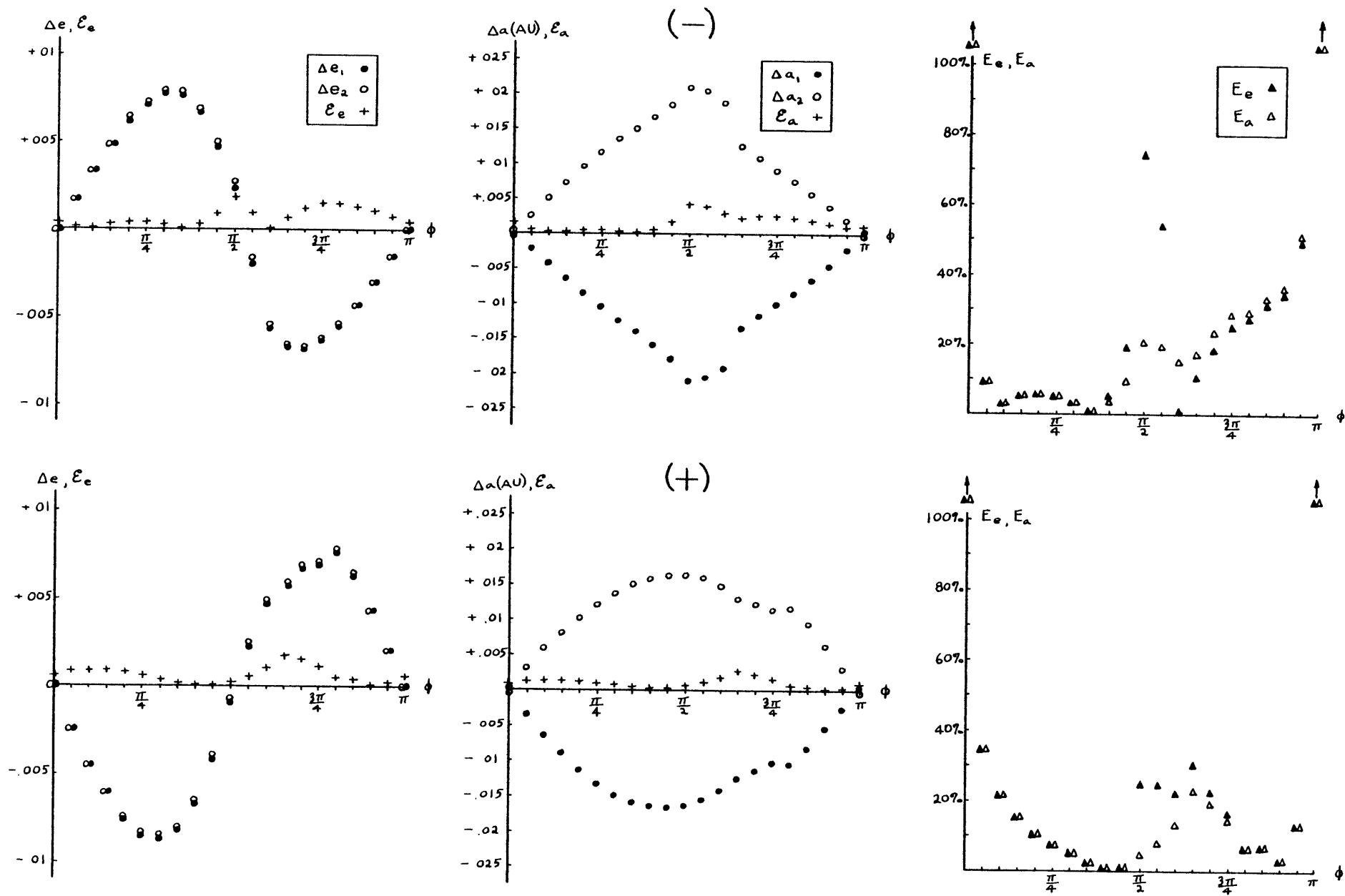


Figure 8

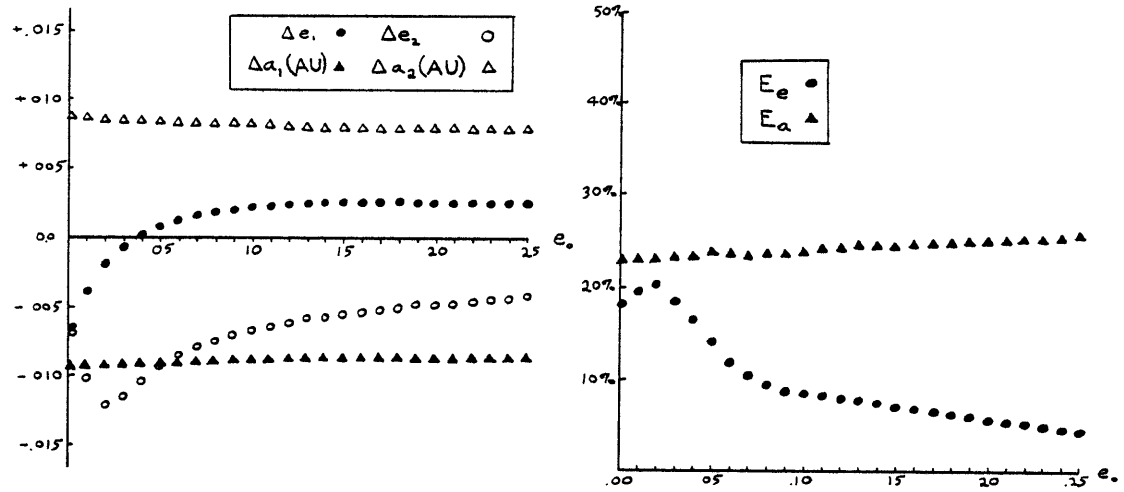
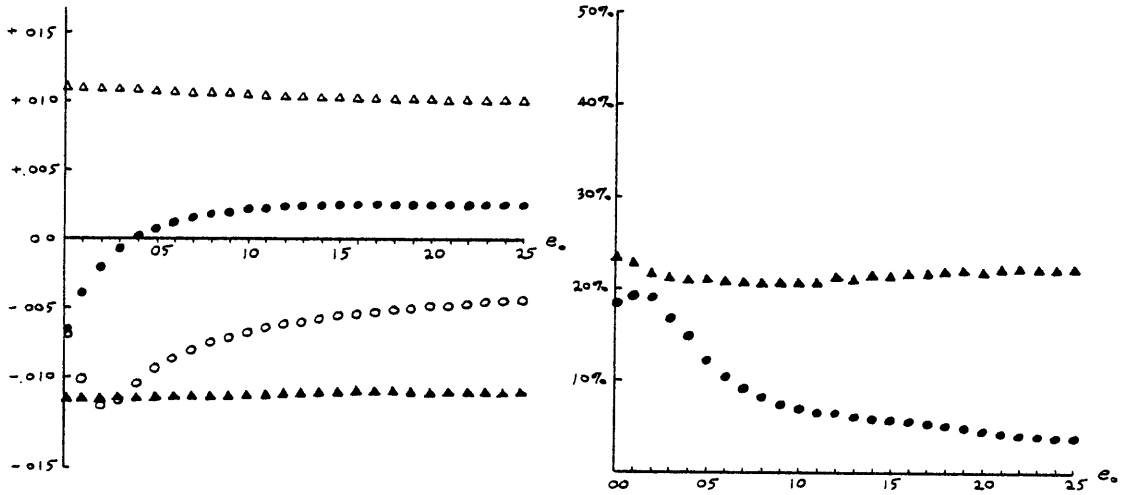
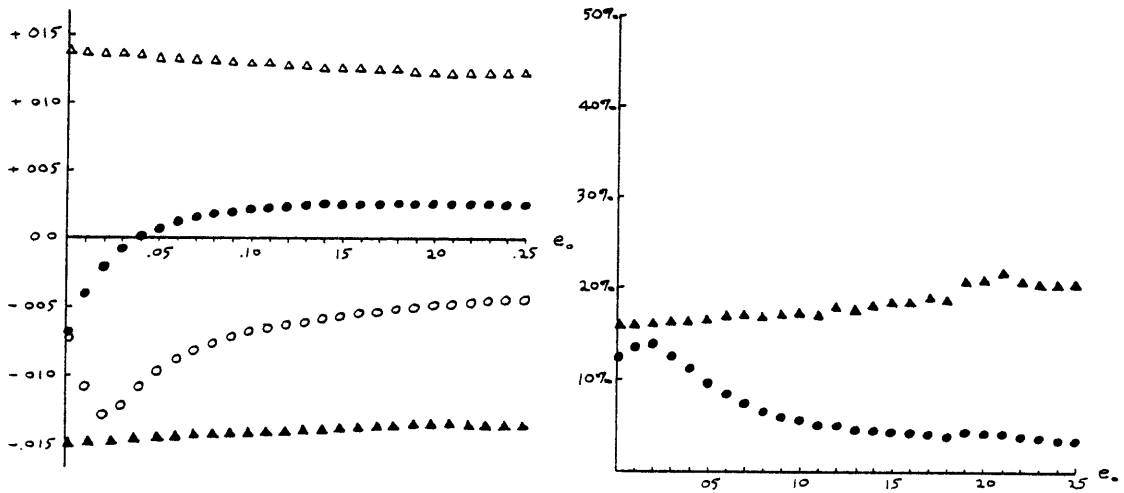
$R_0 = .80 \text{ AU}$  $R_0 = 1.0 \text{ AU}$  $R_0 = 1.20 \text{ AU}$ 

Figure 9

Figure 10

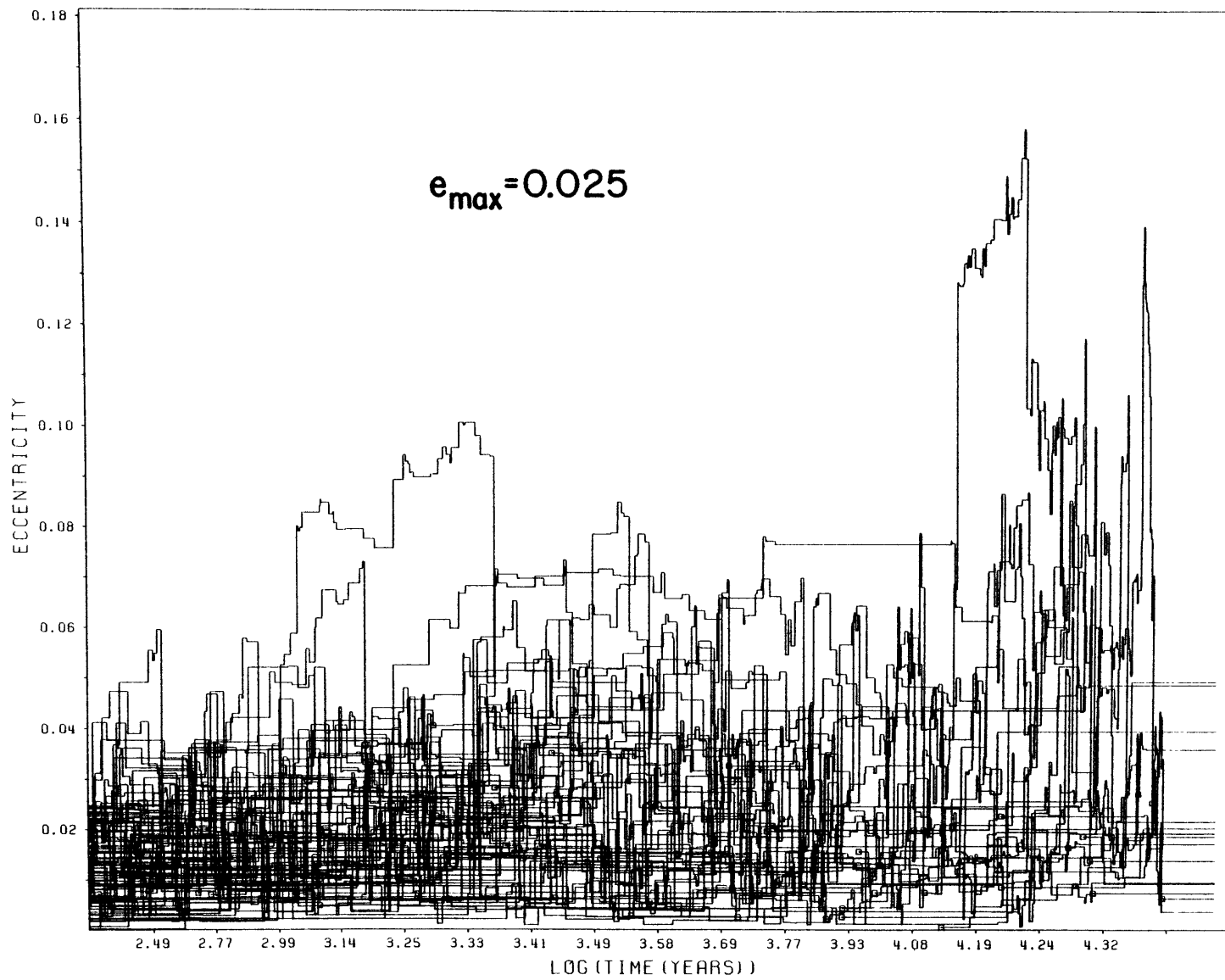


Figure 11

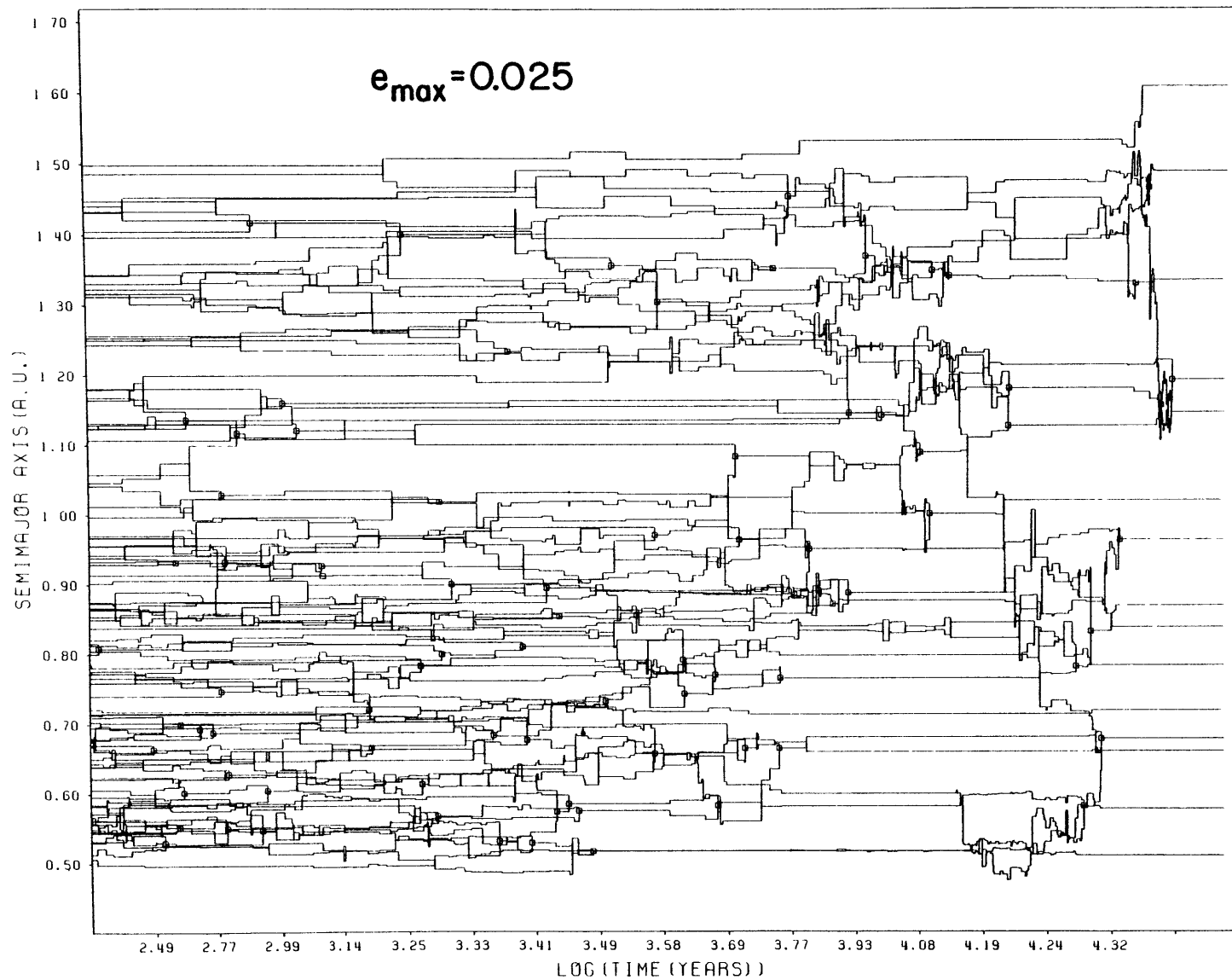


Figure 12

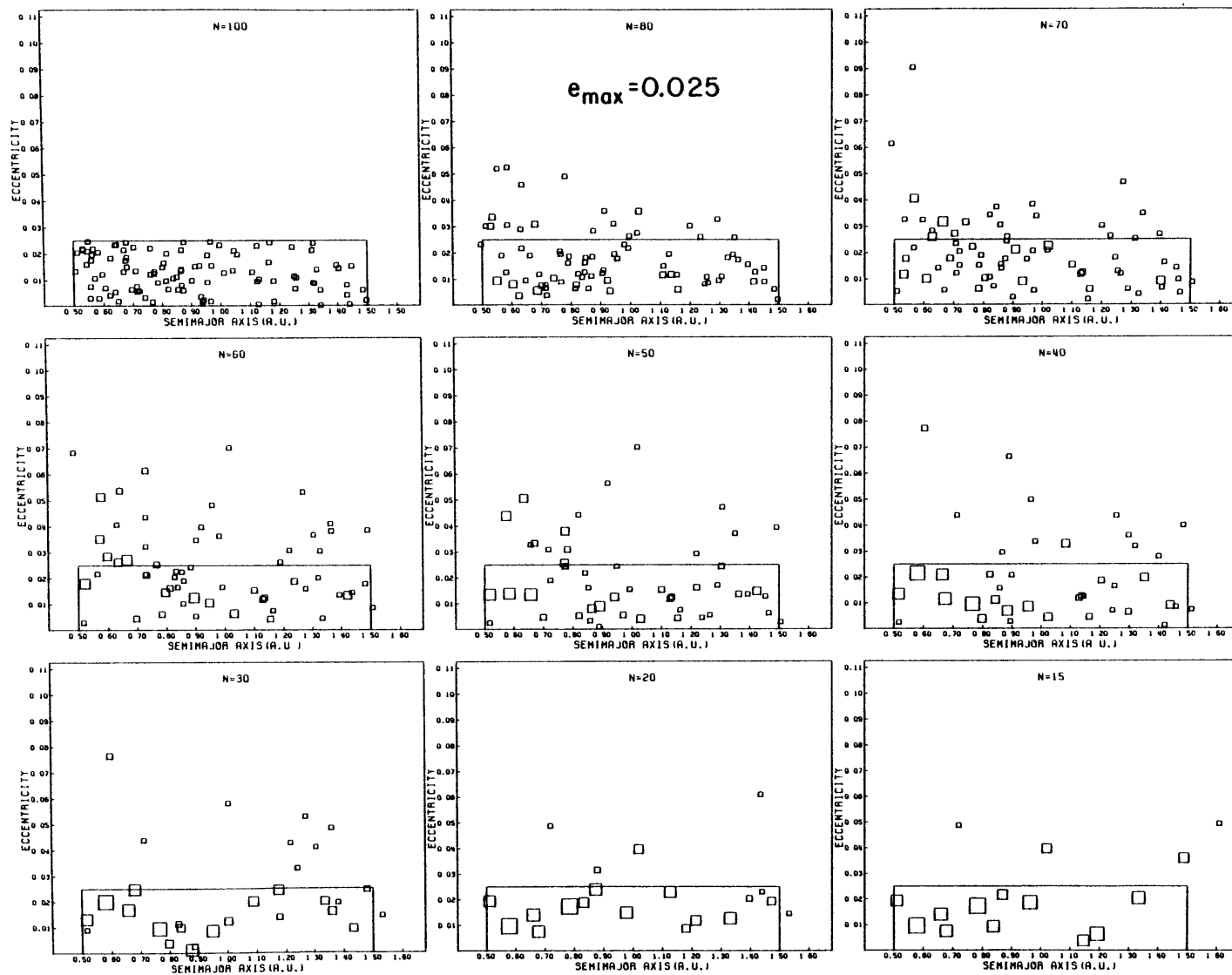


Figure 13

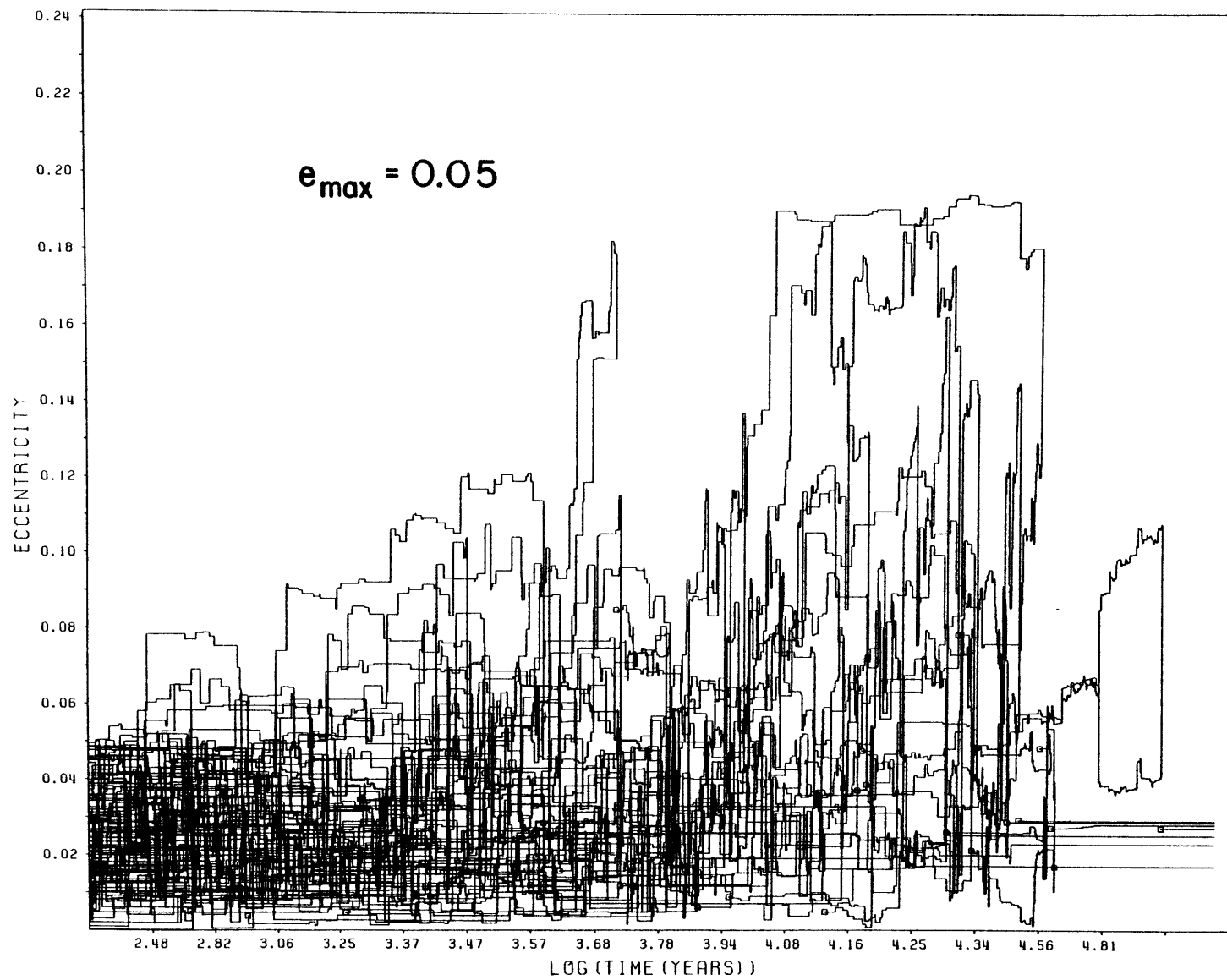


Figure 14

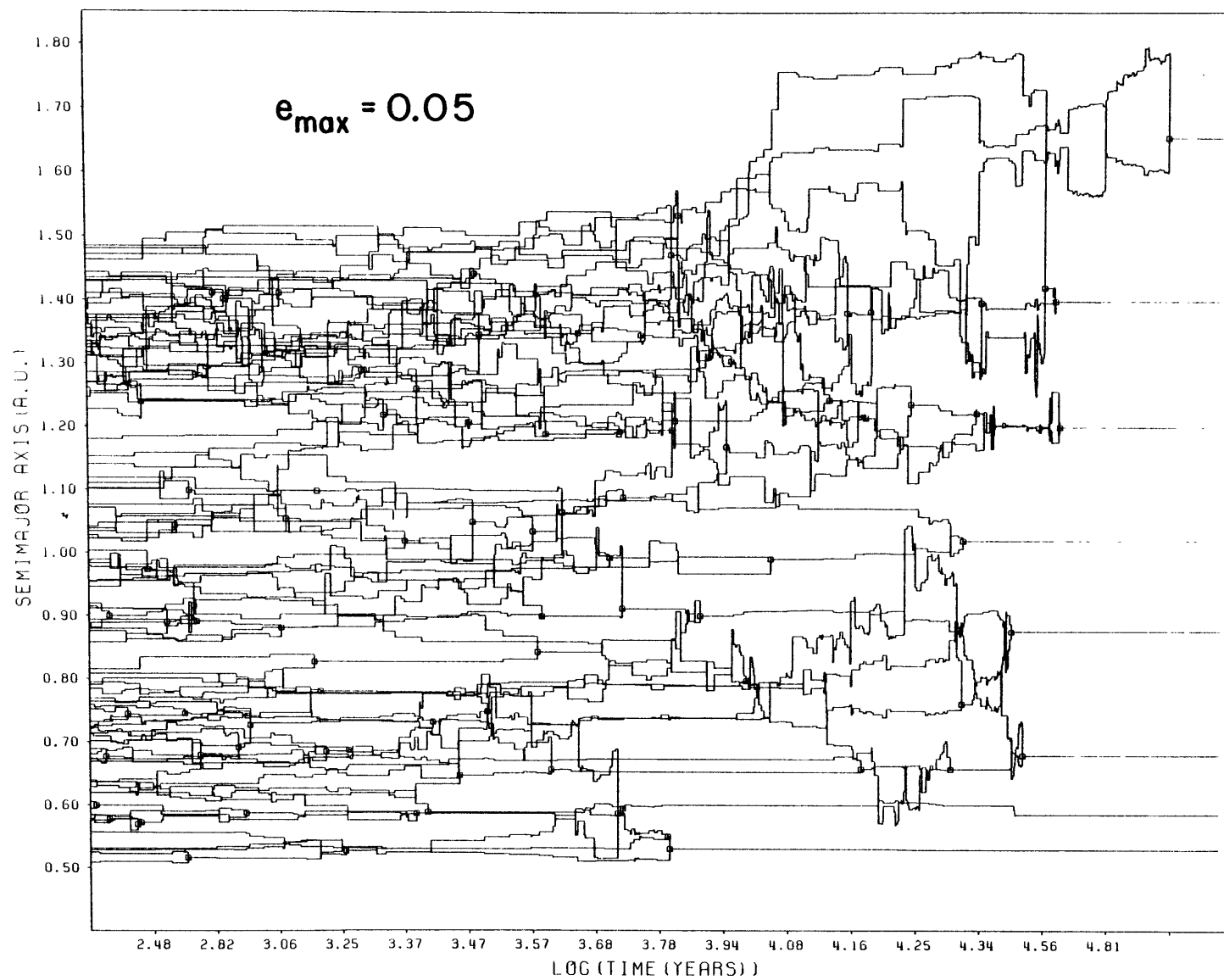


Figure 15

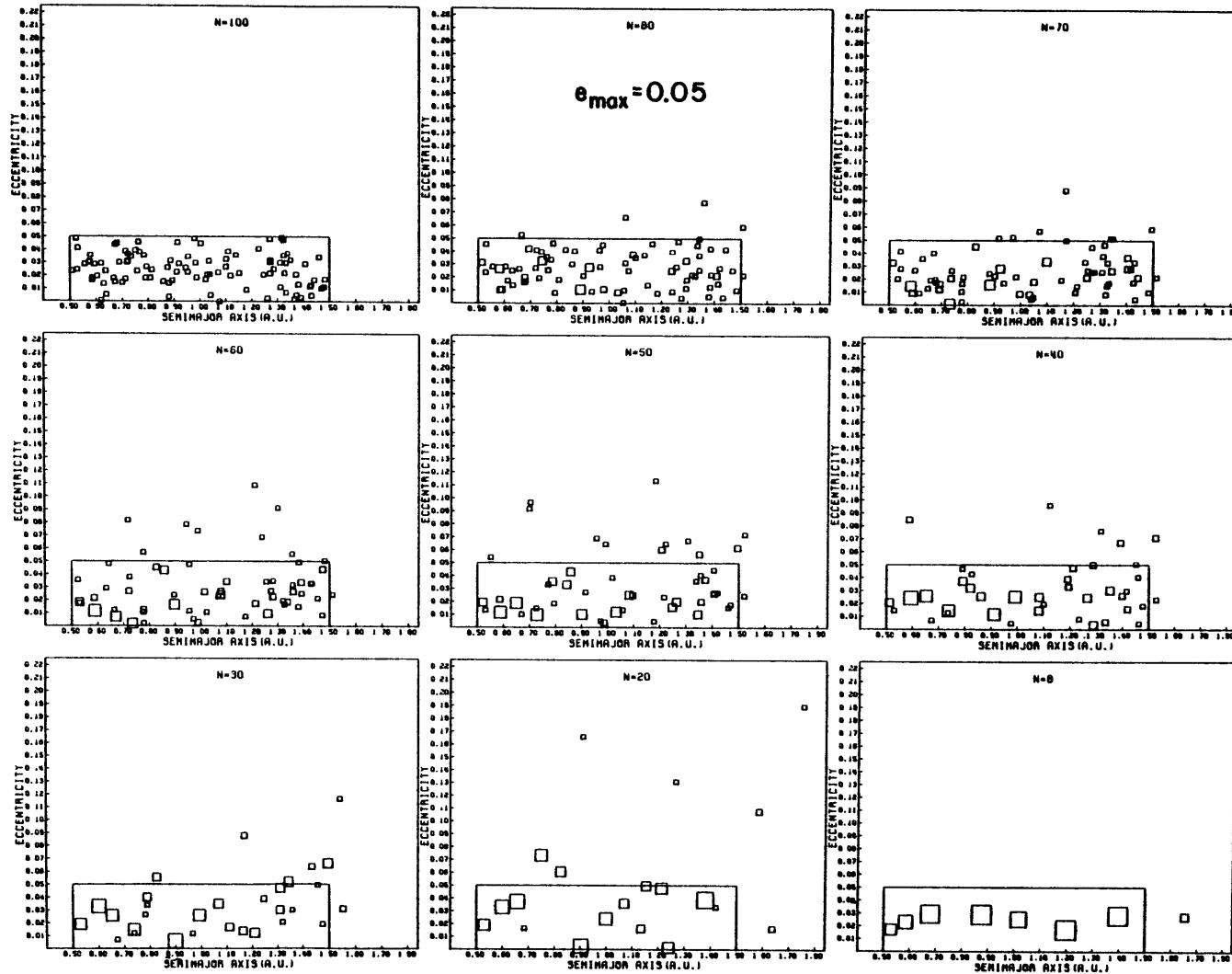


Figure 16

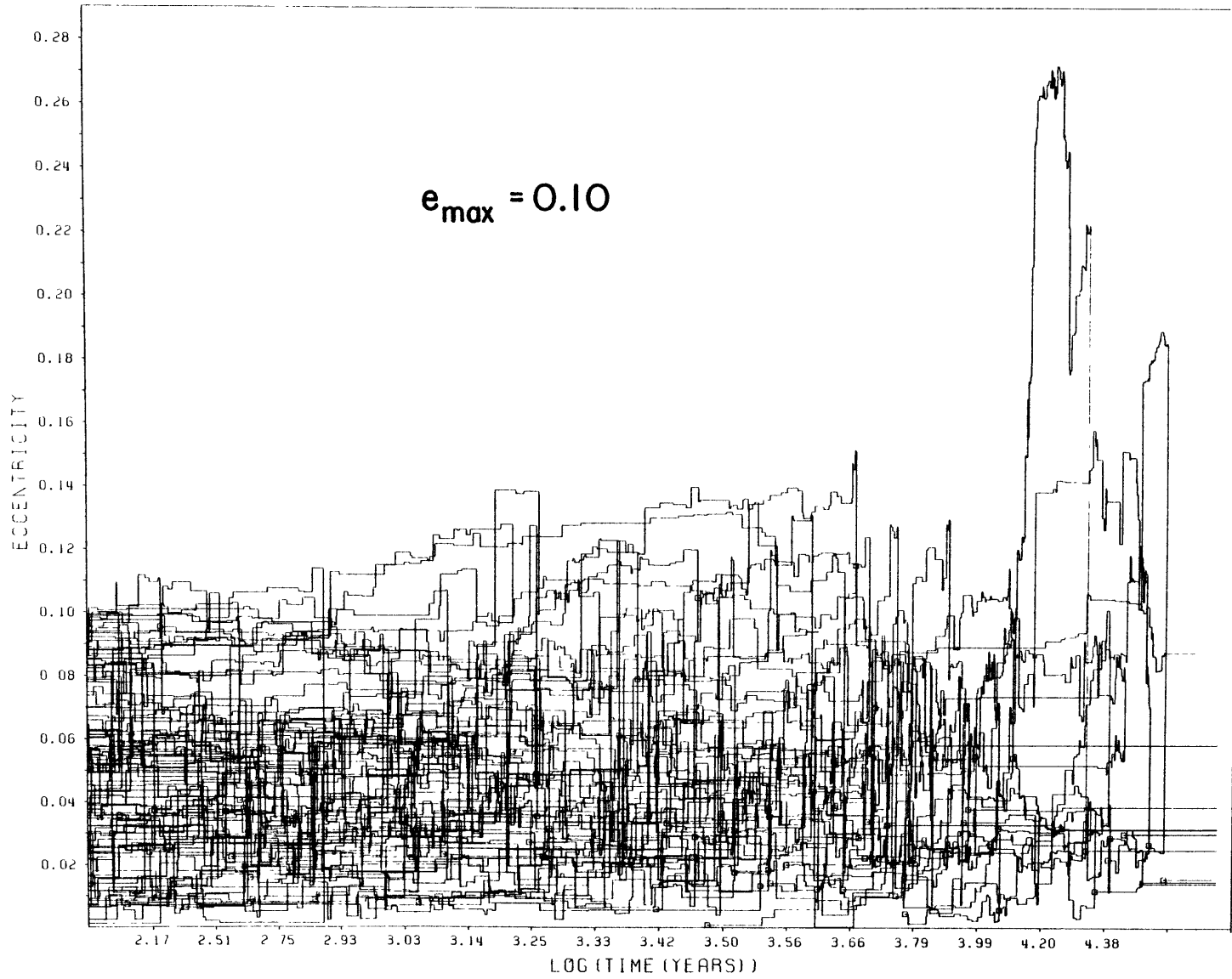


Figure 17

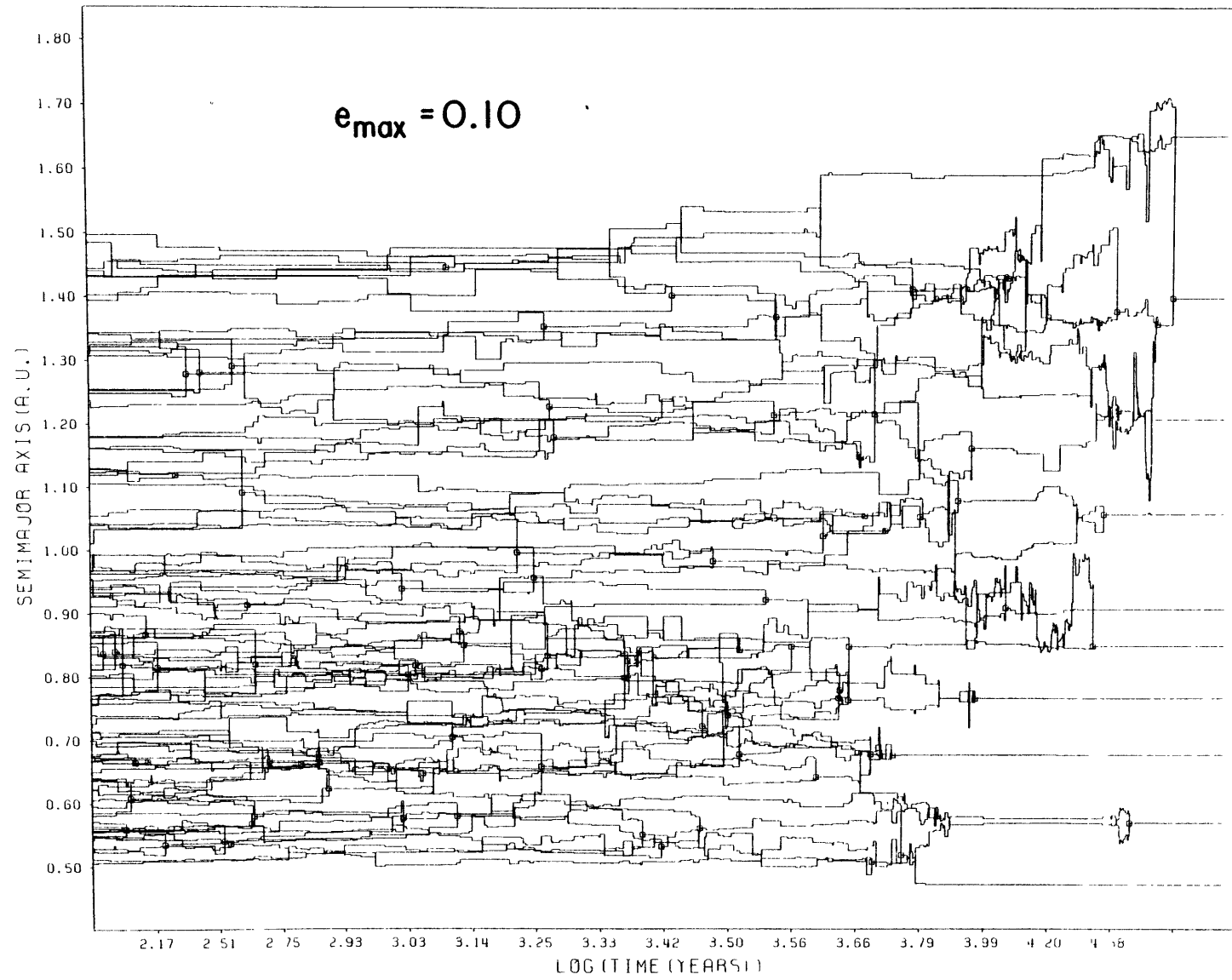


Figure 18

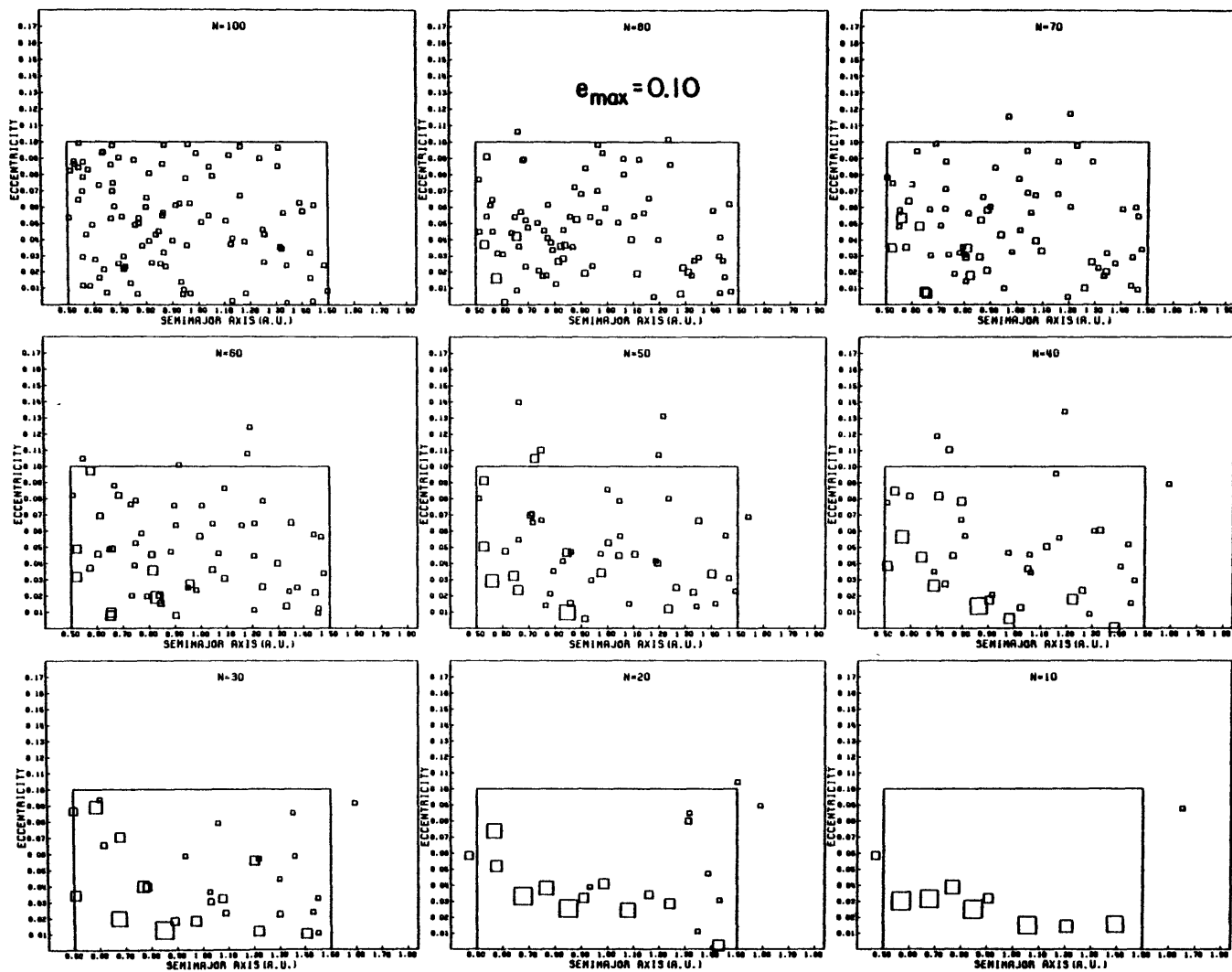


Figure 19

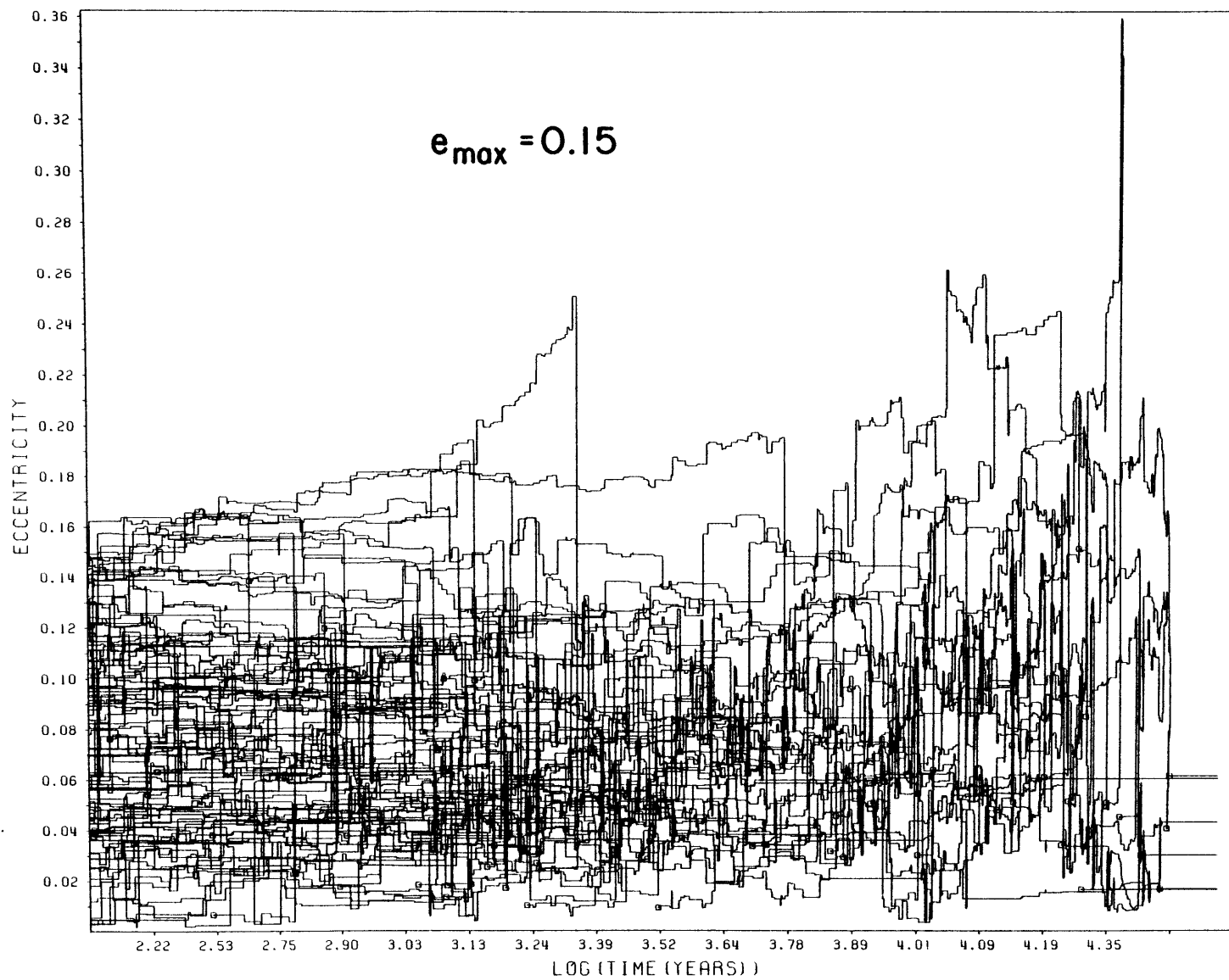


Figure 20

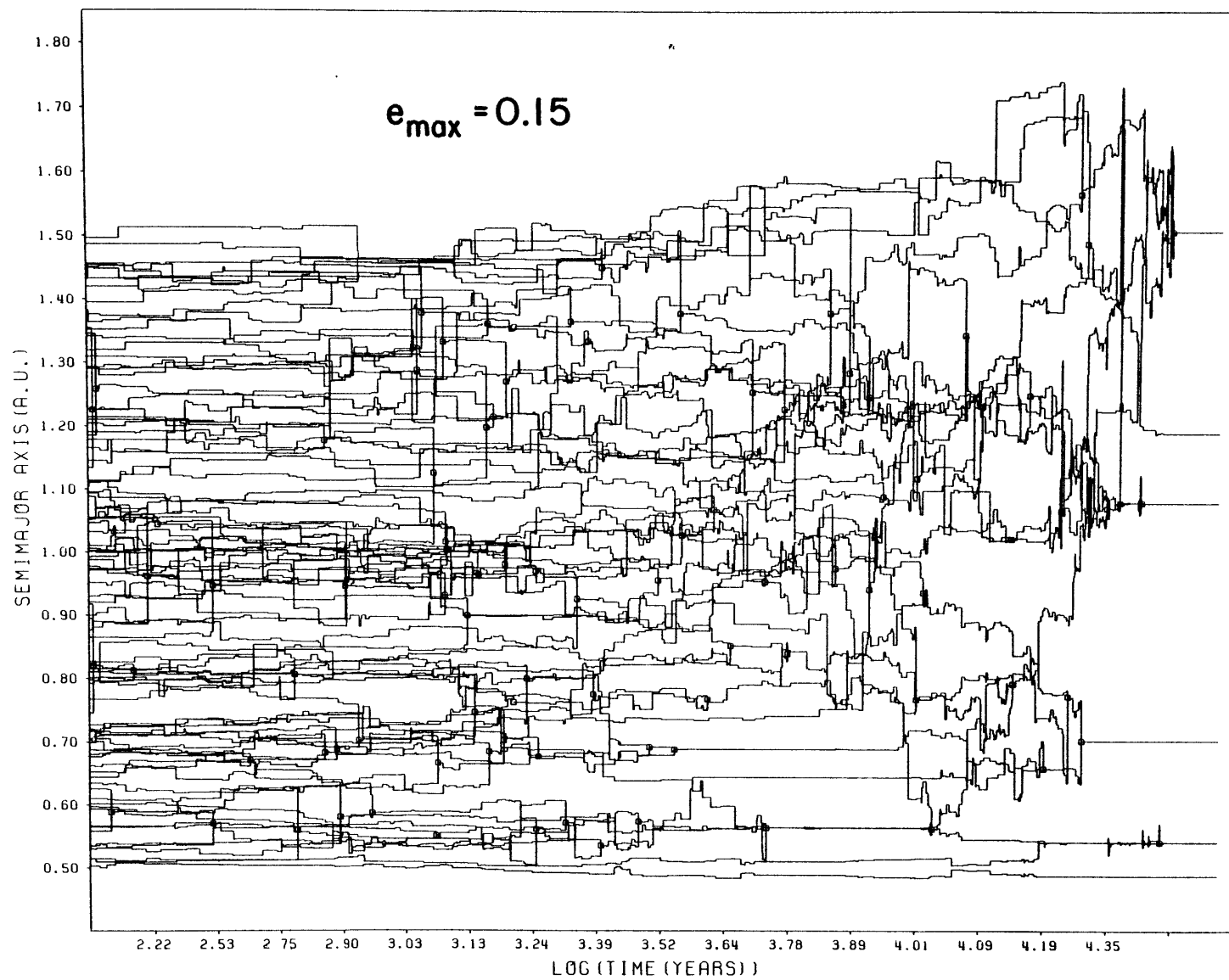


Figure 21

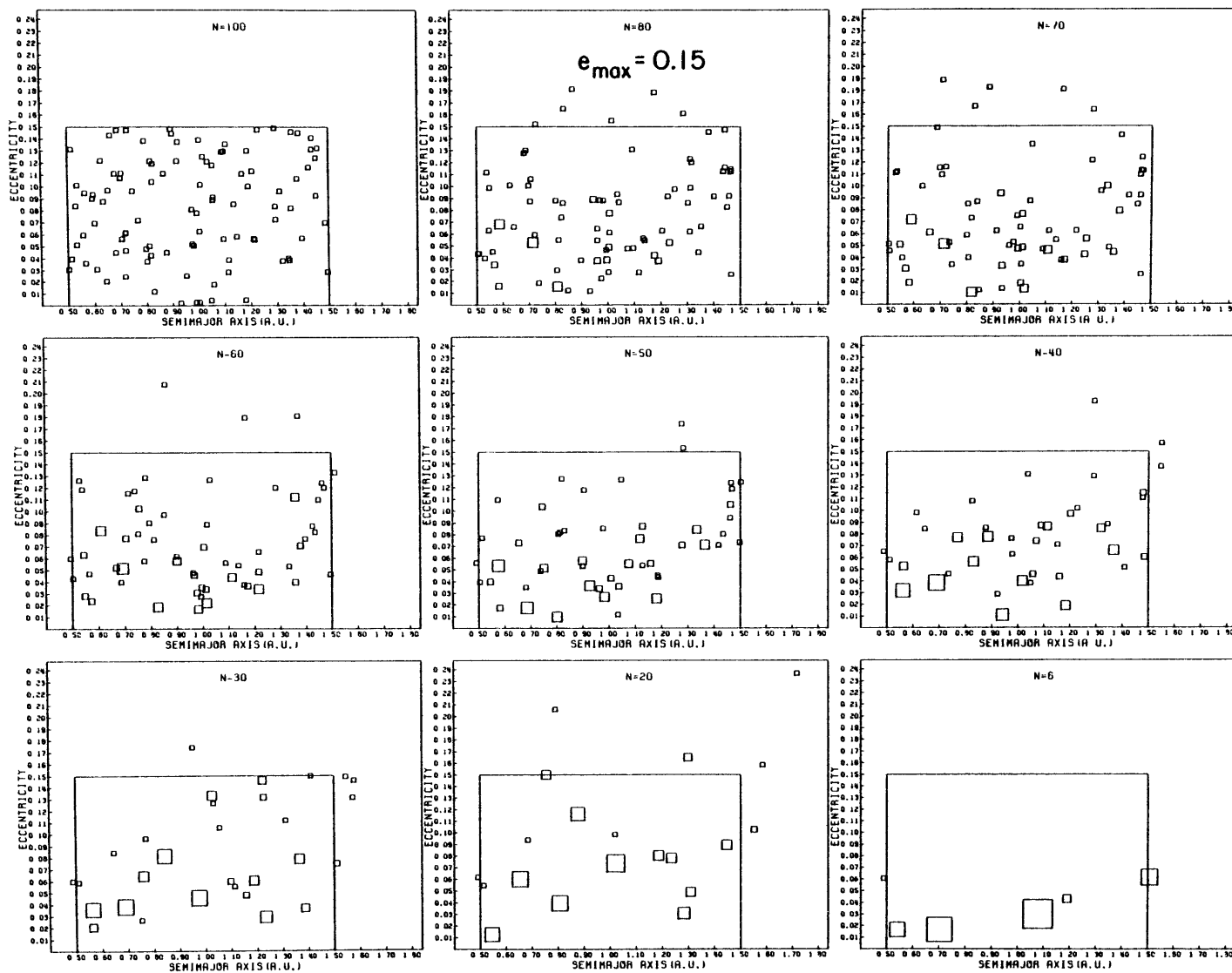


Figure 22

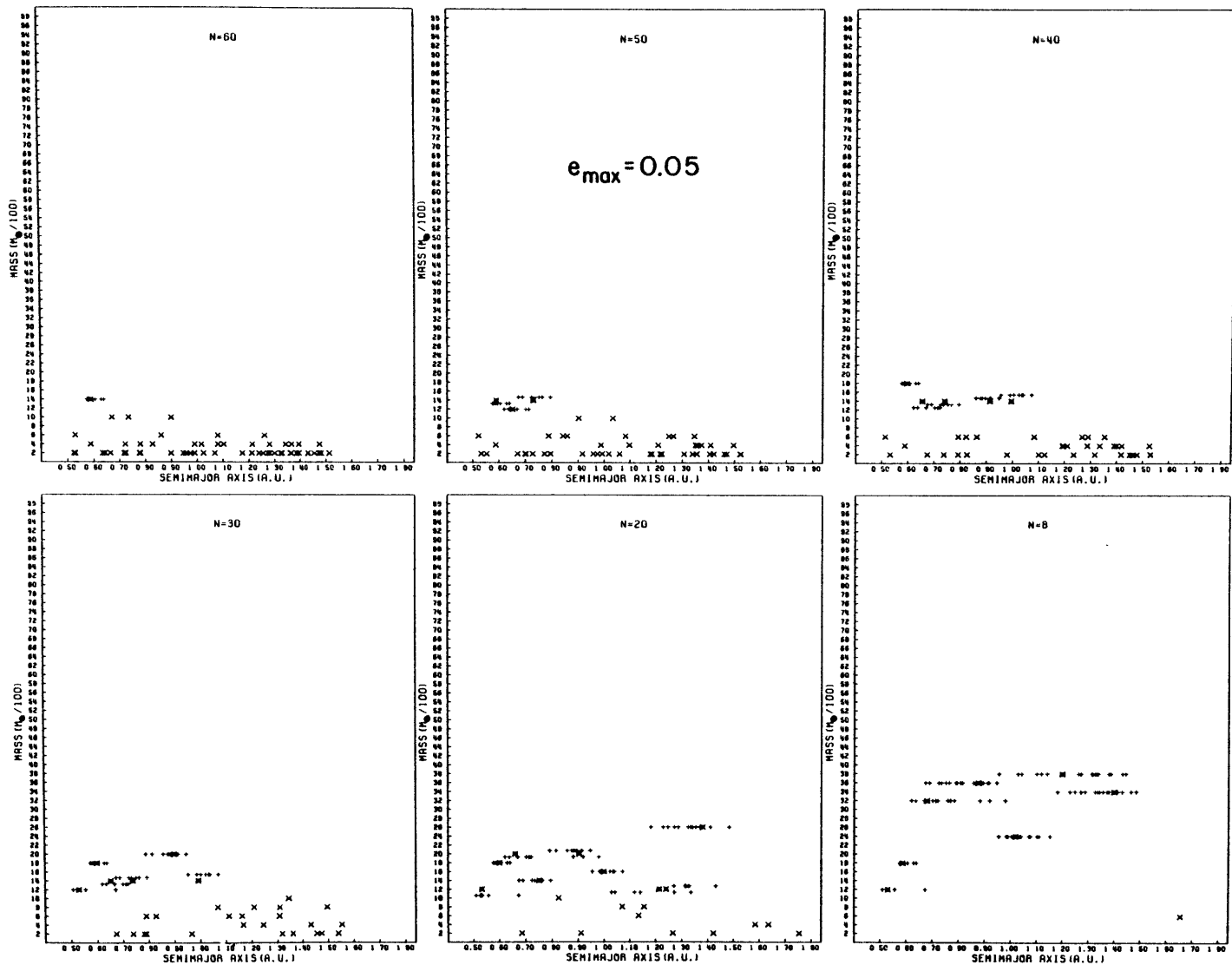
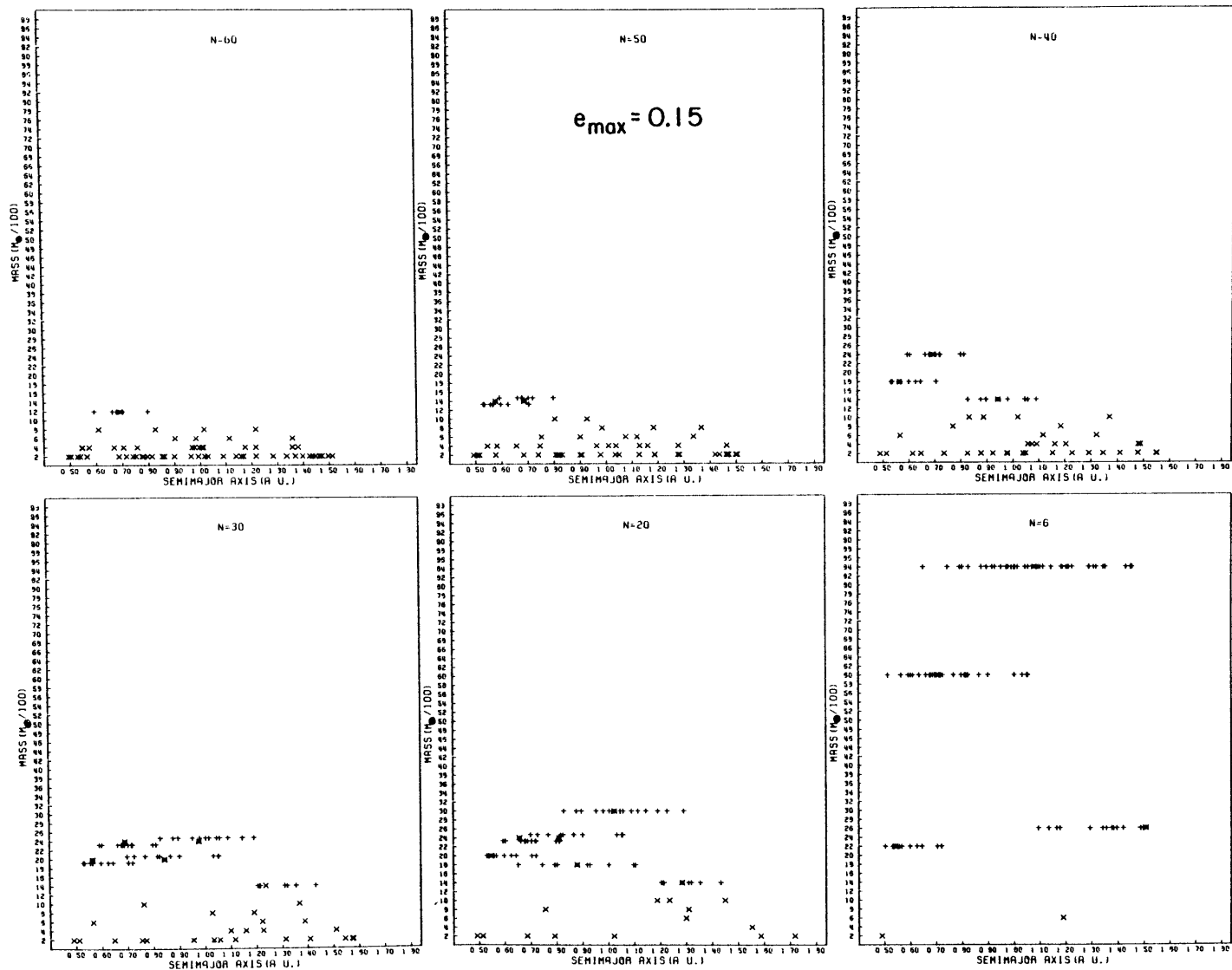


Figure 23



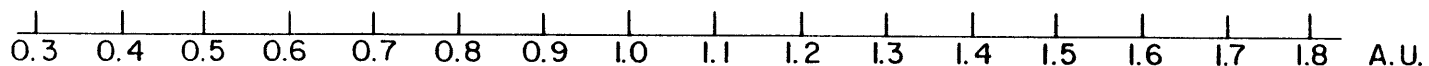
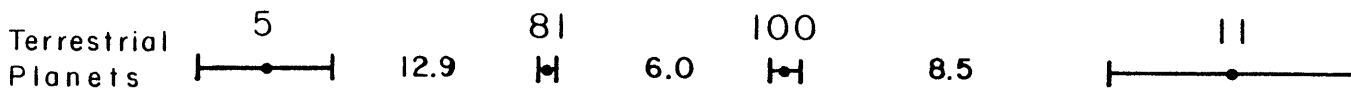
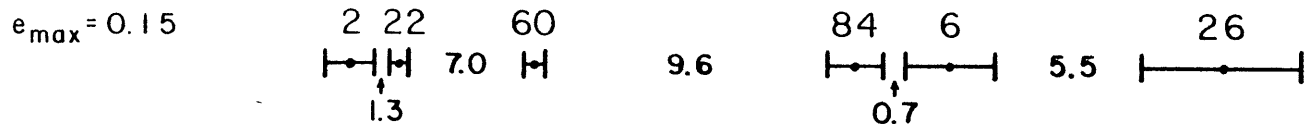
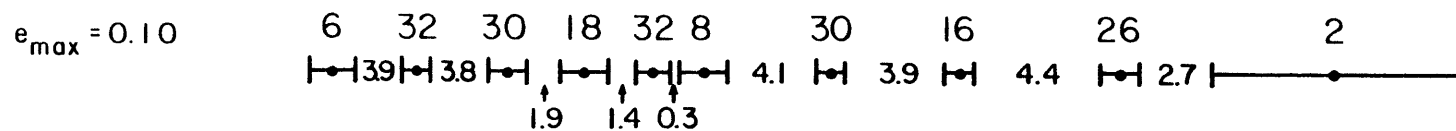
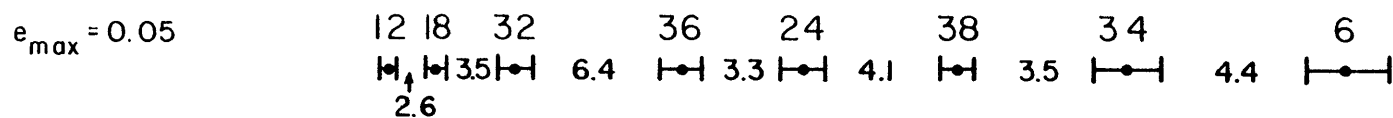
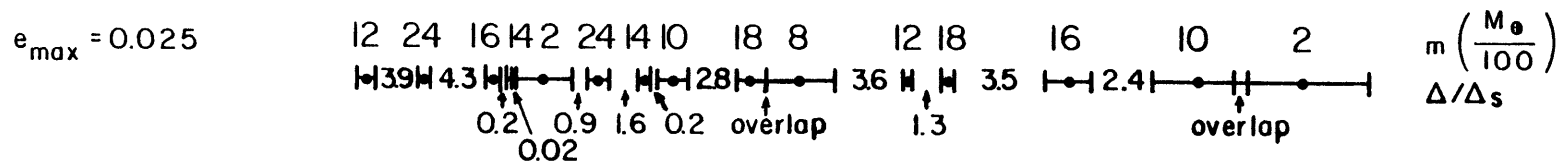


Figure 24

BIOGRAPHICAL NOTE

Larry Paul Cox was born and reared in Birmingham, Alabama. He was graduated from Ensley High School, Ensley, Alabama in 1962. He attended the Massachusetts Institute of Technology and received an S.B. in Physics in 1969. Research for his senior thesis led to publication with J.V. Evans of "Seasonal Variation of the F_1 -Region Ion Composition" (J.G.R., 75, 159-164). Following graduation he continued to do research with J.V. Evans as a staff member of the Millstone Hill Ionospheric Observatory, Lincoln Laboratory. This research led to a further publication with J.V. Evans of "Seasonal Variation of the O/N_2 Ratio in the F_1 -Region" (J.G.R., 75, 6271-6286).

As a graduate student in the Department of Earth and Planetary Sciences the author has held a National Defense Education Act Fellowship, a Teaching Assistantship in planetary physics, and Research Assistantships in the Department of Mathematics as well as in the Department of Earth and Planetary Sciences. His research work has been in the fields of ionospheric physics, galactic dynamics, and planetary accretion dynamics.

He married Candace Lenoir Kelton of Denver, Colorado in August, 1969. His wife has taught English in junior high school since 1970.